NATIONAL ADVISORY COMMITTEE FOR AERONAUTICS

TECHNICAL NOTE 2597

INVESTIGATION OF LAMINAR BOUNDARY LAYER IN COMPRESSIBLE FLUIDS USING THE CROCCO METHOD

By E. R. Van Driest

North American Aviation, Inc.

NACA

Washington
January 1952

1G

NATIONAL ADVISORY COMMITTEE FOR AERONAUTICS

TECHNICAL NOTE 2597

INVESTIGATION OF LAMINAR BOUNDARY LAYER IN COMPRESSIBLE FLUIDS USING THE CROCCO METHOD

By E. R. Van Driest

SUMMARY

In the present investigation of the flow of air in a thin laminar boundary layer on a flat plate, the Crocco method has been used to solve the simultaneous differential equations of momentum and energy involved in such flow. The Crocco method was used because it gave accurate results for arbitrary Prandtl number near unity. The Prandtl number was taken at 0.75, the specific heat was held constant, and the Sutherland law of viscosity-temperature variation was assumed to represent the viscosity data starting with an initial ambient temperature of -67.6° F. The main results presented here are the skin-friction and heat-transfer coefficients as functions of Reynolds number, Mach number, and wall-to-free-stream temperature ratio. Variations of shear, velocity, temperature, and Mach number across the boundary layer are included. The Crocco method is discussed in detail.

INTRODUCTION

In the present investigation of the flow of air in a thin laminar boundary layer on a flat plate, the Crocco method (reference 1) has been used to solve the simultaneous differential equations of momentum and energy involved in such flow. The Crocco method was used because it gave accurate results for arbitrary Prandtl number near unity. The first assumptions for the present discussion are as follows:

(1) The boundary layer is thin

(2) The pressure gradient is zero

(3) The plate surface is smooth

(4) The motion is two-dimensional and steady

(5) The Prandtl number is constant

This work was done by North American Aviation, Inc., and has been made available to the National Advisory Committee for Aeronautics for publication because of its general interest. The author gratefully acknowledges the assistance of Messrs. Warren W. Gollos, John N. Hale, and Frederick G. Etheridge and Mrs. Phyllis M. Watté in the publication of this report.

SYMBOLS

Variables, parameters, and functions

x,y	geometrical coordinates parallel and perpendicular to flat plate, respectively
u,v	velocity components of boundary-layer flow in x- and y-directions, respectively
ρ	mass density
μ	coefficient of viscosity
k	coefficient of thermal conductivity
T	absolute temperature
i	enthalpy
c_p	specific heat at constant pressure
γ	ratio of specific heat at constant pressure to specific heat at constant volume
τ	shear stress
M	Mach number
Pr	Prandtl number $\left(c_p\mu/k\right)$
g_*	shear function $\left(\sqrt{\frac{2}{\rho_\infty\mu_\infty u_\infty^3}}\, g_2(u)\right)$
ω	exponent of viscosity-temperature power law
S	Sutherland constant
δ	thickness of boundary layer

θ ratio of Sutherland constant to free-stream temperature $\left(110^{\circ}\ K/T_{\infty}{}^{\circ}\ K\right)$

$I, J, \theta^{I}, \theta^{II}$ functions connected with enthalpy distribution

$\overline{\overline{g_*}}$ shear function near outer edge of boundary layer

δg_* correction to $\overline{\overline{g_*}}$ near outer edge of boundary layer (in computations, at $u_* = 0.98$)

R_{∞} Reynolds number $\left(\rho_{\infty} u_{\infty} x/\mu_{\infty}\right)$

c_f local skin-friction coefficient $\left(2\tau_w/\rho_{\infty} u_{\infty}{}^2\right)$

C_f mean skin-friction coefficient $\left(2\int_0^x \tau_w\, dx \Big/ \rho_{\infty} u_{\infty}{}^2 x\right)$

q rate of heat transfer

h local heat-transfer coefficient, difference between u_* and unity as u_* approaches unity

C_H Stanton number

r recovery factor

$i_* = i/i_{\infty}$

$u_* = u/u_{\infty}$

$\rho_* = \rho/\rho_{\infty}$

$\mu_* = \mu/\mu_{\infty}$

$M_* = M/M_{\infty}$

$T_* = T/T_{\infty}$

y_* distance parameter $\left(\frac{y}{x}\sqrt{R_{\infty}}\right)$

$f(u_*) = 2u_*\rho_*\mu_*$

$g_2(u) = \tau\sqrt{2x}$

Subscripts

∞ free-stream conditions

w wall conditions

TRANSFORMATION OF BOUNDARY-LAYER EQUATIONS

The equations governing the steady two-dimensional motion of a compressible fluid in a thin boundary layer on a flat plate with zero pressure gradient are:

$$\frac{\partial}{\partial x}(\rho u) + \frac{\partial}{\partial y}(\rho v) = 0 \qquad \text{(continuity)} \tag{1}$$

$$\rho u \frac{\partial u}{\partial x} + \rho v \frac{\partial u}{\partial y} = \frac{\partial}{\partial y}\left(\mu \frac{\partial u}{\partial y}\right) \qquad \text{(momentum)} \tag{2}$$

$$\rho u \frac{\partial}{\partial x}(i) + \rho v \frac{\partial}{\partial y}(i) = \mu\left(\frac{\partial u}{\partial y}\right)^2 + \frac{\partial}{\partial y}\left(k \frac{\partial T}{\partial y}\right) \qquad \text{(energy)} \tag{3}$$

Because of the thinness of the layer, $\partial p/\partial y = 0$, and hence for a perfect gas the density varies inversely with the temperature. Upon assumption that the Prandtl number $c_p\mu/k$ is constant and use of $c_p = \partial i/\partial T$, equation (3) becomes

$$\rho u \frac{\partial i}{\partial x} + \rho v \frac{\partial i}{\partial y} = \mu\left(\frac{\partial u}{\partial y}\right)^2 + \frac{1}{Pr} \frac{\partial}{\partial y}\left(\mu \frac{\partial i}{\partial y}\right) \tag{4}$$

The independent variables are first transformed from x and y to x and u by means of

$$u = u(x,y)$$

Use of $\tau = \mu \partial u/\partial y$ and the elimination of ρv then yield the following two equations:

$$u \frac{\partial}{\partial x}\left(\frac{\rho\mu}{\tau}\right) + \frac{\partial^2 \tau}{\partial u^2} = 0 \tag{5}$$

$$(1 - Pr)\frac{\partial i}{\partial u} \tau \frac{\partial \tau}{\partial u} + \left(\frac{\partial^2 i}{\partial u^2} + Pr\right)\tau^2 - Pr\ u\rho\mu \frac{\partial i}{\partial x} = 0 \tag{6}$$

with boundary conditions

$$\tau = \infty \qquad \text{at} \qquad x = 0, \quad 0 < u < u_\infty \tag{7a}$$

$$\frac{\partial \tau}{\partial u} = 0, \quad i = i_w \qquad \text{at} \qquad x > 0, \quad u = 0 \tag{7b}$$

$$\tau = 0, \quad i = i_\infty \qquad \text{at} \qquad x > 0, \quad u = u_\infty \tag{7c}$$

It is now assumed that the enthalpy is a function of u only; that is, $\partial i/\partial x = 0$. (This can be shown (reference 2) to be the case for a Prandtl number equal to unity, whether the wall is insulated or not.) Hence it follows from equation (6) that a type of solution is $\tau = g_1(x)g_2(u)$. Whence, since ρ and μ are functions of temperature, and therefore enthalpy, and therefore velocity u alone, there results from equation (5) and boundary condition (7a) that $\tau = g_2(u)/\sqrt{2x}$. Equations (5) and (6) now become

$$g_2 g''_2 + u\rho\mu = 0 \tag{8}$$

$$(i'' + Pr)g_2 + (1 - Pr)i'g'_2 = 0 \tag{9}$$

with boundary conditions

$$g'_2 = 0, \ i = i_w \qquad \text{at} \ u = 0 \tag{10a}$$

$$g_2 = 0, \ i = i_\infty \qquad \text{at} \ u = u_\infty \tag{10b}$$

where the prime signifies differentiation with respect to u. When the variables i, u, ρ, and μ are made dimensionless by putting $i_* = i/i_\infty$, $u_* = u/u_\infty$, $\rho_* = \rho/\rho_\infty$, and $\mu_* = \mu/\mu_\infty$, it is seen that g_* must then be equal to $\sqrt{\frac{2}{\rho_\infty \mu_\infty u_\infty^3}}\, g_2(u)$. Equations (8) and (9) become finally

$$g_* g_*'' + 2u_* \rho_* \mu_* = 0 \tag{11}$$

$$\left(i_*'' + Pr \frac{u_\infty^2}{i_\infty}\right) g_* + (1 - Pr) i_*' g_*' = 0 \tag{12}$$

with boundary conditions

$$g_*' = 0, \quad i_* = i_w/i_\infty \qquad \text{at} \quad u_* = 0 \tag{13a}$$

$$g_* = 0, \quad i_* = 1 \qquad \text{at} \quad u_* = 1 \tag{13b}$$

The factor 2 is inserted in equation (11) so that when $\rho_* \mu_* = 1$, equation (11) will become the Blasius equation (reference 3), the exact solution of which will be used as the first step in the Crocco method of solving equations (11) and (12) in the case of gases.

The boundary-layer equations (equations (1), (2), and (3)) have thus been transformed into two simultaneous ordinary differential equations which lend themselves more readily to solution. Having the solution of equations (11) and (12), one can then compute the coefficients of skin friction and heat transfer and also the variation of certain properties across the boundary layer.

SOLUTION OF EQUATIONS FOR ARBITRARY PRANDTL NUMBER NEAR UNITY AND ARBITRARY VISCOSITY LAW

In order to solve equations (11) and (12), it is necessary to assume a law of variation of viscosity with temperature. Two laws have been frequently used to represent viscosity data, namely, the power law and the Sutherland law. The power law is

$$\left.\begin{aligned} \mu_* &= (T_*)^\omega \\ T_* &= T/T_\infty \end{aligned}\right\} \tag{14}$$

where, in the case of air, ω ranges from 0.76 for ordinary temperatures to 0.5 for higher temperatures. The Sutherland law is

$$\left.\begin{aligned} \mu_* &= T_*^{1/2}\frac{1+\theta}{1+(\theta/T_*)} \\ \theta &= S/T_\infty \end{aligned}\right\} \qquad (15)$$

where S is a constant depending upon the gas used. From data of Tribus and Boelter (reference 4), the constant S is found to be 110° K for air. Both laws are plotted in figure 1 using initial conditions corresponding to the standard isothermal altitude range of 35,332 to 104,987 feet. It is seen that the Sutherland law fits the data much better than the power law; therefore, since both ω and θ depend upon the free-stream temperature T_∞, it follows that the Sutherland law is most suitable for use in equation (11). When it is assumed that the specific heat is constant and i_∞ is set equal to c_pT_∞, then i_* can replace T_* in equation (14) or (15), and $\rho_* = i_*^{-1}$. If the variation of the specific heat is to be taken into account, then it is only necessary that the relation between enthalpy and temperature (from gas tables) be available in order to convert the viscosity and density to functions of enthalpy.

Following Crocco, equation (12) is written in the form

$$\frac{d}{du_*}\left(i_*'g_*^{1-Pr}\right) + Pr\frac{u_\infty^2}{i_\infty}g_*^{1-Pr} = 0$$

the solution of which is, in terms of g_* and boundary conditions $i_*(0)$ and $i_*'(0)$,

$$i_*(u_*) = i_*(0) + i_*'(0)I(u_*) - Pr\frac{u_\infty^2}{i_\infty}J(u_*) \qquad (16)$$

where

$$I = \int_0^{u_*}\left[\frac{g_*}{g_*(0)}\right]^{Pr-1}du_*$$

$$J = \int_0^{u_*}\left[\frac{g_*}{g_*(0)}\right]^{Pr-1}du_{*_1}\int_0^{u_{*_1}}\left[\frac{g_*}{g_*(0)}\right]^{1-Pr}du_{*_2}$$

This solution can be written in terms of the boundary condition in equation (13b) instead of $i_*'(0)$ by letting $i_* = 1$ at $u_* = 1$ in equation (16) and eliminating $i_*'(0)$ between the resulting equation and equation (16). Thus

$$1 = i_*(0) + i_*'(0)I(1) - Pr\frac{u_\infty^2}{i_\infty}J(1) \tag{16a}$$

from which and equation (16),

$$i_*(u_*) = i_*(0) - \left[i_*(0) - 1\right]\frac{I(u_*)}{I(1)} + Pr\frac{u_\infty^2}{i_\infty}\left[\frac{I(u_*)}{I(1)}J(1) - J(u_*)\right]$$

or

$$i_*(u_*) = \frac{i_w}{i_\infty} - \left(\frac{i_w}{i_\infty} - 1\right)\theta^I(u_*) + \frac{u_\infty^2}{i_\infty}\theta^{II}(u_*) \tag{17}$$

where

$$\theta^I(u_*) = \frac{I(u_*)}{I(1)}$$

$$\theta^{II}(u_*) = Pr\left[\theta^I(u_*)J(1) - J(u_*)\right]$$

The method of successive approximations suggests itself for calculation of the shear function from equations (11) and (17). That is, a first approximation to g_* would yield from equation (17) an i_* which in turn would lead to a new g_* through solution of equation (11), upon satisfaction, of course, of the boundary conditions in equation (13). The new g_* could then be used to compute another i_* which would give another g_*, and so on.

After extensive calculations Crocco observed, however, that the enthalpy distribution $i_*(u_*)$ was practically independent of the law of variation of $\rho_*\mu_*$ with enthalpy, that is, essentially independent of the law of variation of viscosity with temperature. This can be deduced upon inspection of the expressions for I and J in which g_* and $g_*(0)$ appear as a ratio. It is apparent that although a change in the viscosity-temperature law would affect the absolute value of g_* in equation (11), nevertheless such a change could hardly affect the value of $g_*/g_*(0)$, because $g_*(0)$ would be affected in much the same

way as g_* because of the variation in viscosity law. Furthermore, for Prandtl numbers near unity, the effect of viscosity-law variation on enthalpy distribution would be even less. In his numerical proof of this important observation, Crocco used values of ω from 1/2 to $1\frac{1}{4}$ and values of θ from 0 to 3 when $i_* = T_*$ in equations (14) and (15).

As a result of the above observation, one concludes that it is not necessary to carry through a lengthy iteration process between equations (11) and (17). Rather, the enthalpy distribution can be immediately computed using the shear function corresponding to any viscosity law. The final shear function is then obtained as the solution of equation (11) by using an exact viscosity-temperature law. This simplification of solution of the simultaneous equations (11) and (17) is the crux of the Crocco method of laminar-boundary-layer analysis.

The shear function which may be readily used to compute the enthalpy distribution is that corresponding to the viscosity law such that $\rho_*\mu_* = 1$. (Since $\rho_* = T_*^{-1}$, it is then necessary that $\mu_* = T_*$, whence $\omega = 1$ in equations (14).) Therefore, equation (11) reduces to the Blasius equation which has already been solved exactly.

Table I gives the Blasius solution of equation (11) when $\rho_*\mu_* = 1$. Table II gives the values of I and J based upon the Blasius solution; table III gives the values of θ^I and θ^{II}.

It may be well to interject here that the special case $\rho_*\mu_* = 1$ represents a gas or state of a gas for which there is no effect of compressibility on skin friction for thin laminar boundary layers, although the temperature of the fluid rises because of dissipation of the kinetic energy, and properties of the fluid vary accordingly.

Now that the enthalpy distribution has been calculated, attention will be directed toward the details of solution of equation (11). Writing equation (11) in integral form, taking into consideration the boundary conditions (13), one obtains the integral equation

$$g_*(u_*) = \int_{u_*}^{1} du_{*_1} \int_{0}^{u_{*_1}} \frac{2u_*\rho_*\mu_*}{g_*(u_*)}\, du_{*_2} \tag{18}$$

in which $\rho_*\mu_*$ is a known function of u_* depending upon the viscosity law assumed. The method of successive approximations will again be utilized. However, as Crocco pointed out, the direct method of

substitution, integration, resubstitution, and reintegration does not converge upon a single solution but yields values of g_* which oscillate about the exact value. For, if an initial value of the shear function g_{*_1} equal to Ag_{*_e}, in which A is a constant and g_{*_e} is the exact value, is substituted into the right-hand side of equation (18), the new g_{*_2} obtained upon integration will be equal to g_{*_e}/A, resubstitution of which will yield $g_{*_3} = Ag_{*_e} = g_{*_1}$. Therefore, it is seen that the next substitution should be $\sqrt{g_{*_1} g_{*_2}} = g_{*_e}$. In the iterative process of solving equation (11) (equation (18)), it then follows that successive values g_* for resubstitution into equation (18) should be the geometric mean of the two previous substitutions. Although an exact viscosity-temperature relation is now used in equation (18), the iterative process may be started with the Blasius solution (table I) which corresponds to a linear viscosity-temperature law.

It is next observed that a singularity exists at $u_* = 1$ owing to the boundary condition (13b) that $g_* = 0$ at that point. Therefore, integration is carried out only to an upper value of $u_* = 1 - h$, where h is an arbitrarily small value greater than zero. Equation (18) becomes then

$$g_*(u_*) = g_*(1 - h) + \int_{u_*}^{1-h} du_{*_1} \int_0^{u_{*_1}} \frac{f(u_*)}{g_*(u_*)} du_{*_2} \tag{19}$$

where $f(u_*) = 2u_*\rho_*\mu_*$. In order to avoid double integration, equation (19) is written in the form

$$g_*(u_*) = g_*(1 - h) + (1 - u_*) \int_0^{u_*} \frac{f(u_*)}{g_*(u_*)} du_* - h \int_0^{1-h} \frac{f(u_*)}{g_*(u_*)} du_* + \int_{u_*}^{1-h} (1 - u_*) \frac{f(u_*)}{g_*(u_*)} du_* \tag{20}$$

Since the first term $g_*(1 - h)$ on the right-hand side of equation (20) is unchanged by successive iteration, it is necessary to derive a method to adjust $g_*(1 - h)$ in each iteration so that the boundary condition $g_*(1) = 0$ is more nearly approached. Hence the problem is now reduced to that of determining an accurate value of $g_*(1 - h)$ which is compatible with the boundary condition $g_*(1) = 0$. A method of estimating $g_*(1 - h)$ is now given.

Following Crocco, one notes that for $u_* \longrightarrow 1$ equation (11) approaches

$$\overline{\overline{g_*}}\,\overline{\overline{g_*}}'' + 2 = 0 \tag{21}$$

which can be integrated in closed form. The double bar is used to designate the solution of this approximate equation. The first integral of equation (21) yields

$$\overline{\overline{g_*}}' = -2\sqrt{\log_e(B/\overline{\overline{g_*}})} \tag{22}$$

where B is an arbitrary constant and the minus sign is chosen because of the sense of $\overline{\overline{g_*}}'$. Further integration gives

$$1 - u_* = -\frac{1}{2}\int_0^{\overline{\overline{g_*}}} \frac{d\overline{\overline{g_*}}}{\sqrt{\log_e(B/\overline{\overline{g_*}})}} \tag{23}$$

in which the boundary condition $g_*(1) = 0$ is satisfied. Upon substitution of $\log_e(B/\overline{\overline{g_*}}) = t^2$, this equation can be expressed in terms of the tabulated error function $\phi(x) = \frac{2}{\sqrt{\pi}}\int_0^x e^{-t^2}\,dt$, thus

$$1 - u_* = \frac{1}{2}B\sqrt{\pi}\left\{1 - \phi\left[\sqrt{\log_e(B/\overline{\overline{g_*}})}\right]\right\} \tag{24}$$

The constant B can be eliminated between equations (22) and (24). Hence

$$(1 - u_*)/\overline{\overline{g_*}} = \frac{\sqrt{\pi}}{2}e^{(\overline{\overline{g_*}}'/2)^2}\left[1 - \phi(-\overline{\overline{g_*}}'/2)\right] \tag{25}$$

from which $\overline{\overline{g_*}}(1 - h)$ can be calculated, given $h = 1 - u_*$ and the slope $\overline{\overline{g_*}}'(1 - h)$. Since the slopes of g_* and $\overline{\overline{g_*}}$ are to match at $u_* = 1 - h$, one puts

$$\overline{\overline{g_*}}'(1 - h) = g_*'(1 - h) \tag{26}$$

which is computed from the first integral of equation (11), namely,

$$g_*'(1 - h) = -\int_0^{1-h} \frac{f(u_*)}{g_*(u_*)}\, du_* \tag{27}$$

The ratio $h/\overline{\overline{g_*}}(1 - h)$ is plotted against $\overline{\overline{g_*}}'(1 - h)$ in figure 2. Crocco noticed that the combination $\frac{1}{|\overline{\overline{g_*}}'(1 - h)|}\left[\frac{\overline{\overline{g_*}}(1 - h)}{h} - 1\right]$ can be represented by the straight line $0.7828 + 0.0178\,|\overline{\overline{g_*}}'(1 - h)|$ over the practical range of $\overline{\overline{g_*}}'(1 - h)$ between -2.2 and -4 (fig. 2).

Now the error between $\overline{\overline{g_*}}(1 - h)$ and $g_*(1 - h)$ will depend upon the smallness of the h, that is, upon how well the approximate equation (21) represents the exact equation (11). As Crocco points out, i_*, and therefore $\rho_*\mu_*$, varies rapidly for $Pr < 1$ when u_* approaches unity (cf. tables II and III and equation (17)); hence it may be necessary to apply a correction so that

$$g_*(1 - h) = \overline{\overline{g_*}}(1 - h) + \delta g_* \tag{28}$$

Rewriting equation (18) in the form

$$g_*(u_*) = (1 - u_*)\int_0^{u_*} \frac{f(u_*)}{g_*(u_*)}\, du_* + \int_{u_*}^{1} (1 - u_*)\,\frac{f(u_*)}{g_*(u_*)}\, du_* \tag{29}$$

and combining with the integral of equation (11), namely,

$$g_*'(u_*) = -\int_0^{u_*} \frac{f(u_*)}{g_*(u_*)}\, du_* = g_*'(1 - h) - \int_{1-h}^{u_*} \frac{f(u_*)}{g_*(u_*)}\, du_* \tag{30}$$

there is obtained

$$g_*(u_*) = -(1 - u_*)g_*'(1 - h) + (1 - u_*)\int_{1-h}^{u_*} \frac{f(u_*)}{g_*(u_*)}\,du_* +$$

$$\int_{u_*}^{1} (1 - u_*)\,\frac{f(u_*)}{g_*(u_*)}\,du_* \tag{31}$$

Similarly from equation (21) one obtains

$$\overline{\overline{g_*}}(u_*) = -(1 - u_*)\overline{\overline{g_*}}'(1 - h) + (1 - u_*)\int_{1-h}^{u_*} \frac{2}{\overline{\overline{g_*}}(u_*)}\,du_* +$$

$$\int_{u_*}^{1} (1 - u_*)\,\frac{2}{\overline{\overline{g_*}}(u_*)}\,du_* \tag{32}$$

Subtraction of this equation from the preceding one gives

$$\delta g_*(u_*) = (1 - u_*)\int_{1-h}^{u_*} \left(\frac{f}{g_*} - \frac{2}{\overline{\overline{g_*}}}\right)du_* + \int_{u_*}^{1} (1 - u_*)\left(\frac{f}{g_*} - \frac{2}{\overline{\overline{g_*}}}\right)du_* \tag{33}$$

which can be solved in principle by iteration since f is a known function of u_*. That is, starting with an assumed g_{*_1}, $\overline{\overline{g_*}}_1$ is available from equation (25), whence $\delta g_{*_2}(u_*)$ is computed, whence $g_{*_2}(u_*) = \overline{\overline{g_*}}_2(u_*) + \delta g_{*_2}(u_*)$, and so forth.

However, the above iterative process can be rearranged as follows: Write equation (33) thus

$$\delta g_*(u_*) = (1 - u_*)\int_{1-h}^{u_*} \left(\frac{f}{g_*} - \frac{f}{\overline{\overline{g_*}}} - \frac{2}{\overline{\overline{g_*}}} + \frac{f}{\overline{\overline{g_*}}}\right)du_* +$$

$$\int_{u_*}^{1} (1 - u_*)\left(\frac{f}{g_*} - \frac{f}{\overline{\overline{g_*}}} - \frac{2}{\overline{\overline{g_*}}} + \frac{f}{\overline{\overline{g_*}}}\right)du_* \tag{34}$$

$$\delta g_*(u_*) = (1 - u_*) \int_{1-h}^{u_*} \frac{f - 2}{\overline{\overline{g_*}}}\, du_* + \int_{u_*}^{1} (1 - u_*) \frac{f - 2}{\overline{\overline{g_*}}}\, du_* +$$

$$(1 - u_*) \int_{1-h}^{u_*} \left(\frac{1}{g_*} - \frac{1}{\overline{\overline{g_*}}}\right) f\, du_* + \int_{u_*}^{1} (1 - u_*) \left(\frac{1}{g_*} - \frac{1}{\overline{\overline{g_*}}}\right) f\, du_* \tag{35}$$

The term $\frac{1}{g_*} - \frac{1}{\overline{\overline{g_*}}}$ can now be expanded in the form

$$\frac{1}{g_*} - \frac{1}{\overline{\overline{g_*}}} = -\frac{\delta g_*}{\overline{\overline{g_*}}^2} + \frac{\delta g_*^2}{\overline{\overline{g_*}}^3} - \cdots \tag{36}$$

whereupon, when $\frac{\delta g_*^2}{\overline{\overline{g_*}}^3}$ is neglected since $\frac{\delta g_*}{\overline{\overline{g_*}}}$ is small, equation (35) becomes

$$\delta g_*(u_*) = (1 - u_*) \int_{1-h}^{u_*} \frac{f - 2}{\overline{\overline{g_*}}}\, du_* + \int_{u_*}^{1} (1 - u_*) \frac{f - 2}{\overline{\overline{g_*}}}\, du_* -$$

$$(1 - u_*) \int_{1-h}^{u_*} \frac{\delta g_*}{\overline{\overline{g_*}}^2} f\, du_* - \int_{u_*}^{1} (1 - u_*) \frac{\delta g_*}{\overline{\overline{g_*}}^2} f\, du_* \tag{37}$$

If the first approximation to δg_* is obtained by letting $\delta g_* = 0$ on the right-hand side of equation (37), then

$$\delta g_{*_1}(u_*) = (1 - u_*) \int_{1-h}^{u_*} \frac{f - 2}{\overline{\overline{g_*}}}\, du_* + \int_{u_*}^{1} (1 - u_*) \frac{f - 2}{\overline{\overline{g_*}}}\, du_*$$

$$\delta g_{*_2}(u_*) = \delta g_{*_1}(u_*) - (1 - u_*) \int_{1-h}^{u_*} \frac{\delta g_{*_1}}{\overline{\overline{g_*}}^2} f\, du_* - \int_{u_*}^{1} (1 - u_*) \frac{\delta g_{*_1}}{\overline{\overline{g_*}}^2} f\, du_*$$

$$\delta g_{*_3}(u_*) = \delta g_{*_1}(u_*) - (1 - u_*) \int_{1-h}^{u_*} \frac{\delta g_{*_2}}{\overline{\overline{g_*}}^2} f \, du_* - \int_{u_*}^{1} (1 - u_*) \frac{\delta g_{*_2}}{\overline{\overline{g_*}}^2} f \, du_*$$

and so forth. Stopping with the third approximation, the value of δg_* at $u_* = 1 - h$ is then

$$\delta g_*(1 - h) = \int_{1-h}^{1} (1 - u_*) \frac{f - 2}{\overline{\overline{g_*}}} du_* - \int_{1-h}^{1} (1 - u_*) \frac{\delta g_{*_2}}{\overline{\overline{g_*}}^2} f \, du_* \qquad (38)$$

Crocco now gives an approximate expression for equation (38) in the form

$$\delta g_*(1 - h) = 2\frac{h^2}{\overline{\overline{g_*}}}\left\{a(i_* - 1)\left[A_0 - A_1\left(\frac{h}{\overline{\overline{g_*}}}\right)^2 + A_2\left(\frac{h}{\overline{\overline{g_*}}}\right)^4 - A_3 a(i_* - 1)\left(\frac{h}{\overline{\overline{g_*}}}\right)^2 + \ldots\right] + b(i_* - 1)^2\left[B_0 - B_1\left(\frac{h}{\overline{\overline{g_*}}}\right)^2 + \ldots\right] + c(i_* - 1)^3\left[C_0 - C_1\left(\frac{h}{\overline{\overline{g_*}}}\right)^2 + \ldots\right] - h^2\left[D_0 - D_1\left(\frac{h}{\overline{\overline{g_*}}}\right)^2 + \ldots\right]\right\} \qquad (39)$$

where

$$a = \frac{1}{2} - \frac{1}{\theta + 1}$$

$$b = -\frac{1}{8} - \frac{a}{\theta + 1}$$

$$c = \frac{1}{16} - \frac{b}{\theta + 1}$$

are the coefficients in a Taylor series expansion of $\rho_*\mu_*$ about the point $i_* = 1$ using the Sutherland law (equation (15)) for

viscosity-temperature variation. The other coefficients in equation (39) are

$$A_o = \frac{1}{3 - (2 - Pr)\eta}$$

$$A_1 = \frac{2}{2 - (2 - Pr)\eta}\left[\frac{1}{1 + 2(1 - \eta)} - \frac{A_o}{5 - (4 - Pr)\eta}\right]$$

$$A_2 = \frac{4}{2 - (2 - Pr)\eta}\left\{\frac{1}{\left[1 + 2(1 - \eta)\right]\left[1 + 4(1 - \eta)\right]} - \frac{A_o}{\left[5 - (4 - Pr)\eta\right]\left[7 - (6 - Pr)\eta\right]}\right\}$$

$$A_3 = \frac{2}{2 - (2 - Pr)\eta}\left[\frac{1}{4 - (3 - Pr)\eta} - \frac{A_o}{6 - (5 - 2Pr)\eta}\right]$$

$$B_o = \frac{1}{4 - (3 - 2Pr)\eta}$$

$$B_1 = \frac{2}{3 - (3 - 2Pr)\eta}\left[\frac{1}{1 + 2(1 - \eta)} - \frac{B_o}{6 - (5 - 2Pr)\eta}\right]$$

$$C_o = \frac{1}{5 - (4 - 3Pr)\eta}$$

$$C_1 = \frac{2}{4 - (4 - 3Pr)\eta}\left[\frac{1}{1 + 2(1 - \eta)} - \frac{B_o}{6 - (5 - 2Pr)\eta}\right]$$

$$D_o = \frac{1}{3 - \eta}$$

$$D_1 = \frac{2}{2 - \eta}\left[\frac{1}{1 + 2(1 - \eta)} - \frac{D_o}{2 + 3(1 - \eta)}\right]$$

where $\eta = -\frac{h}{\overline{\overline{g_*}}}\overline{\overline{g_*}}'$. In equation (39), the values of $\overline{\overline{g_*}}$, $\overline{\overline{g_*}}'$, and i_*

are to be determined at $u_* = 1 - h$. It will be found that the terms included in equation (39) will give sufficient accuracy to $\delta g_*(1 - h)$. In fact, in the calculations carried out in the present report it was found that δg_* was negligible, being of the order of 10^{-4}.

SKIN-FRICTION AND HEAT-TRANSFER COEFFICIENTS

Since $\tau = \frac{g_2(u)}{\sqrt{2x}}$ and $g_* = \sqrt{\frac{2}{\rho_\infty \mu_\infty u_\infty^3}}\, g_2(u)$, it follows that the shear stress τ and the shear function g_* are related by

$$\tau = \frac{1}{2}\rho_\infty u_\infty^2 \frac{g_*}{\sqrt{R_\infty}}$$

where $R_\infty = \frac{\rho_\infty u_\infty x}{\mu_\infty}$, the Reynolds number in terms of the length x from the leading edge to the point in question on the plate. The surface stress is then

$$\tau_w = \frac{1}{2}\rho_\infty u_\infty^2 \frac{g_*(0)}{\sqrt{R_\infty}} \tag{40}$$

In terms of the local skin-friction coefficient c_f defined by

$$\tau_w = c_f \frac{1}{2}\rho_\infty u_\infty^2 \tag{41}$$

there results

$$c_f \sqrt{R_\infty} = g_*(0) \tag{42}$$

Furthermore, in terms of the mean skin-friction coefficient C_f defined by

$$\int_0^x \tau_w \, dx = C_f \frac{1}{2}\rho_\infty u_\infty^2 x \tag{43}$$

there follows

$$C_f \sqrt{R_\infty} = 2g_*(0) \tag{44}$$

Comparison of equations (42) and (44) shows that regardless of Mach number, Reynolds number, or wall-to-free-stream temperature ratio

$$C_f = 2c_f \tag{45}$$

The heat transferred from the wall to the fluid per unit width of plate is given by

$$\begin{aligned} q_w &= -k_w\left(\frac{\partial T}{\partial y}\right)_w \\ &= -\frac{k_w}{c_{p_w}}\left(\frac{di}{du}\right)_w\left(\frac{\partial u}{\partial y}\right)_w \\ &= -\frac{k_w}{c_{p_w}\mu_w}\frac{i_\infty}{u_\infty}\, i_*'(0)\tau_w \\ &= -\frac{i_\infty}{Pr\ u_\infty}\, i_*'(0)\tau_w \end{aligned} \tag{46}$$

From equation (16a) one has

$$i_*'(0) = \frac{1}{I(1)}\left[1 - i_*(0) + Pr\ J(1)\frac{u_\infty^2}{i_\infty}\right]$$

so that equation (46) becomes

$$q_w = -\frac{1}{Pr\ I(1)}\frac{i_\infty}{u_\infty}\tau_w\left[1 + Pr\ J(1)\ \frac{u_\infty^2}{i_\infty} - i_*(0)\right] \tag{47}$$

for variable specific heat, or

$$q_w = -\frac{1}{Pr\ I(1)}\frac{c_p}{u_\infty}\tau_w\left\{T_\infty\left[1 + 2Pr\ J(1)\frac{\gamma - 1}{2}M_\infty^2\right] - T_w\right\} \tag{48}$$

for constant specific heat.

Defining the local heat-transfer coefficient by

$$h = \frac{1}{Pr\ I(1)} \frac{c_{p_\infty} \tau_w}{u_\infty} \tag{49}$$

and the Stanton number by $C_H = h \Big/ \left(c_{p_\infty} \rho_\infty u_\infty\right)$, there follows, utilizing equation (41), that

$$C_H = \frac{1}{Pr\ I(1)} \frac{c_f}{2} \tag{50}$$

It is now interesting to observe from table II, that, closely,

$$Pr\ I(1) \approx Pr^{2/3}$$

and

$$2Pr\ J(1) \approx Pr^{1/2}$$

so that practically

$$C_H = \frac{1}{Pr^{2/3}} \frac{c_f}{2} \tag{51}$$

and

$$q_w = -C_H \rho_\infty u_\infty \left[\left(i_\infty + Pr^{1/2} \frac{u_\infty^2}{2} \right) - i_w \right] \tag{52}$$

when the specific heat is variable, or

$$q_w = -C_H c_p \rho_\infty u_\infty \left[T_\infty \left(1 + Pr^{1/2} \frac{\gamma - 1}{2} M_\infty^2 \right) - T_w \right] \tag{53}$$

when the specific heat is constant. (Specifically, for $Pr = 0.75$, $Pr\ I(1) = 0.8302$ and $Pr^{2/3} = 0.8258$; $2Pr\ J(1) = 0.8654$ and $Pr^{1/2} = 0.8660$.)

Suppose now there is no heat transfer into or out of the boundary layer (insulated wall). Then $q_w = 0$ and

$$i_w = i_\infty + Pr^{1/2} \frac{u_\infty^2}{2} \qquad \text{(variable } c_p\text{)} \tag{54}$$

or

$$T_w = T_\infty\left(1 + Pr^{1/2} \frac{\gamma - 1}{2} M_\infty^2\right) \qquad \text{(constant } c_p\text{)} \tag{55}$$

which is the wall temperature due to viscous action alone. However, the "recovery factor" is defined by

$$r = \frac{i_w - i_\infty}{u_\infty^2/2} \tag{56}$$

Hence, it follows upon comparison of equations (54) and (56) that, closely,

$$\text{Recovery factor} = r = Pr^{1/2} \tag{57}$$

for laminar boundary layers.

In the determination of the friction and heat transfer at the plate, it was not necessary to know the internal geometric distribution of properties of the boundary layer. However, if the geometric distribution of properties, such as velocity and temperature in a stability analysis, are desired, then a suitable distance parameter is

$$y_* = \frac{y}{x}\sqrt{R_\infty} = 2\int_0^{u_*} \frac{\mu_*\, du_*}{g_*} \tag{58}$$

since $\tau = \mu \frac{\partial u}{\partial y}$.

RESULTS OF CALCULATIONS

Calculations of the skin-friction and heat-transfer coefficients for laminar boundary layers on flat plates have been carried out for Mach numbers up to 20 and wall-to-free-stream temperature ratios of 1/4 to 6. Although the results for the higher Mach numbers are academic because of the assumptions made concerning the variation of properties

of the gas at high temperatures, these calculations were performed in order to indicate trends and compare with more accurate results. The Prandtl number was taken at 0.75, the specific heat was held constant, and the Sutherland law for viscosity-temperature variation was assumed to represent the viscosity data starting with an initial ambient temperature of -67.6° F. The ratio of specific heats was taken at 1.400.

The calculation procedure was as follows: The enthalpy distribution was calculated using the Blasius distribution of the dimensionless shear function as given in table I; that is, values of θ^{I} and θ^{II} from table III were used in equation (17). The final shear distribution was computed by integration of equation (11) by the method of successive approximations from $u_* = 0$ to $u_* = 0.98$ starting with the Blasius solution in table I. In the iterative process, the value of the shear function at $u_* = 0.98$ was obtained from the solution of equation (21) (fig. 2). The required accuracy on $g_*(u_*)$ was within 0.0025, hence within 0.5 percent for friction and heat transfer at the plate over the variation of wall-to-free-stream temperature ratios chosen herein. It was unnecessary to apply the correction δg_* of equation (28) because δg_* was always found to be very small (of the order of 10^{-4}). A worksheet for carrying out an iteration for g_* is given in the appendix.

In figure 3 is plotted the mean skin-friction coefficient as function of free-stream Reynolds number, free-stream Mach number, and wall-to-free-stream temperature ratio. Figure 4 gives the local heat-transfer coefficient as function of the same dimensionless variables. In figure 5 are compared results obtained using the Sutherland and power viscosity laws. Figure 6 shows the variation of the thickness of the laminar layer as a function of the above independent variables; the thickness was arbitrarily taken at the velocity ratio $u_* = 0.995$ obtained by estimating the g_* distribution to that point.

Figures 7 to 12 show the dimensionless shear-function distribution for various Mach numbers and temperature ratios including the insulated-plate case. Figures 13 to 15 give the variations of the velocity ratio u_*, the temperature ratio T/T_∞, and the Mach number ratio M/M_∞ as functions of free-stream Mach number M_∞ and distance parameter $\frac{y}{x}\sqrt{R_\infty}$ in the case of the insulated plate; figures 16 to 30 show the same dependent variables as functions of the same independent variables in the case of wall-to-free-stream temperature ratios 1/4, 1, 2, 4, and 6. Figures 31 to 47 show the same dependent variables as above but as lines of constant temperature ratio instead of as lines of constant free-stream Mach number, the distance parameter now being the relative distance y/δ. For purpose of comparison with figures 13 to 15 the internal characteristics of the boundary layer are plotted in figures 48 to 50 for $Pr = 1$.

Figure 51 shows the variation across the boundary layer of the ratio of the total enthalpy per unit mass $\left(E = i + \frac{u^2}{2}\right)$ at any point to that of the free stream for an insulated plate. For $Pr = 1$ the ratio would be constant at unity. The fact that Pr is less than unity in these calculations brings about the transfer of the energy from the inner to the outer layers of the boundary layer; this is due to the readjustment of the relative effects of viscosity, heat capacity, and heat conductivity in favor of the heat conductivity.

Aerophysics Laboratory
North American Aviation, Inc.
Downey, Calif., January 9, 1951

APPENDIX A

WORK SHEET FOR CARRYING OUT AN ITERATION FOR g_*

The following headings and equations are used in carrying out an iteration for g_*:

1	2	3	4	5	6	7	8	9	10
u_*	θ^I (table III)	θ^{II} (table III)	$i_*(0) = \frac{i_w}{i_\infty}$	$\frac{u_\infty^2}{i_\infty}$	$i_*(u_*)$ (equation (17))	$\mu_*(u_*)$ (equation (15) and gas tables)	$\rho_*\mu_*$ (columns 6 and 7 and gas tables)	$2\rho_*\mu_*u_* = f(u_*)$	$g_{*_1}(u_*)$ (assumed)

$$i_*(u_*) = \frac{i_w}{i_\infty} - \left(\frac{i_w}{i_\infty} - 1\right)\theta^I(u_*) + \frac{u_\infty^2}{i_\infty}\,\theta^{II}(u_*) \qquad \text{(column 6)}$$

$$\mu_*(u_*) = T_*^{1/2}\,\frac{1.505}{1 + \frac{0.505}{T_*}} \qquad \text{(column 7)}$$

$$\rho_* = \frac{1}{T_*}$$

With constant specific heat, $\frac{u_\infty^2}{i_\infty} = (\gamma - 1)M_\infty^2$ and $i_* = T_*$ for $i_\infty = c_pT_\infty$.

11	12	13	14	15	16	17	18	19	20
$\frac{f(u_*)}{g_{*_1}(u_*)}$	$\int_0^{u_*} \frac{f}{g_{*_1}}\,du_*$	D (see below)	E (see below)	D - E	$(1 - u_*)\,\frac{f}{g_{*_1}}$	F (see below)	$g_*(1 - h)$	$g_{*_2}(u_*)$ (equation (20))	$g_{*_3} = \sqrt{g_{*_1}g_{*_2}}$

$$D = (1 - u_*)\int_0^{u_*} \frac{f(u_*)}{g_{*_1}(u_*)}\,du_*$$

$$E = h\int_0^{1-h} \frac{f(u_*)}{g_{*_1}(u_*)}\,du_*$$

$$F = \int_{u_*}^{1-h} (1 - u_*)\,\frac{f(u_*)}{g_{*_1}(u_*)}\,du_*$$

$$g_{*_2}(u_*) = g_*(1 - h) + D - E + F$$

$$g_*(1 - h) = \overline{g_*}(1 - h) + \delta g_* \qquad (\delta g_* \text{ is negligible in present calculations})$$

$$\frac{1}{\left|\overline{g_*}'(1 - h)\right|}\left[\frac{\overline{g_*}(1 - h)}{h} - 1\right] = 0.7828 + 0.0178\left|\overline{g_*}'(1 - h)\right|$$

$$\overline{g_*}'(1 - h) = g_*'(1 - h) = -\int_0^{1-h} \frac{f}{g_*}\,du_*$$

REFERENCES

1. Crocco, Luigi: Lo Strato Limite Laminare nei Gas. Monografie Scientifiche di Aeronautica No. 3, Ministero della Difesa-Aeronautica, Roma, Dec. 1946. (Trans. in North American Aviation Aerophysics Lab., Rep. AL-684, July 15, 1948.)

2. Crocco, Luigi: Sulla transmissione del calore da una lamina piana a un fluido scorrente ad alta velocita. L'Aerotechnica, vol. XII, fasc. 2, Feb. 1932, pp. 181-197. (Available in translation as NACA TM 690, 1932.)

3. Blasius, H.: Grenzschichten in Flüssigkeiten mit kleiner Reibung. Zeitschr. Math. und Phys., Bd. 56, Heft 1, 1908, pp. 1-37. (Available in translation as NACA TM 1256, 1950.)

4. Tribus, Myron, and Boelter, L. M. K.: An Investigation of Aircraft Heaters. II - Properties of Gases. NACA ARR, Oct. 1942.

TABLE I

Shear Function g_* When $\rho_*\mu_* = 1$

u_*	g_*	u_*	g_*	u_*	g_*
0	0.66411	0.45	0.61772	0.875	0.27994
.05	.66405	.50	.60013	.900	.23881
.10	.66361	.55	.57836	.925	.19293
.15	.66242	.60	.55183	.95	.14097
.20	.66009	.65	.51985	.96	.11797
.25	.65625	.70	.48161	.97	.09334
.30	.65050	.75	.43607	.98	.06659
.35	.64245	.80	.38189	.99	.03681
.40	.63167	.85	.31715	1.00	0

TABLE II

VALUES OF I AND J BASED UPON BLASIUS SOLUTION FOR g_*

u_*	Pr = 0.5		Pr = 0.725		Pr = 0.75		Pr = 1.00		Pr = 1.25		Pr = 1.50		Pr = 2.00	
	I	J	I	J	I	J	I	J	I	J	I	J	I	J
0	0	0	0	0	0	0	0	0	0	0	0	0	0	0
.1	.1000	.0050	.1000	.0050	.1000	.0050	.1000	.0050	.1000	.0050	.1000	.0050	.1000	.0050
.2	.2002	.0200	.2001	.0200	.2001	.0200	.2000	.0200	.1999	.0200	.1998	.0200	.1997	.0200
.3	.3008	.0452	.3004	.0451	.3004	.0451	.3000	.0450	.2996	.0449	.2992	.0448	.2985	.0447
.4	.4025	.0806	.4014	.0803	.4012	.0803	.4000	.0800	.3988	.0797	.3975	.0794	.3951	.0788
.5	.5062	.1269	.5034	.1260	.5031	.1260	.5000	.1250	.4969	.1240	.4939	.1232	.4881	.1213
.6	.6135	.1849	.6073	.1827	.6066	.1824	.6000	.1800	.5935	.1776	.5872	.1753	.5750	.1708
.7	.7267	.2567	.7144	.2512	.7130	.2507	.7000	.2450	.6875	.2396	.6756	.2342	.6531	.2246
.8	.8505	.3454	.8268	.3337	.8243	.3324	.8000	.3200	.7776	.3086	.7564	.2980	.7186	.2787
.9	.9967	.4612	.9500	.4343	.9451	.4315	.9000	.4050	.8605	.3817	.8251	.3613	.7660	.3276
.92	1.0390	.4899	.9770	.4579	.9715	.4542	.9200	.4232	.8757	.3965	.8367	.3731	.7727	.3353
.94	1.0696	------	1.0056	------	.9991	------	.9400	------	.8901	------	.8472	------	.7780	------
.96	1.1131	.5591	1.0363	.5103	1.0286	.5050	.9600	.4608	.9037	.4245	.8564	.3941	.7824	.3475
.98	1.1671	------	1.0708	------	1.0614	------	.9800	------	.9159	------	.8638	------	.7852	------
.99	------	.6369	------	.5602	------	.5523	.9900	.4901	------	.4429	------	.4060	------	.3527
1.00	1.2806	.7039	1.1210	.5871	1.1070	.5768	1.0000	.5000	.9252	.4473	.8682	.4080	.7863	.3532

TABLE III

VALUES OF θ^{I} AND θ^{II} BASED UPON BLASIUS SOLUTION FOR g_*

u_*	Pr = 0.5		Pr = 0.725		Pr = 0.75		Pr = 1.00		Pr = 1.25		Pr = 1.50		Pr = 2.00	
	θ^{I}	θ^{II}	θ^{I}	θ^{II}	θ^{I}	θ^{II}	θ^{I}	θ^{II}	θ^{I}	θ^{II}	θ^{I}	θ^{II}	θ^{I}	θ^{II}
0	0	0	0	0	0	0	0	0	0	0	0	0	0	0
.1	.0781	.0250	.0892	.0344	.0903	.0353	.1000	.0450	.1081	.0542	.1152	.0630	.1271	.0798
.2	.1562	.0450	.1785	.0615	.1807	.0633	.2000	.0800	.2161	.0958	.2302	.1109	.2539	.1394
.3	.2348	.0601	.2680	.0813	.2713	.0835	.3000	.1050	.3238	.1249	.3446	.1436	.3796	.1788
.4	.3143	.0703	.3580	.0942	.3625	.0966	.4000	.1200	.4310	.1414	.4579	.1611	.5026	.1974
.5	.3953	.0757	.4491	.0998	.4545	.1020	.5000	.1250	.5371	.1452	.5689	.1736	.6206	.1959
.6	.4790	.0761	.5418	.0982	.5480	.1002	.6000	.1200	.6415	.1367	.6763	.1509	.7311	.1749
.7	.5674	.0712	.6373	.0891	.6441	.0906	.7000	.1050	.7431	.1160	.7781	.1250	.8305	.1375
.8	.6641	.0610	.7378	.0720	.7446	.0728	.8000	.0800	.8405	.0842	.8712	.0862	.9139	.0882
.9	.7783	.0431	.8474	.0458	.8538	.0455	.9000	.0450	.9301	.0424	.9503	.0391	.9740	.0328
.92	.8054	.0385	.8715	.0390	.8776	.0390	.9200	.0362	.9465	.0336	.9636	.0301	.9824	.0234
.94	.8352	------	.8970	------	.9026	------	.9400	------	.9621	------	.9757	------	.9894	------
.96	.8692	.0263	.9244	.0235	.9292	.0232	.9600	.0192	.9768	.0155	.9863	.0124	.9948	.0078
.98	.9113	------	.9552	------	.9589	------	.9800	------	.9900	------	.9949	------	.9984	------
.99	.9397	.0123	.9733	.0084	.9760	.0080	.9900	.0050	.9957	.0030	.9981	.0018	.9994	.0006
1.00	1	0	1	0	1	0	1	0	1	0	1	0	1	0

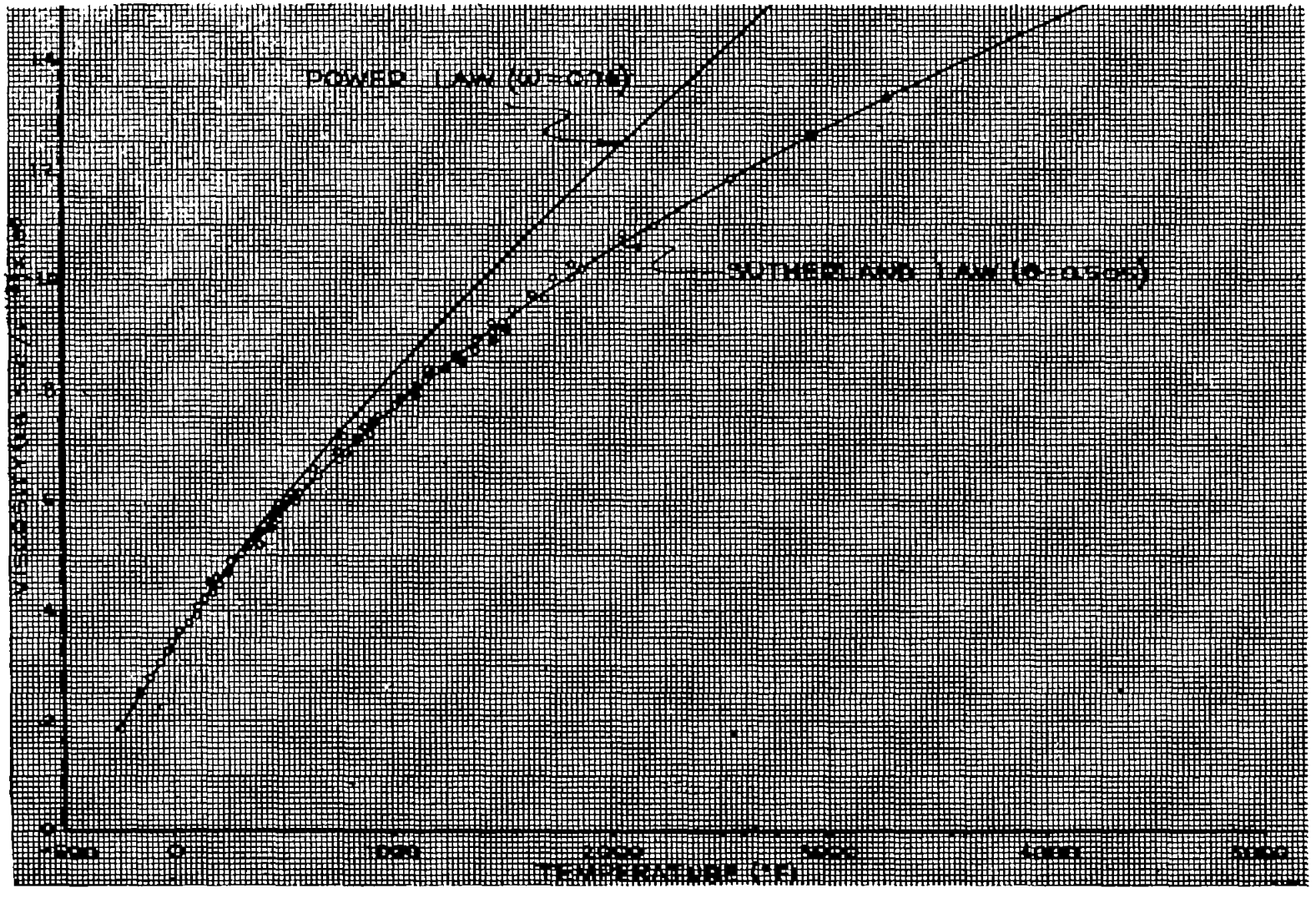

Figure 1.- Viscosity-temperature data.

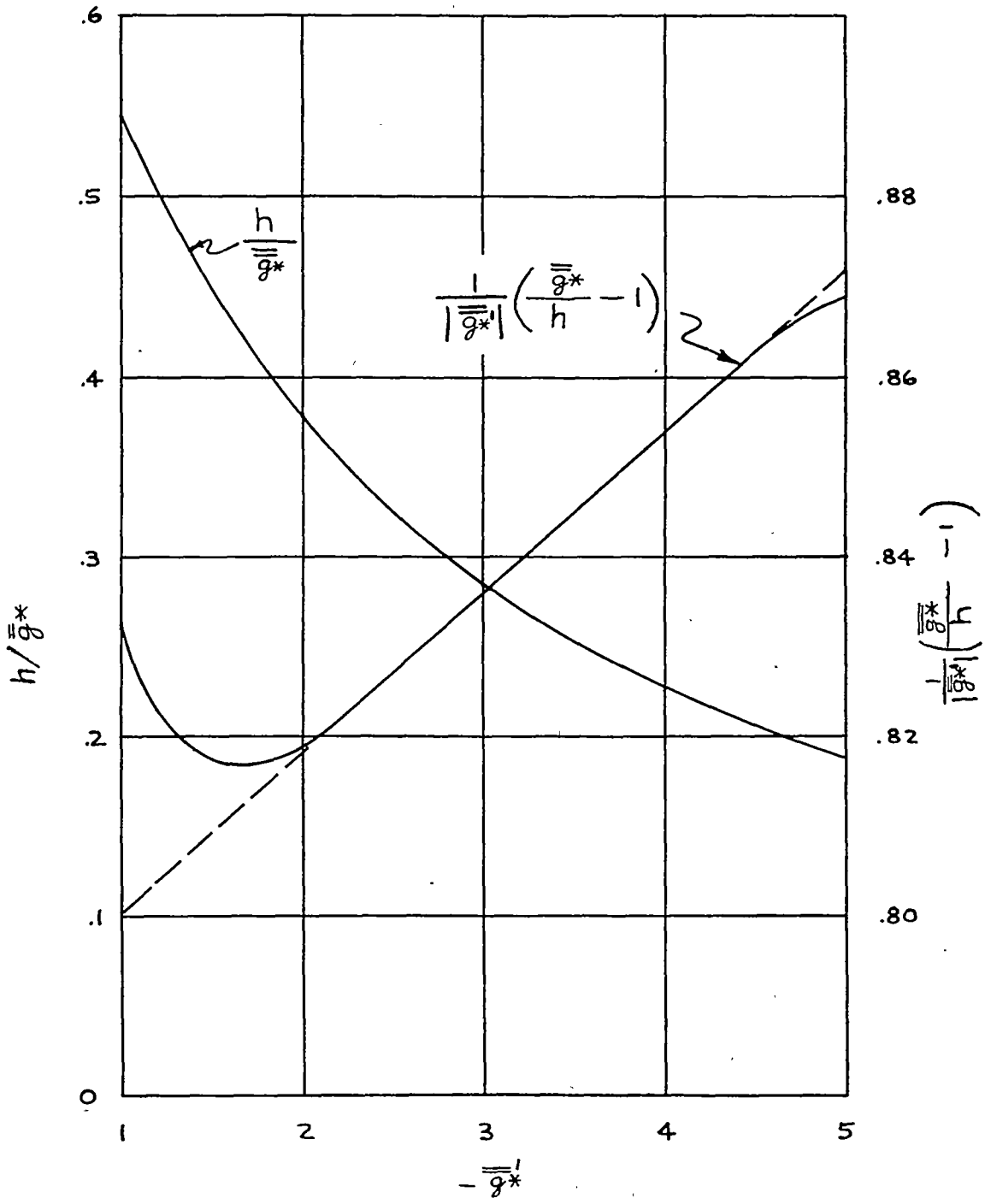

Figure 2.- Shear function $\bar{\bar{g}}_*(1 - h)$ as a function of $\bar{\bar{g}}_*'(1 - h)$.

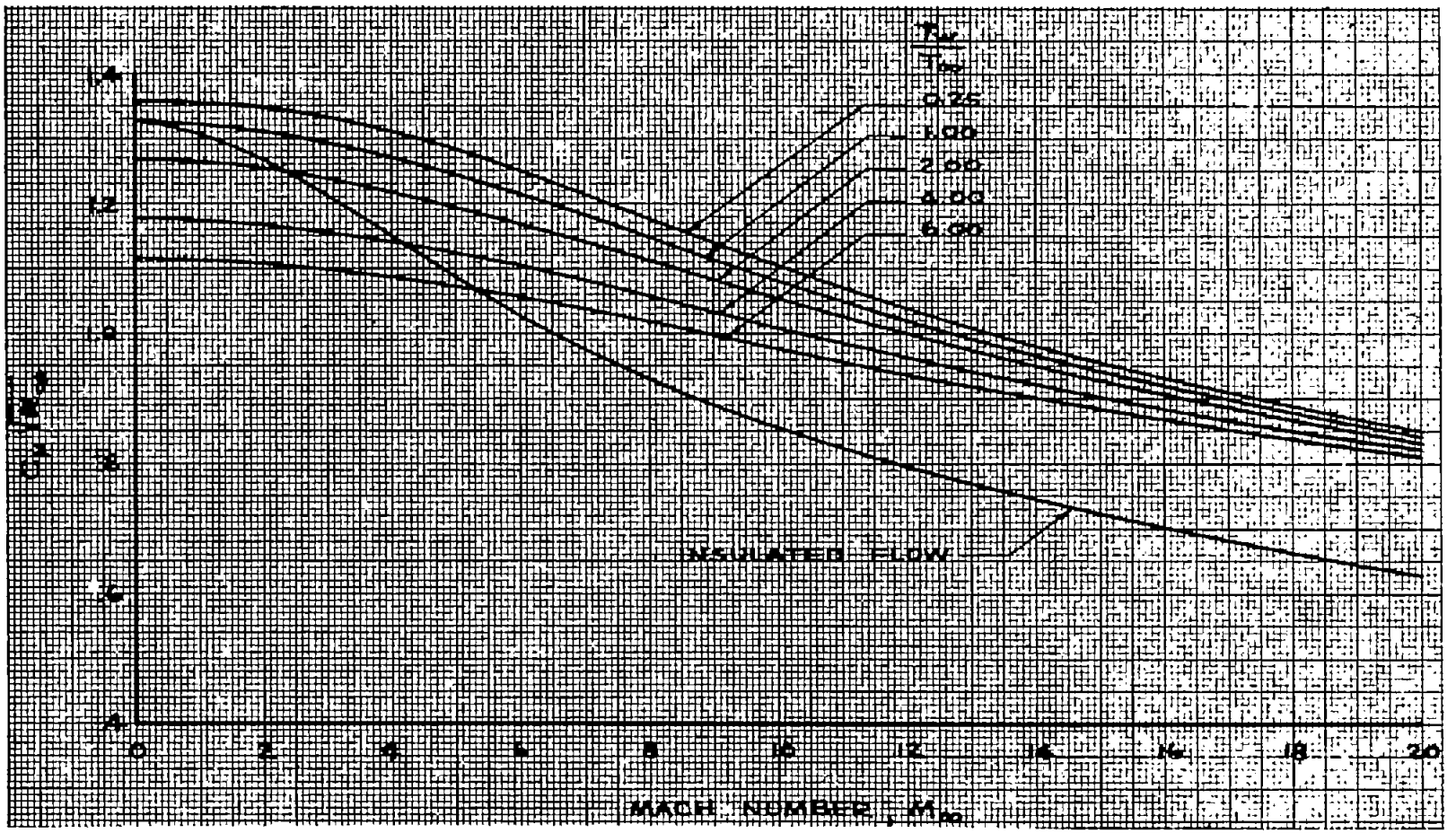

Figure 3.- Mean skin-friction coefficient for laminar boundary layer of a compressible fluid flowing along a flat plate. Prandtl number, 0.75; $\theta = 0.505$.

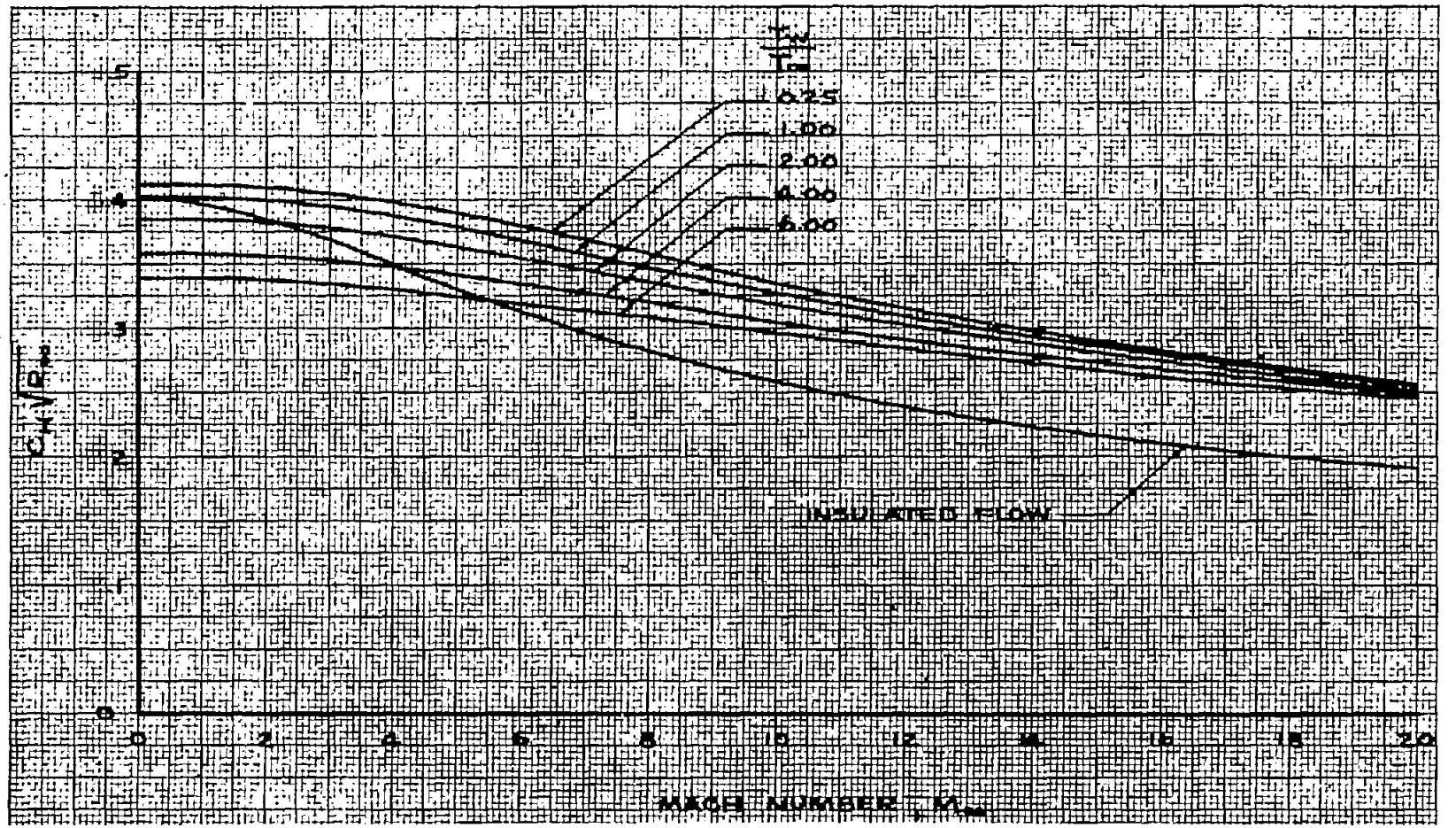

Figure 4.- Local heat-transfer coefficient for laminar boundary layer of a compressible fluid flowing along a flat plate. Prandtl number, 0.75; $\theta = 0.505$.

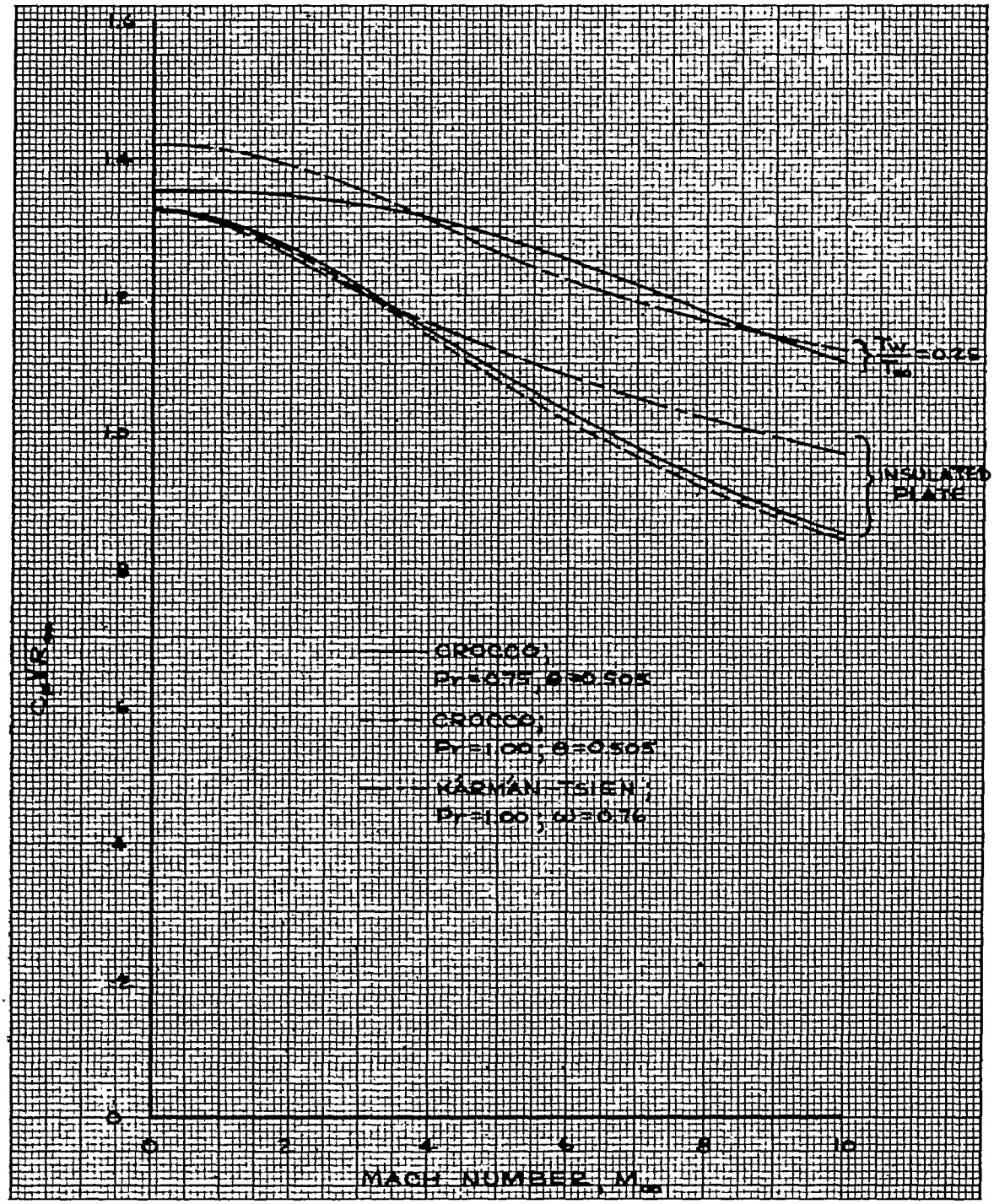

Figure 5.- Comparison of mean skin-friction coefficients using Sutherland and power viscosity laws.

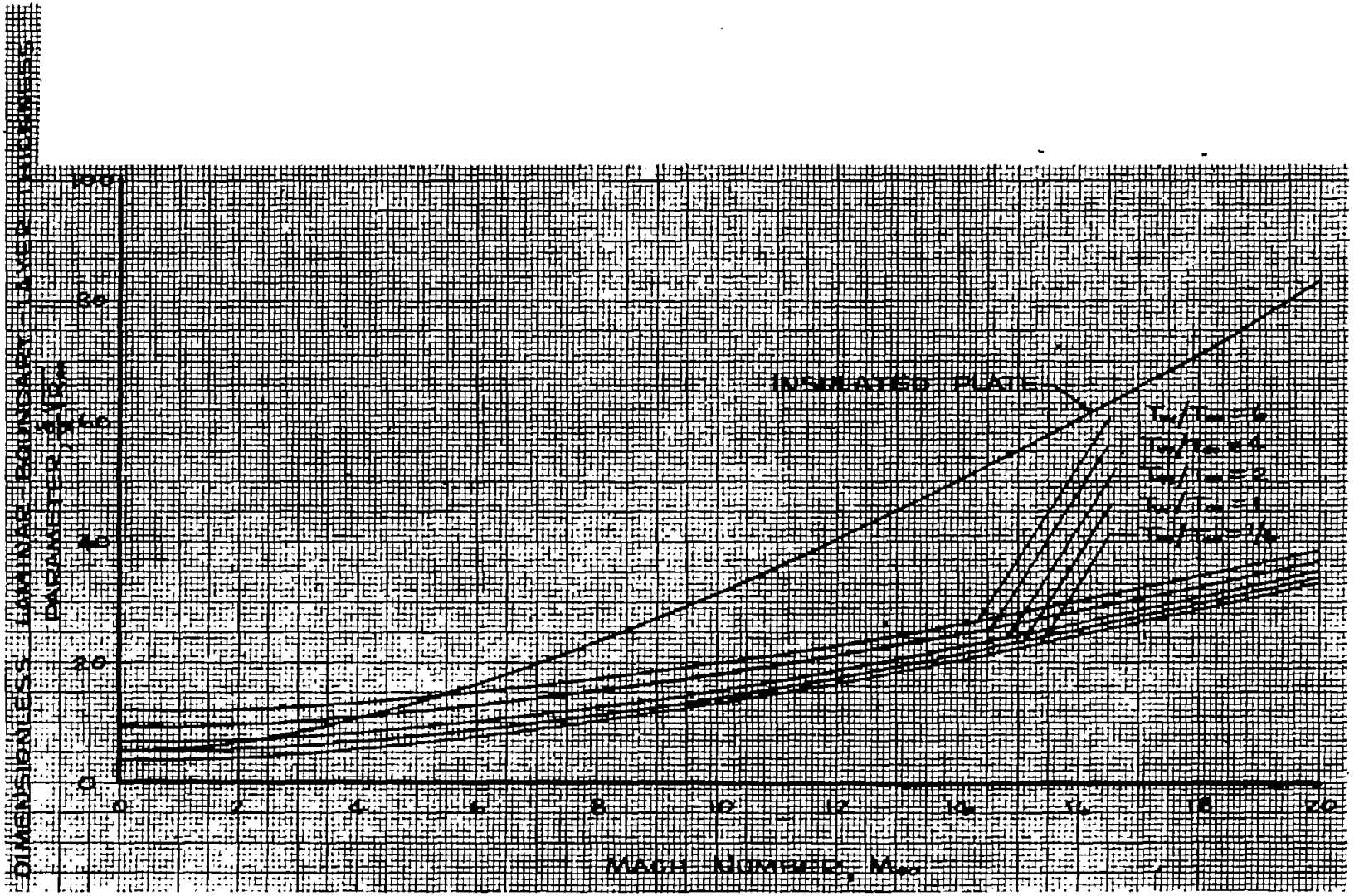

Figure 6.- Thickness of laminar boundary layer of a compressible fluid flowing along a flat plate. Prandtl number, 0.75; $\theta = 0.505$; $y = \delta$ at $u/u_\infty = 0.995$.

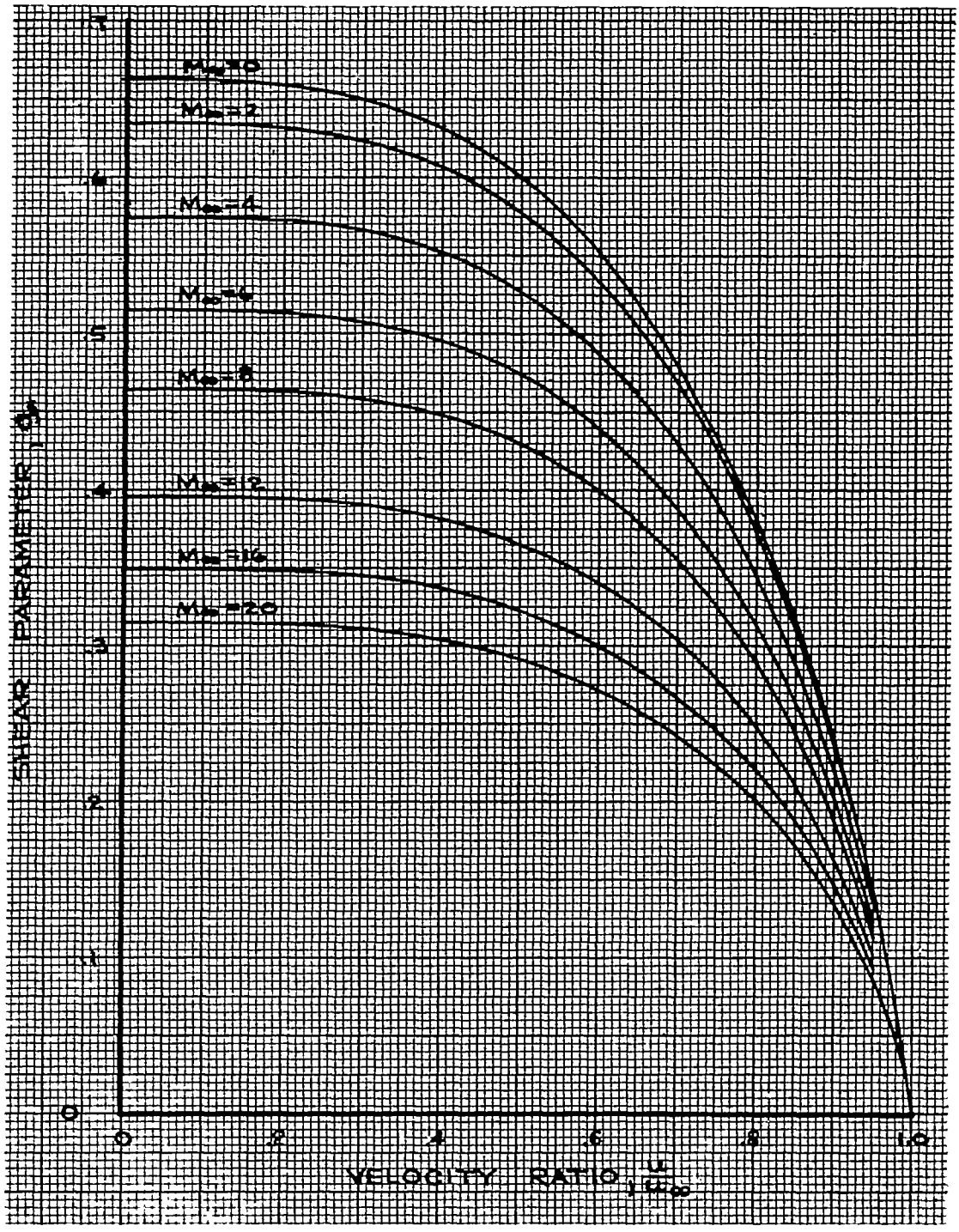

Figure 7.- Shear distribution in laminar boundary layer of a compressible fluid flowing along an insulated flat plate at various free-stream Mach numbers. Prandtl number, 0.75; $\theta = 0.505$.

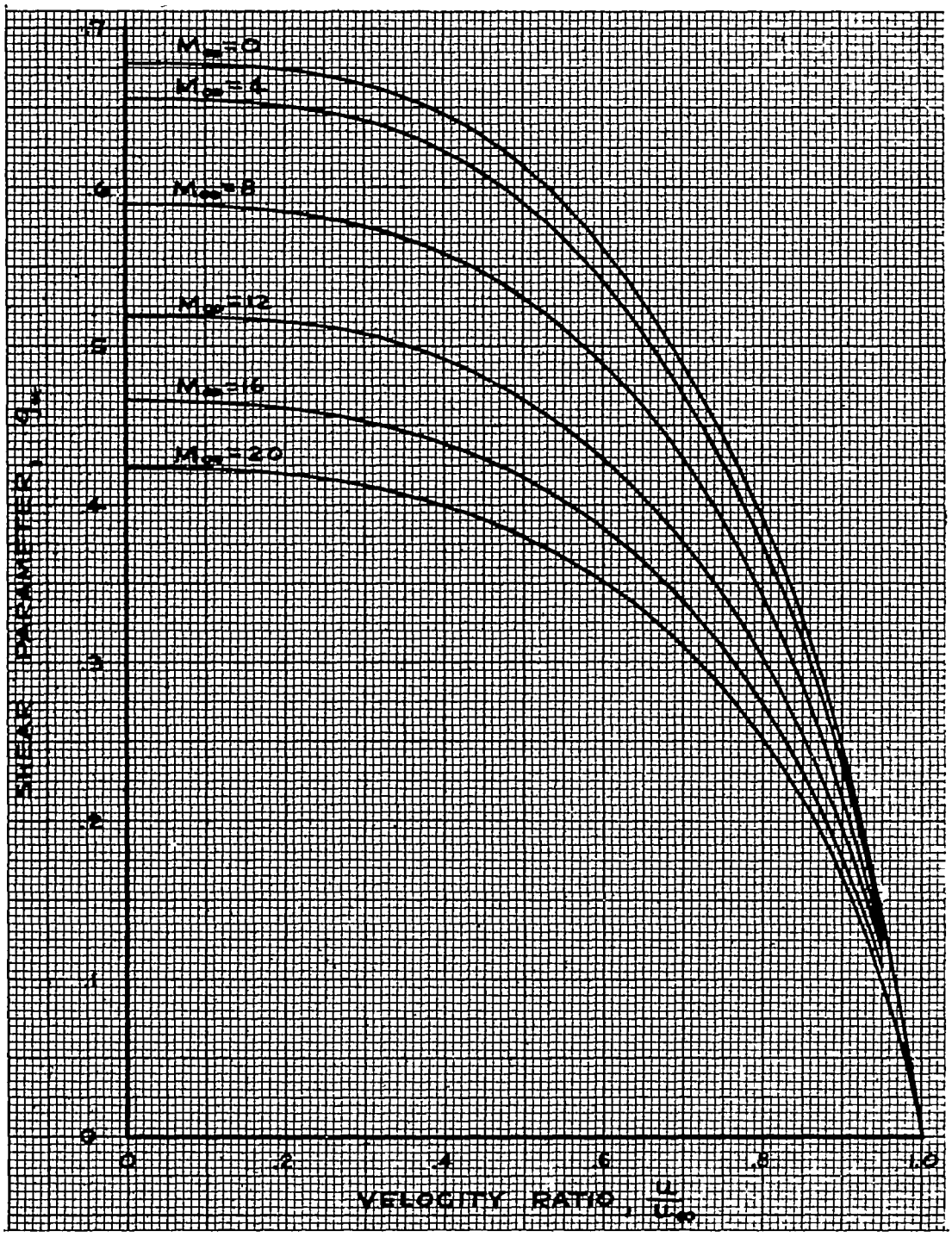

Figure 8.- Shear distribution in laminar boundary layer for wall-to-free-stream temperature ratio of 1/4 and various free-stream Mach numbers. Prandtl number, 0.75; $\theta = 0.505$.

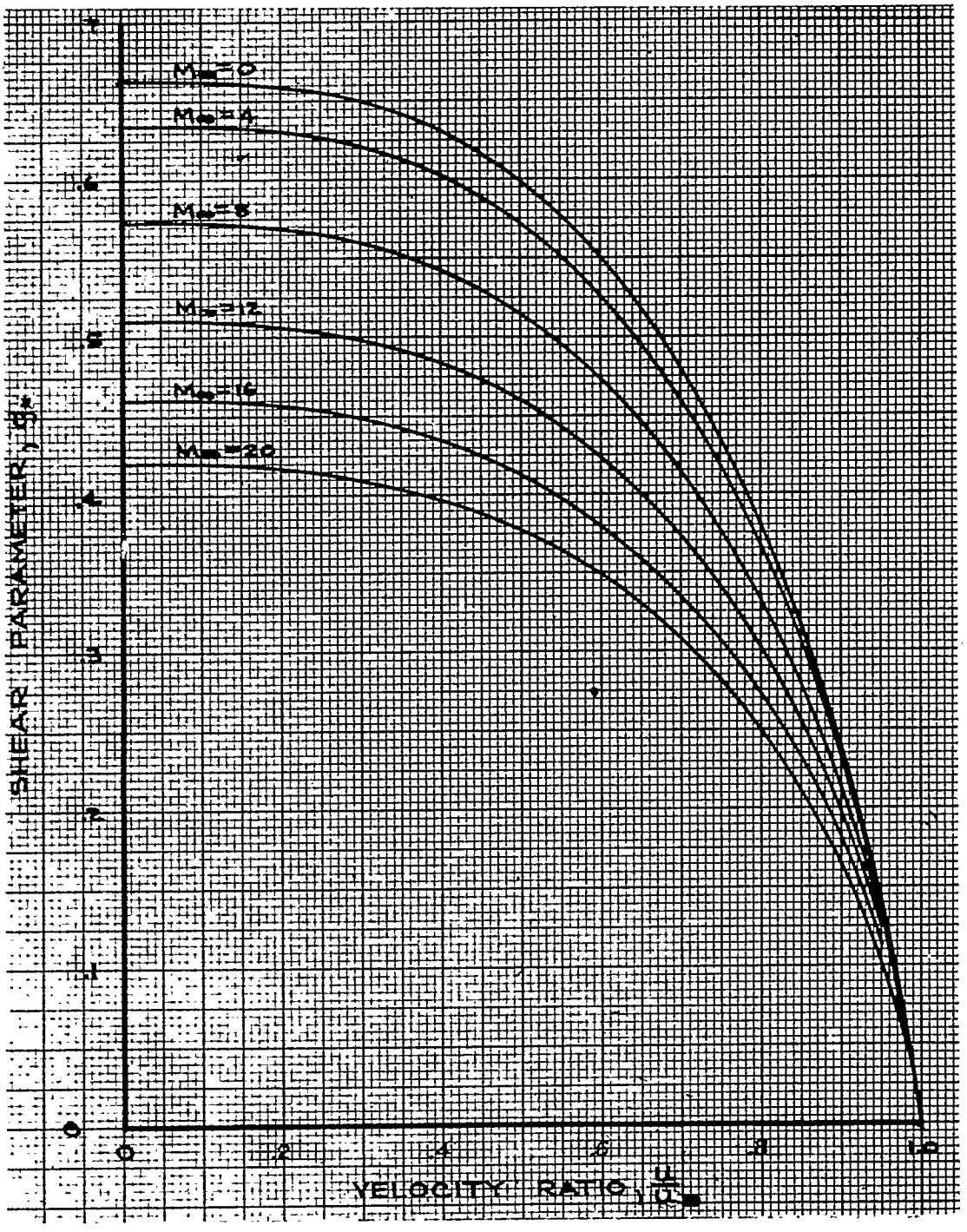

Figure 9.- Shear distribution in laminar boundary layer for wall-to-free-stream temperature ratio of 1 and various free-stream Mach numbers. Prandtl number, 0.75; $\theta = 0.505$.

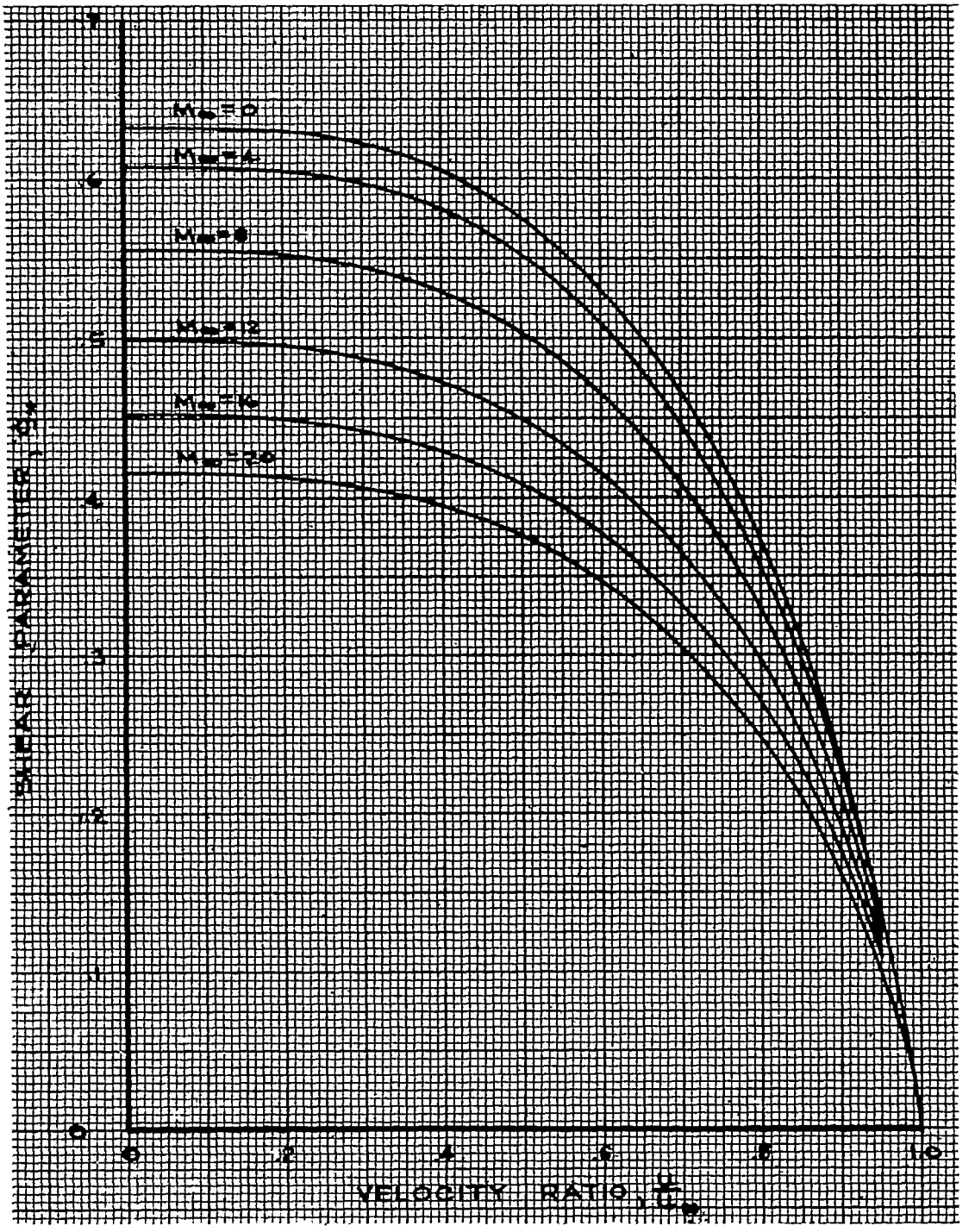

Figure 10.- Shear distribution in laminar boundary layer for wall-to-free-stream temperature ratio of 2 and various free-stream Mach numbers. Prandtl number, 0.75; $\theta = 0.505$.

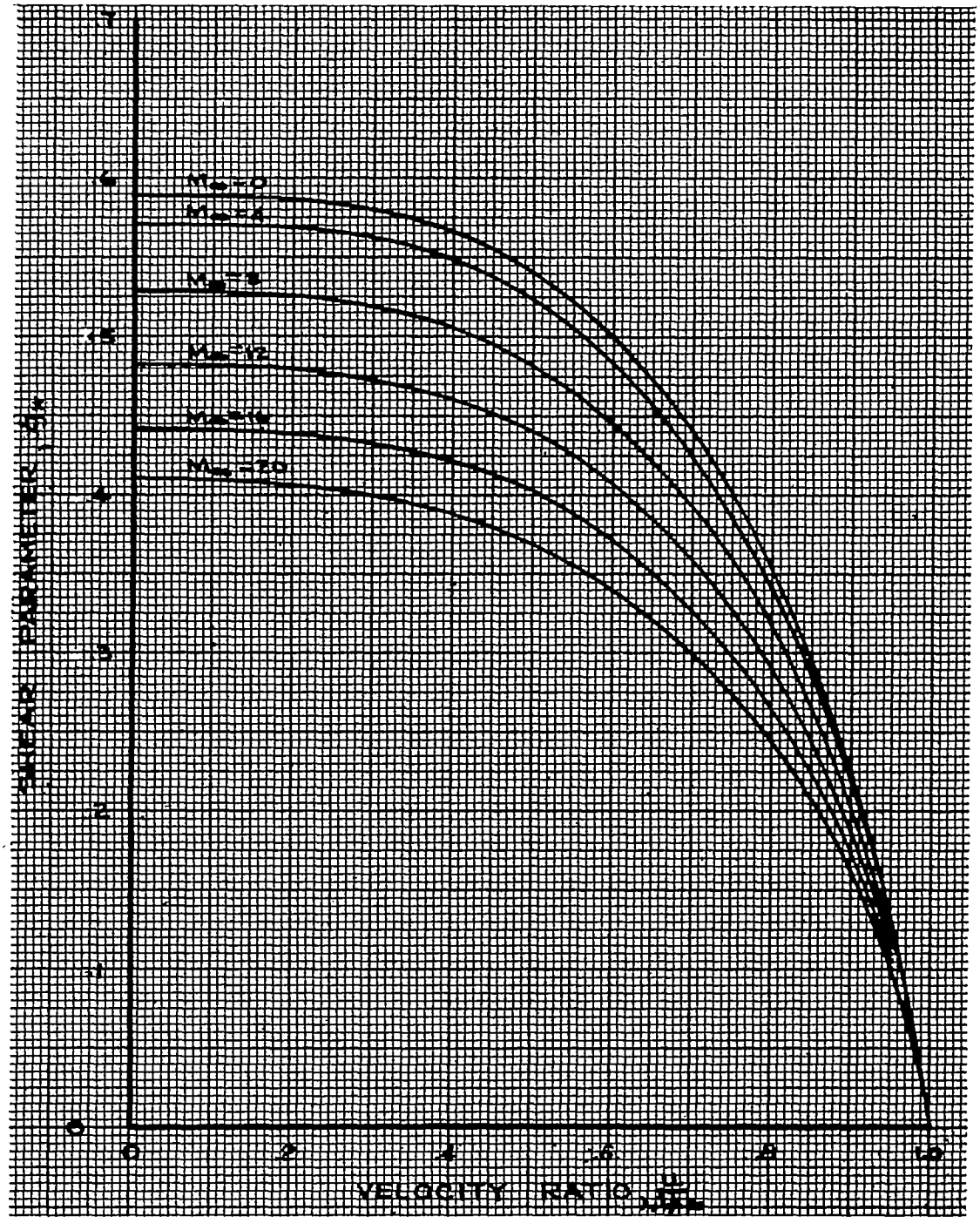

Figure 11.- Shear distribution in laminar boundary layer for wall-to-free-stream temperature ratio of 4 and various free-stream Mach numbers. Prandtl number, 0.75; $\theta = 0.505$.

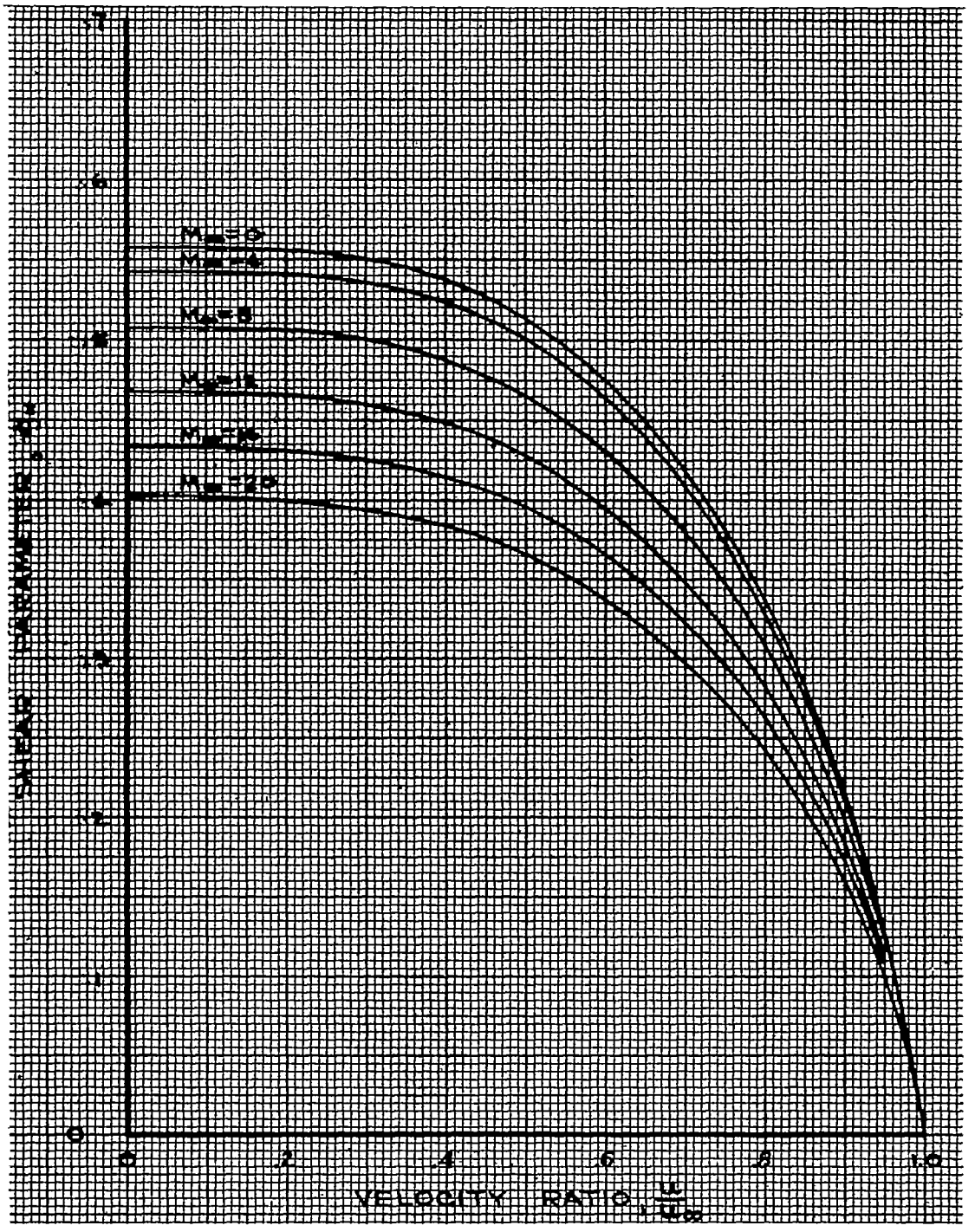

Figure 12.- Shear distribution in laminar boundary layer for wall-to-free-stream temperature ratio of 6 and various free-stream Mach numbers. Prandtl number, 0.75; $\theta = 0.505$.

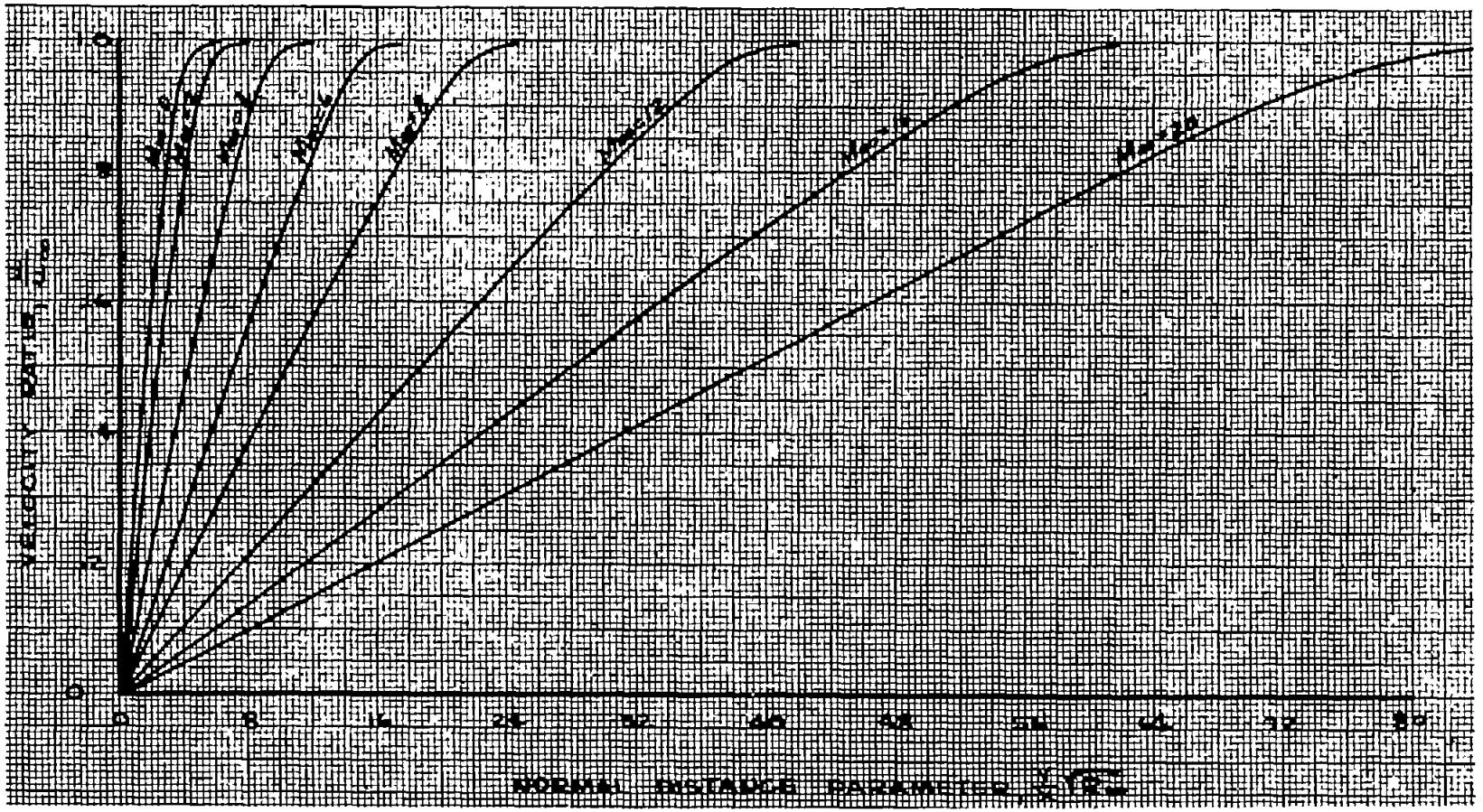

Figure 13.- Velocity distribution across laminar boundary layer on an insulated flat plate for various Mach numbers. Prandtl number, 0.75; $\theta = 0.505$.

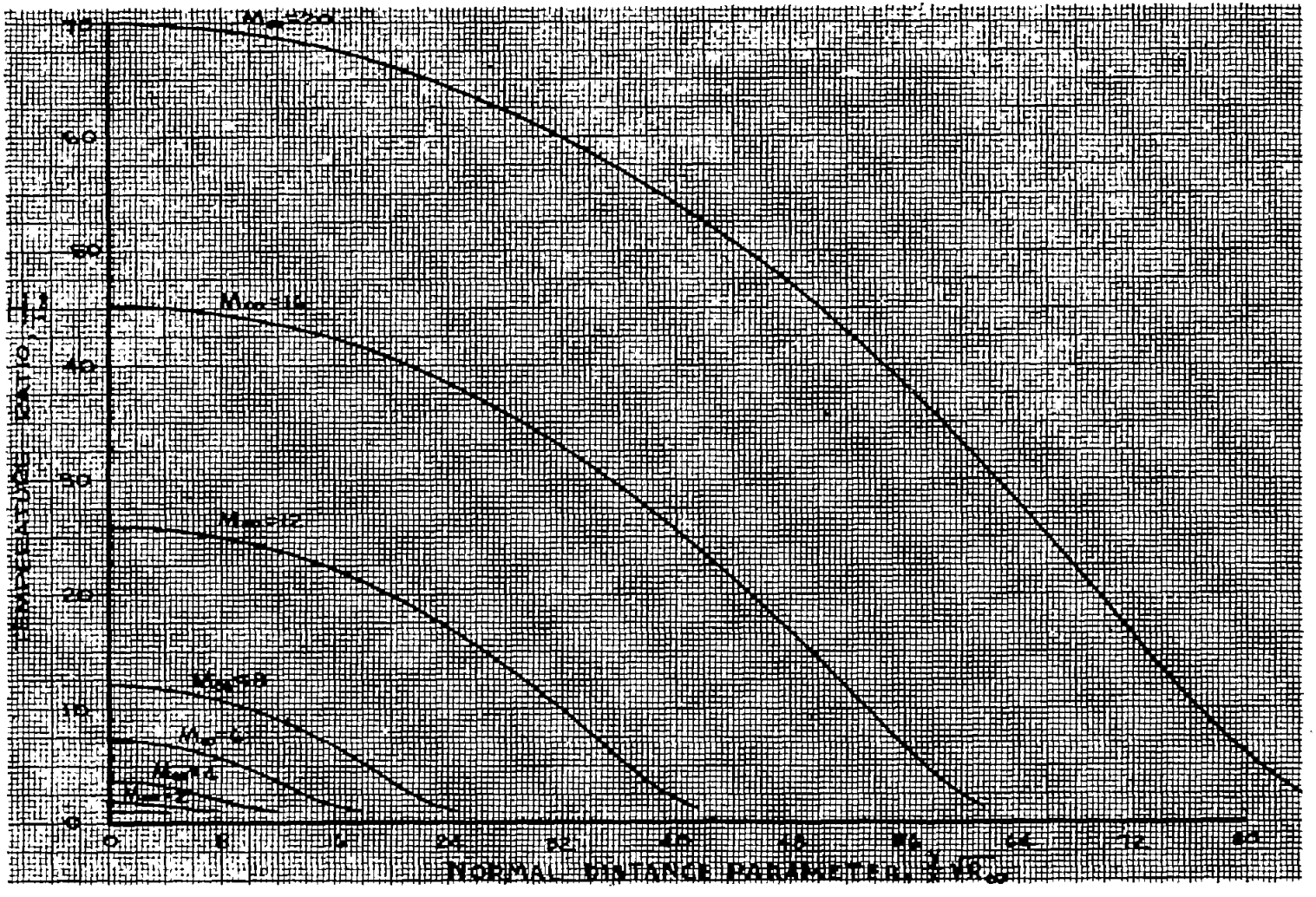

Figure 14.- Temperature distribution across laminar boundary layer on an insulated flat plate for various Mach numbers. Prandtl number, 0.75; $\theta = 0.505$.

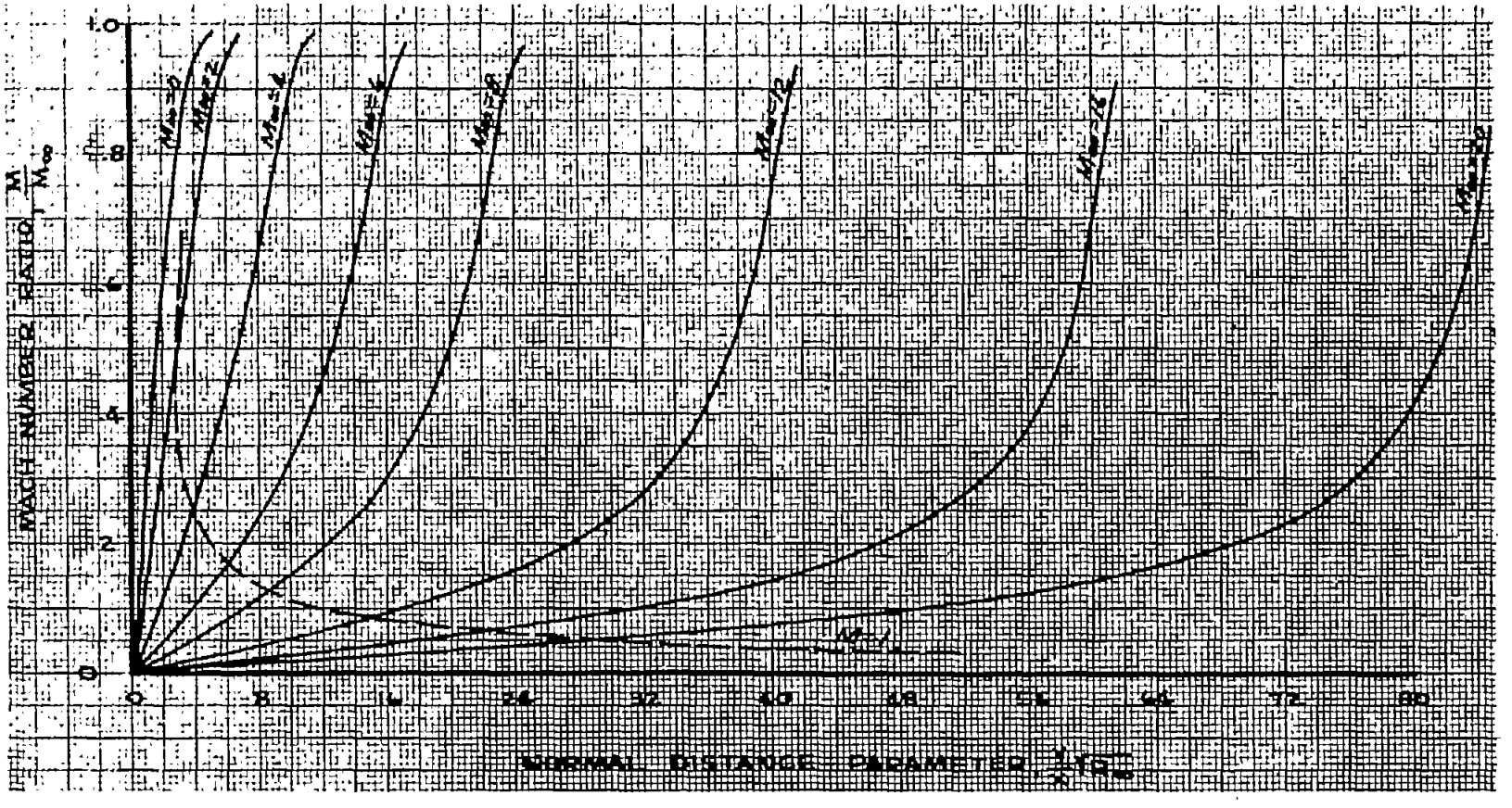

Figure 15.- Mach number distribution across laminar boundary layer on an insulated flat plate for various Mach numbers. Prandtl number, 0.75; $\theta = 0.505$.

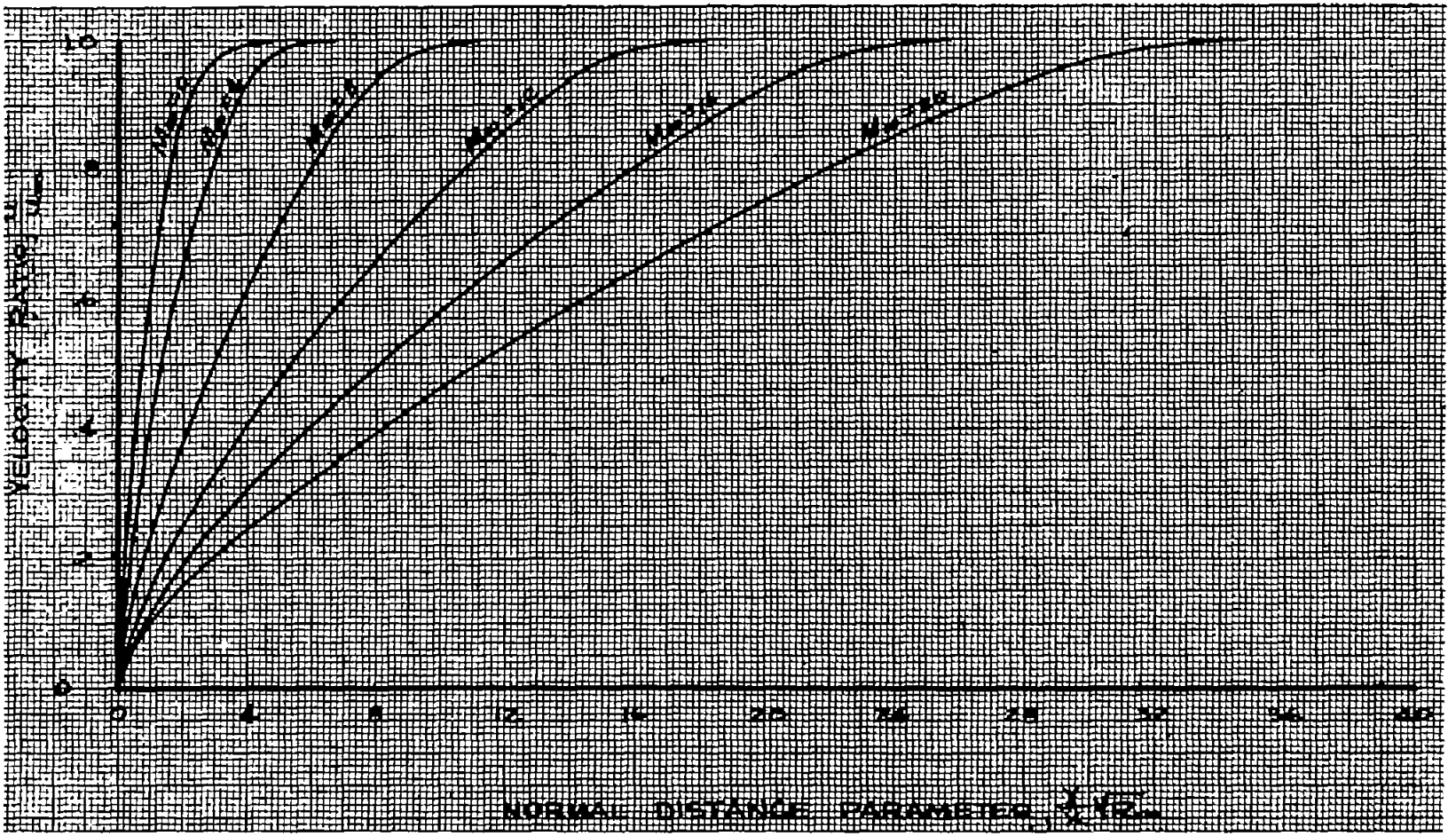

Figure 16.- Velocity distribution across laminar boundary layer for wall-to-free-stream temperature ratio of 1/4 and various Mach numbers. Prandtl number, 0.75; $\theta = 0.505$.

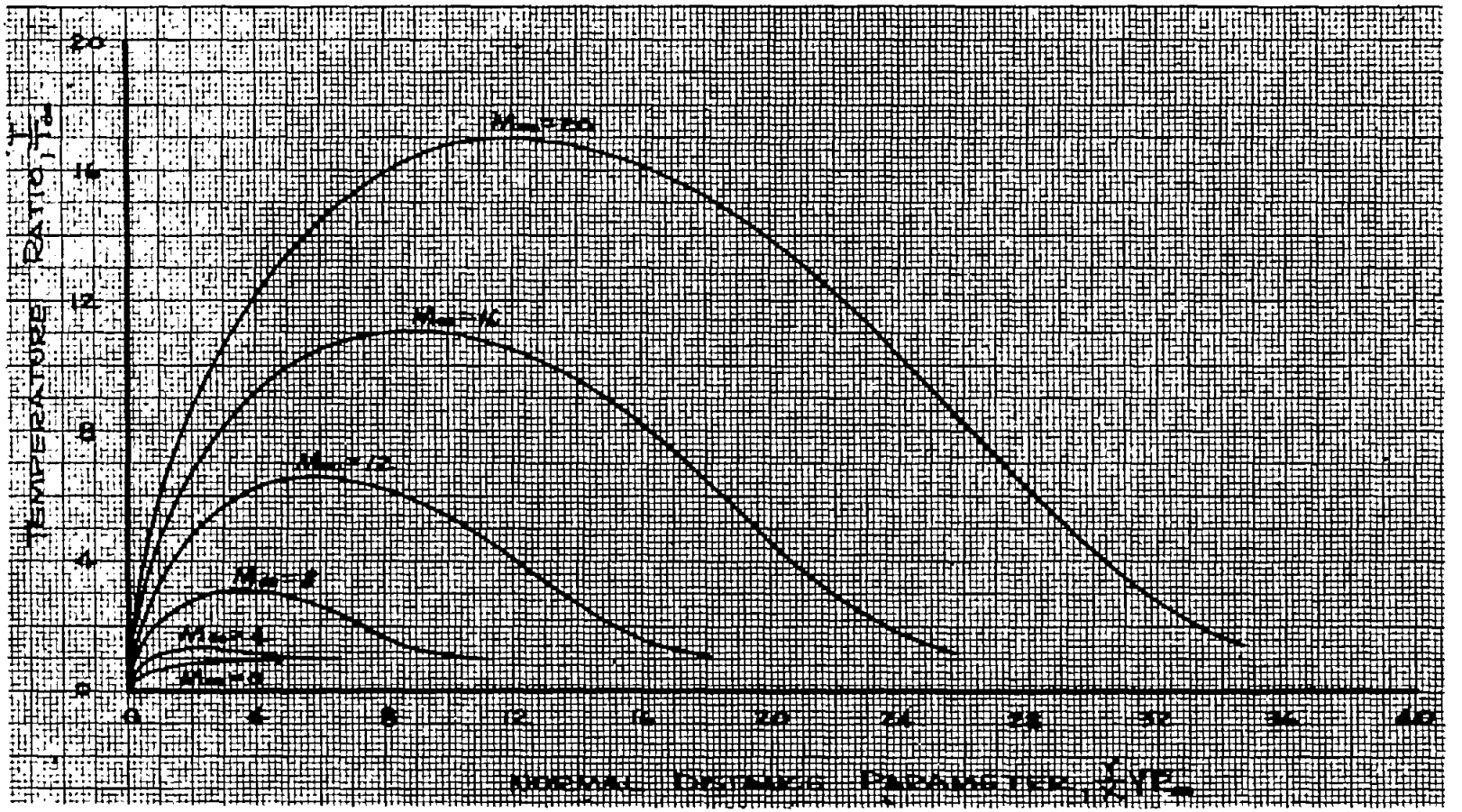

Figure 17.- Temperature distribution across laminar boundary layer for wall-to-free-stream temperature ratio of 1/4 and various Mach numbers. Prandtl number, 0.75; $\theta = 0.505$.

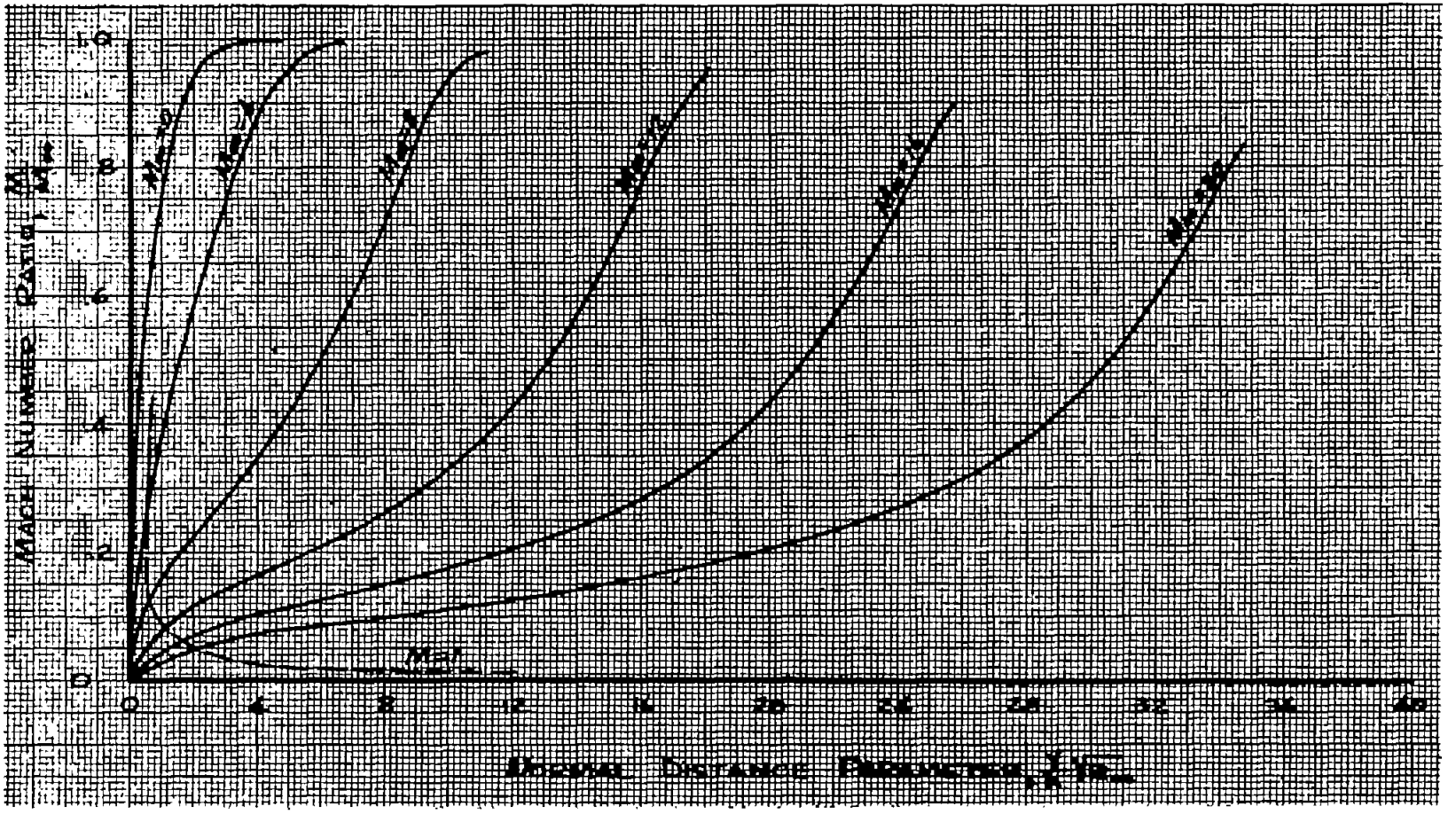

Figure 18.- Mach number distribution across laminar boundary layer for wall-to-free-stream temperature ratio of 1/4 and various Mach numbers. Prandtl number, 0.75; $\theta = 0.505$.

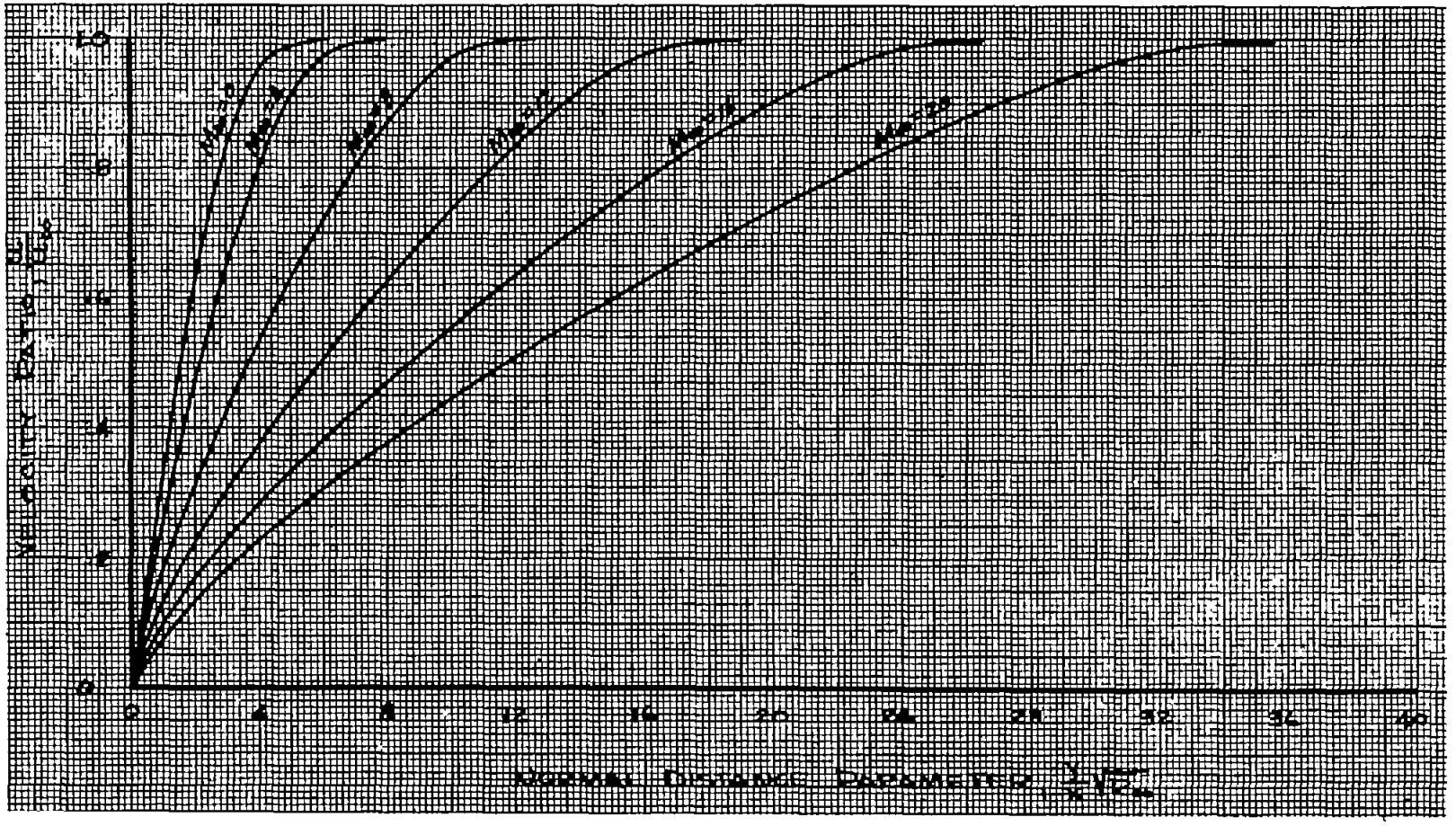

Figure 19.- Velocity distribution across laminar boundary layer for wall-to-free-stream temperature ratio of 1 and various Mach numbers. Prandtl number, 0.75; $\theta = 0.505$.

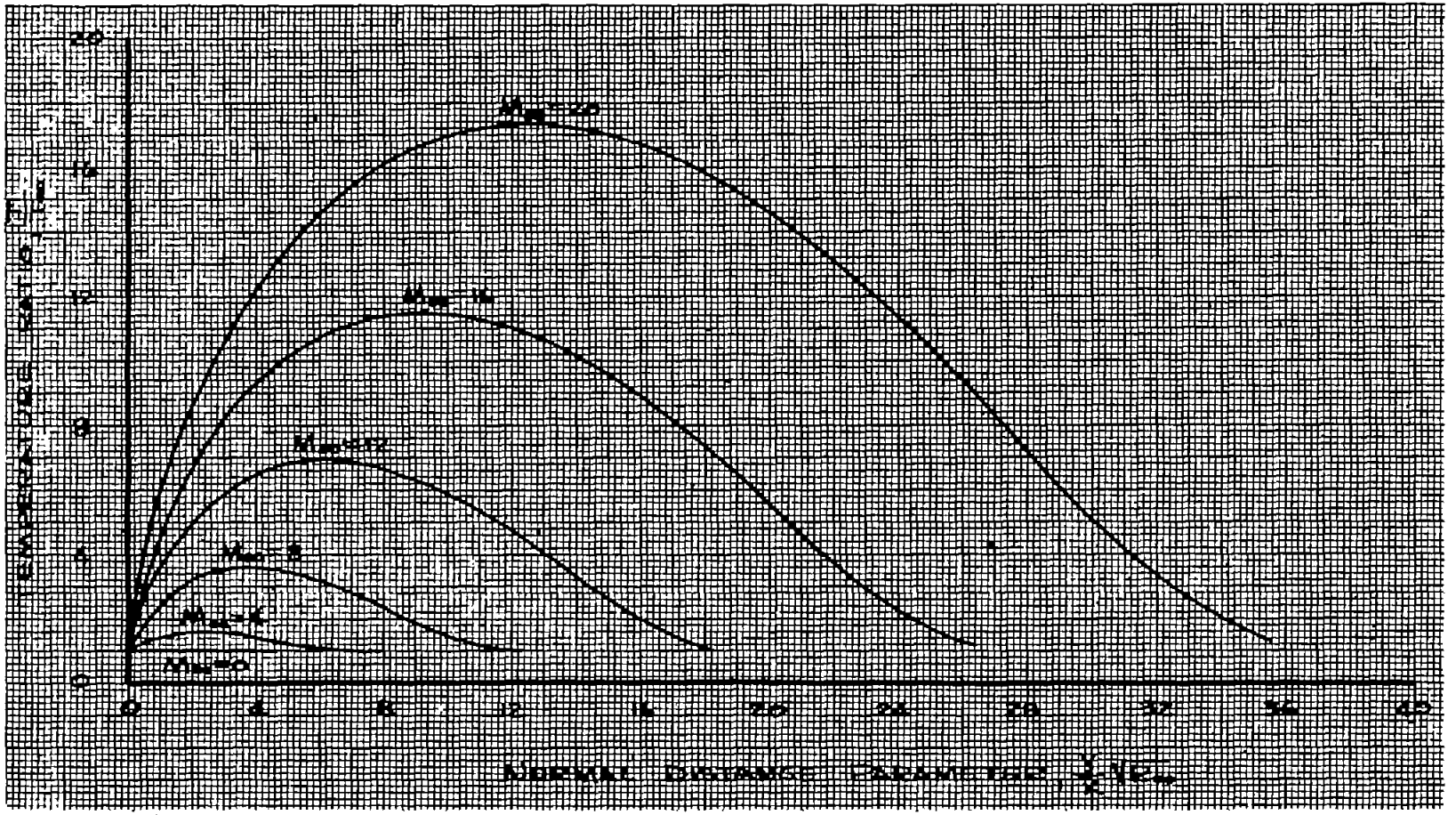

Figure 20.- Temperature distribution across laminar boundary layer for wall-to-free-stream temperature ratio of 1 and various Mach numbers. Prandtl number, 0.75; $\theta = 0.505$.

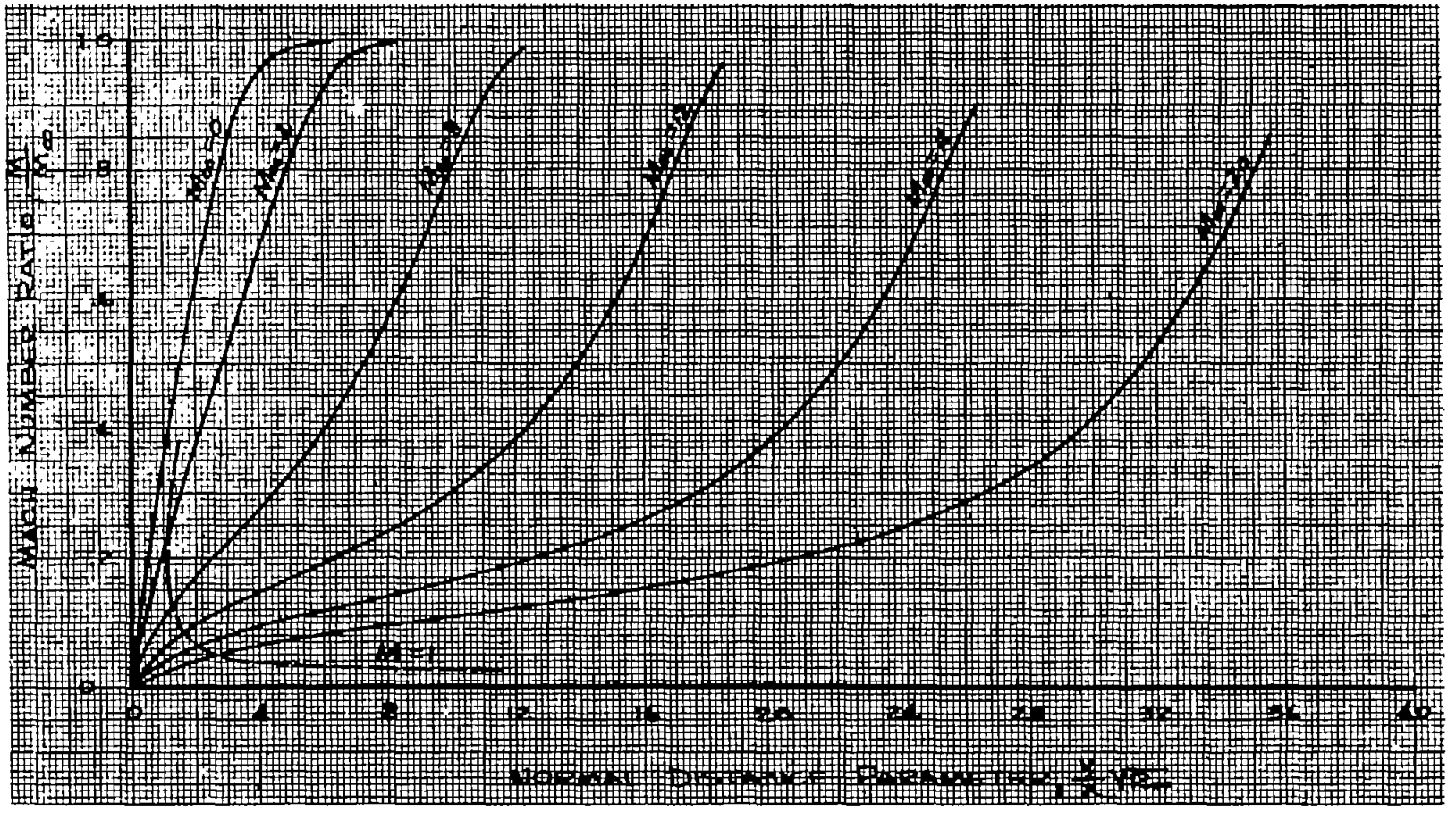

Figure 21.- Mach number distribution across laminar boundary layer for wall-to-free-stream temperature ratio of 1 and various Mach numbers. Prandtl number, 0.75; $\theta = 0.505$.

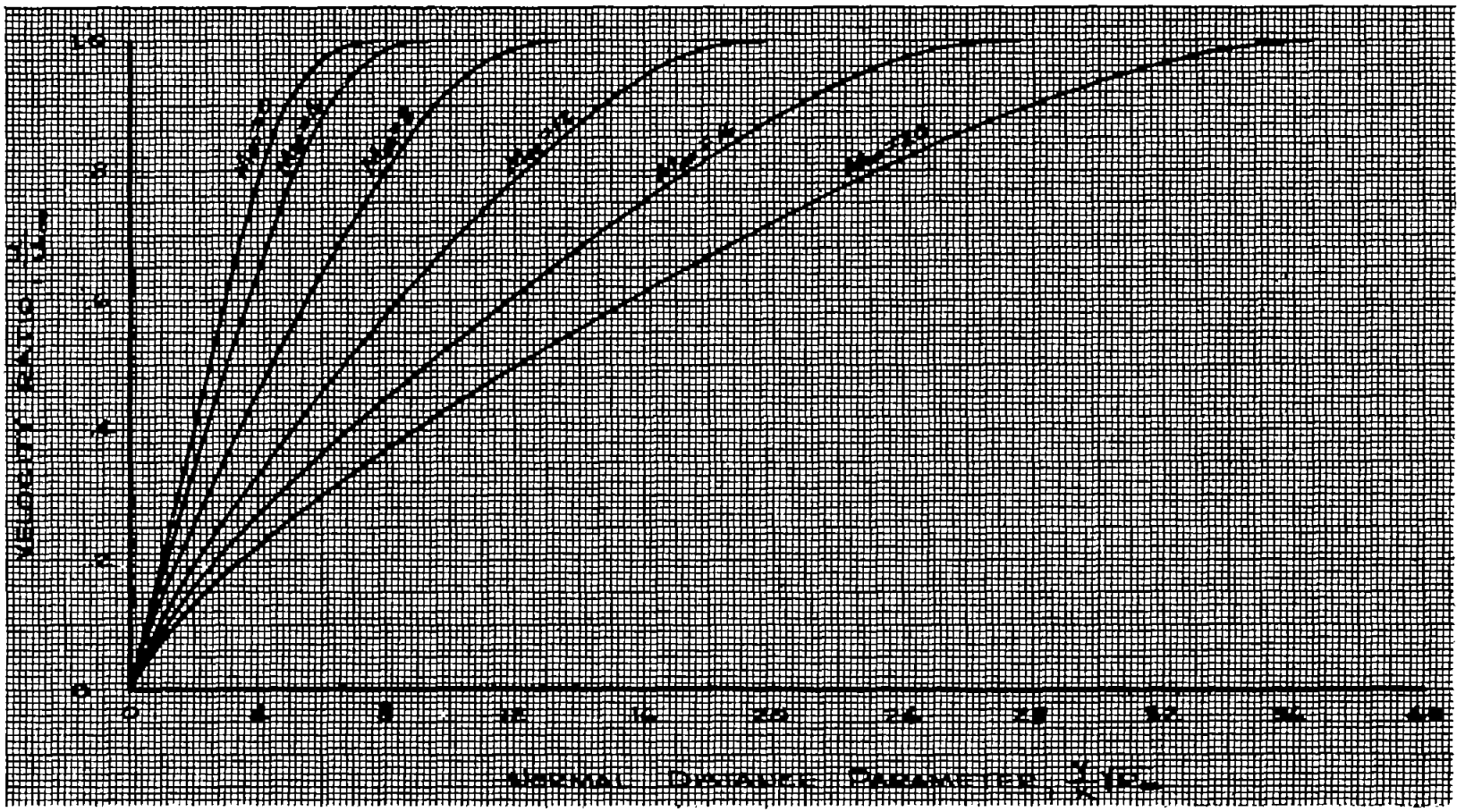

Figure 22.- Velocity distribution across laminar boundary layer for wall-to-free-stream temperature ratio of 2 and various Mach numbers. Prandtl number, 0.75; $\theta = 0.505$.

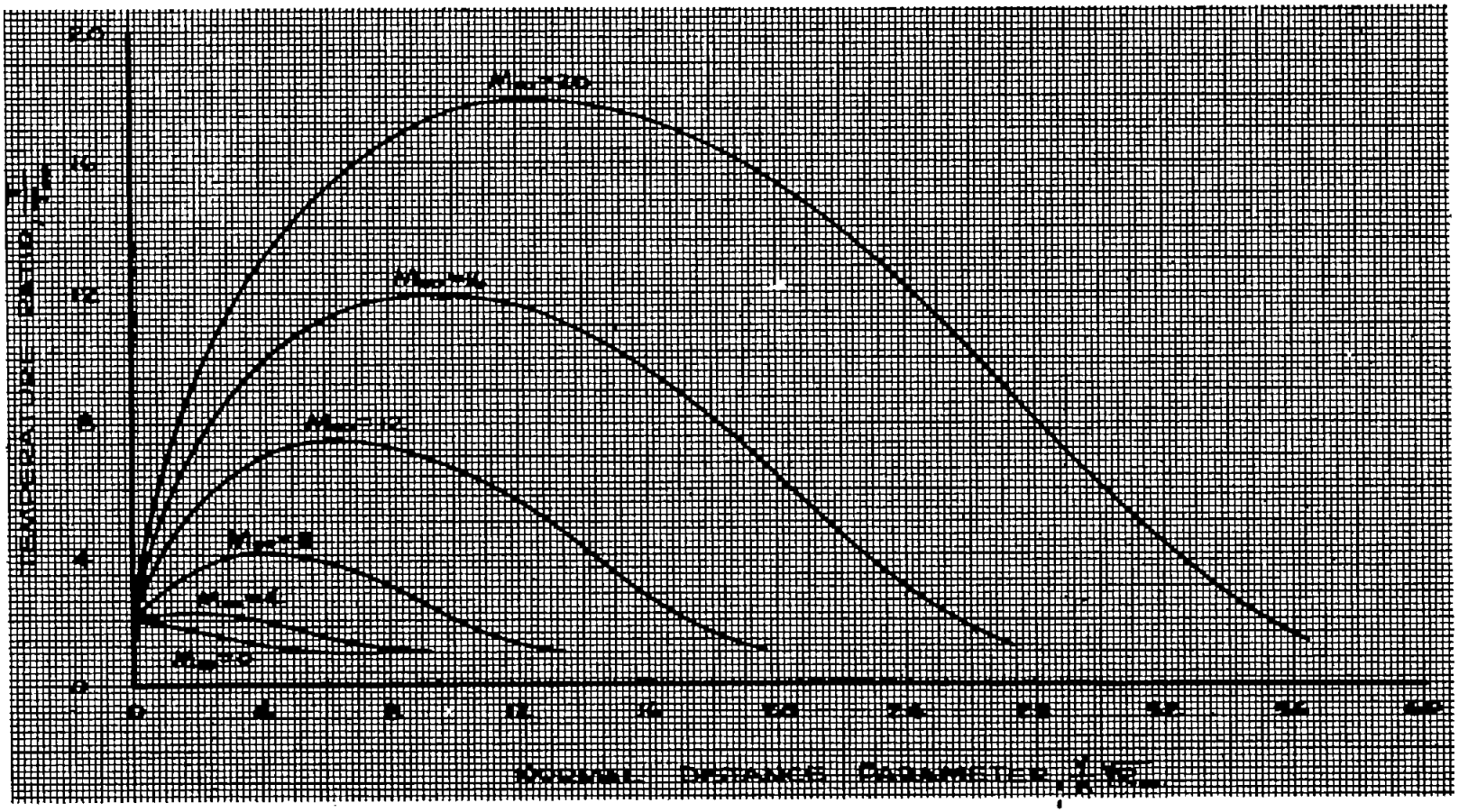

Figure 23.- Temperature distribution across laminar boundary layer for wall-to-free-stream temperature ratio of 2 and various Mach numbers. Prandtl number, 0.75; $\theta = 0.505$.

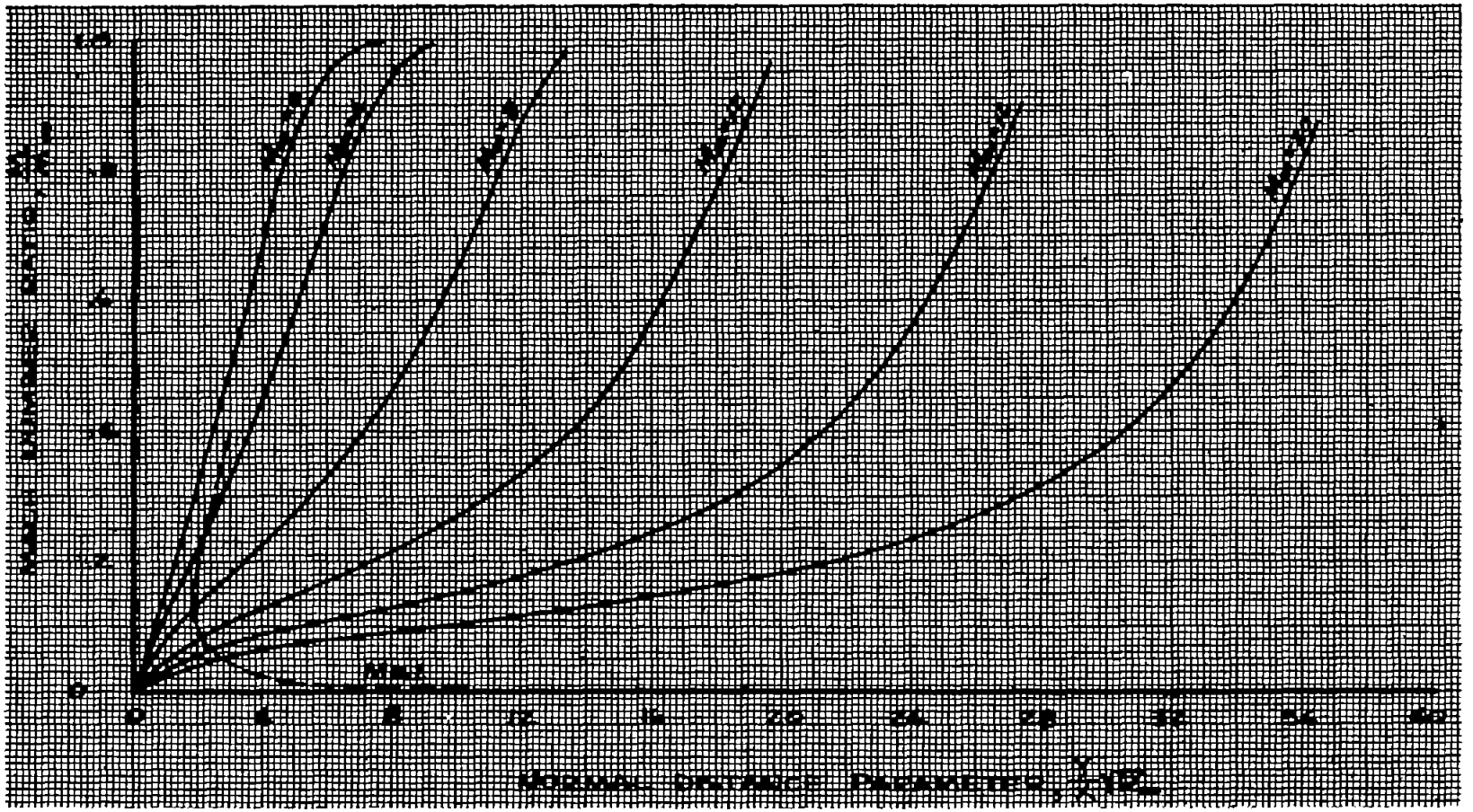

Figure 24.- Mach number distribution across laminar boundary layer for wall-to-free-stream temperature ratio of 2 and various Mach numbers. Prandtl number, 0.75; $\theta = 0.505$.

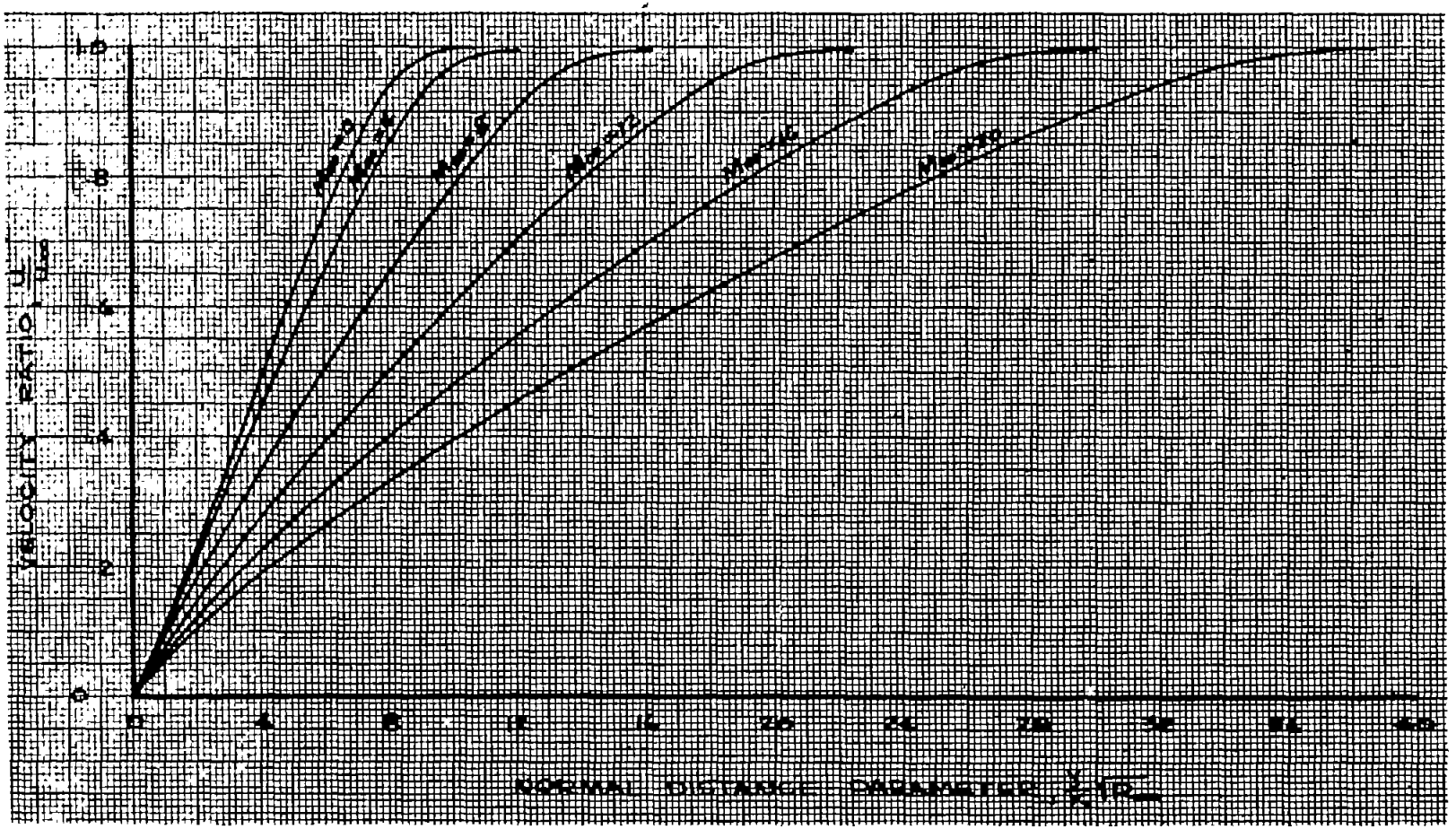

Figure 25.- Velocity distribution across laminar boundary layer for wall-to-free-stream temperature ratio of 4 and various Mach numbers. Prandtl number, 0.75; $\theta = 0.505$.

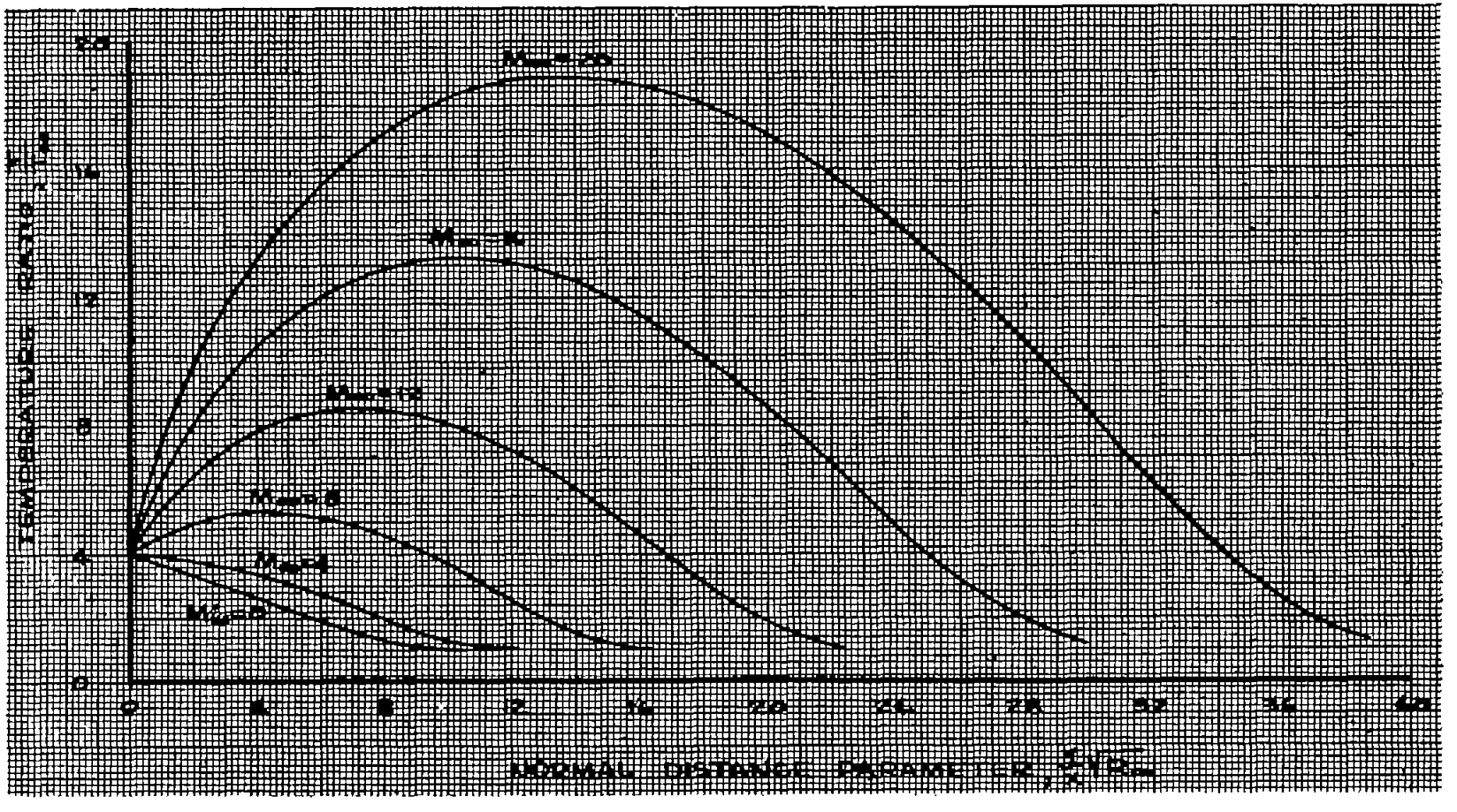

Figure 26.- Temperature distribution across laminar boundary layer for wall-to-free-stream temperature ratio of 4 and various Mach numbers. Prandtl number, 0.75; $\theta = 0.505$.

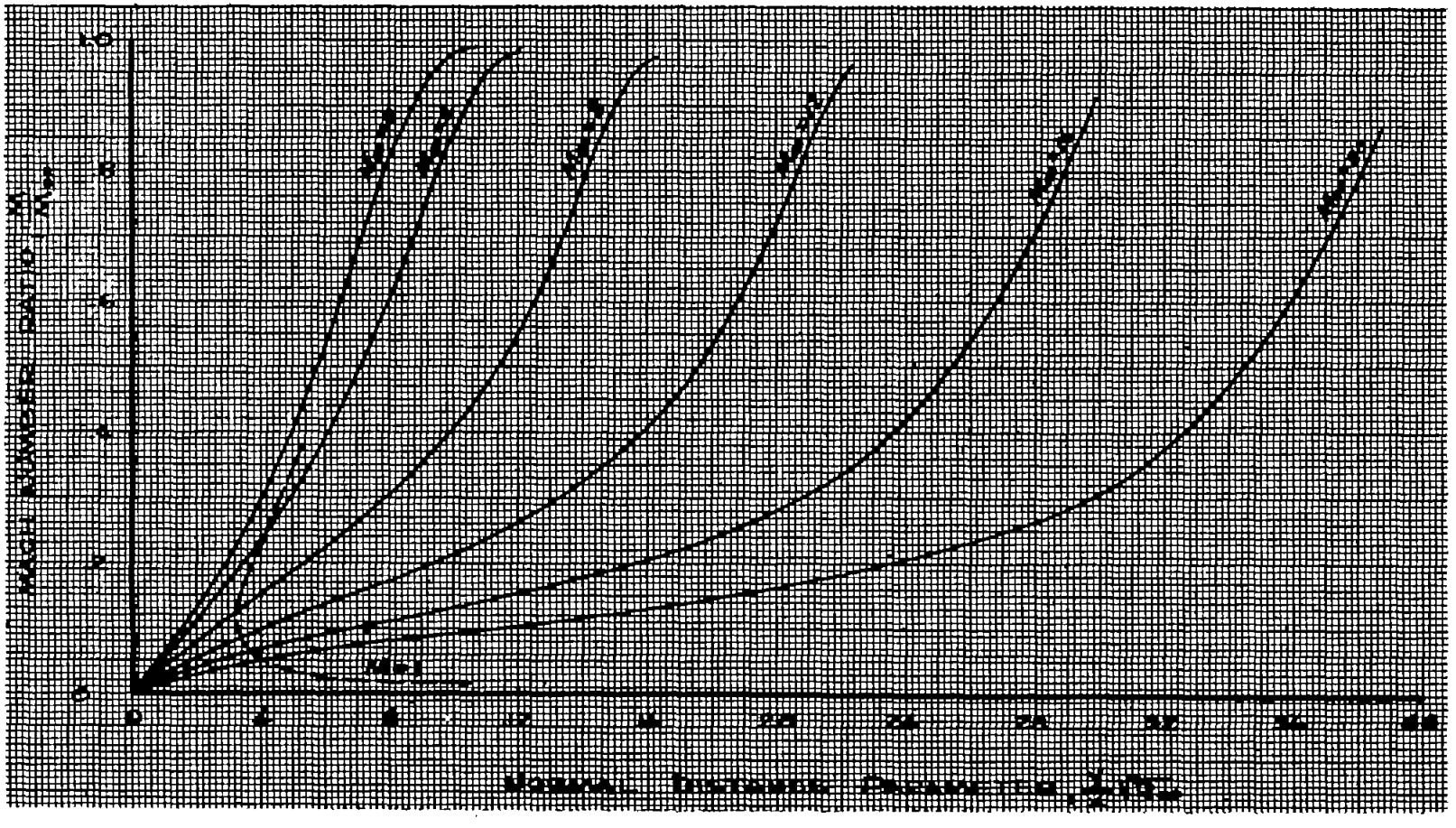

Figure 27.- Mach number distribution across laminar boundary layer for wall-to-free-stream temperature ratio of 4 and various Mach numbers. Prandtl number, 0.75; $\theta = 0.505$.

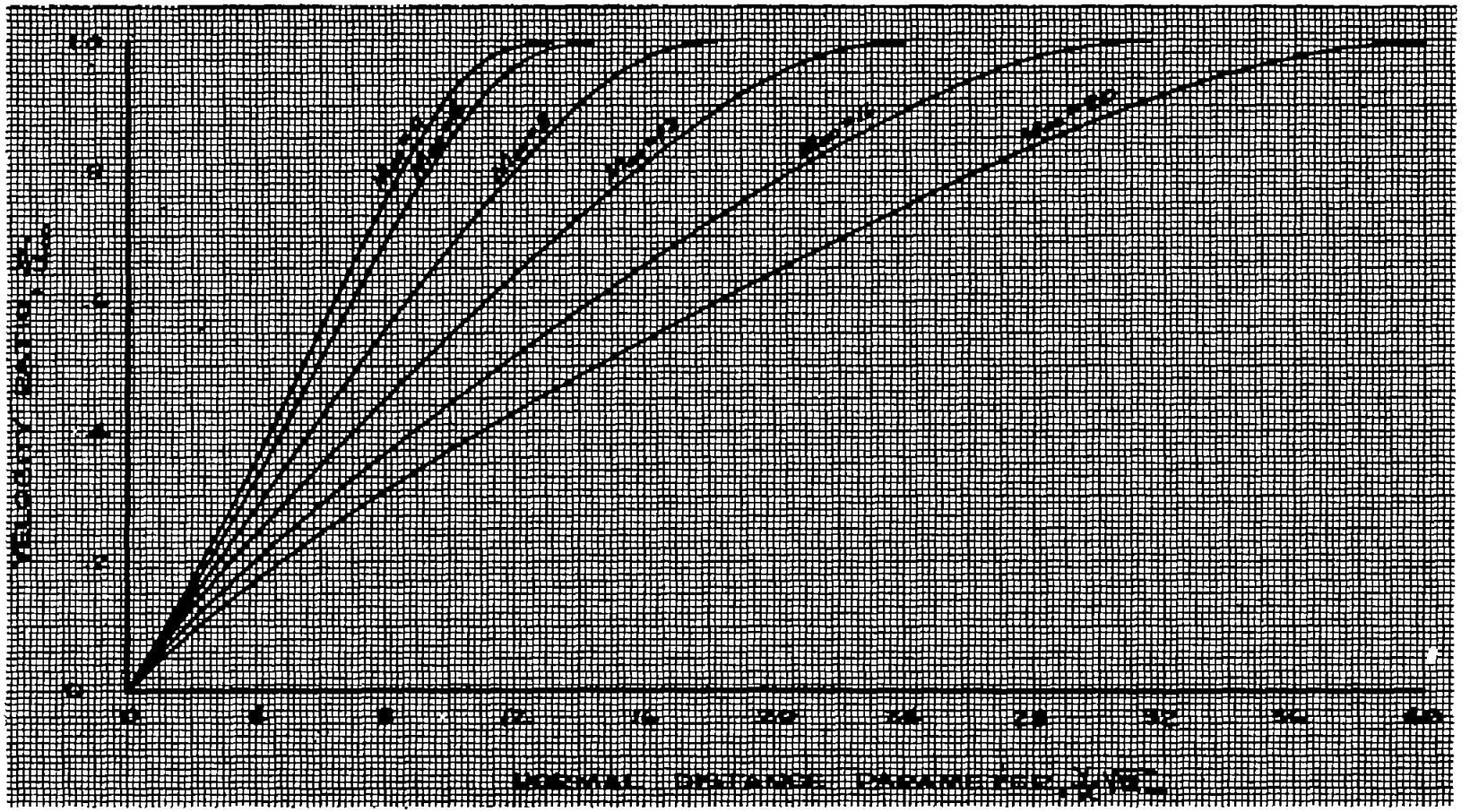

Figure 28.- Velocity distribution across laminar boundary layer for wall-to-free-stream temperature ratio of 6 and various Mach numbers. Prandtl number, 0.75; $\theta = 0.505$.

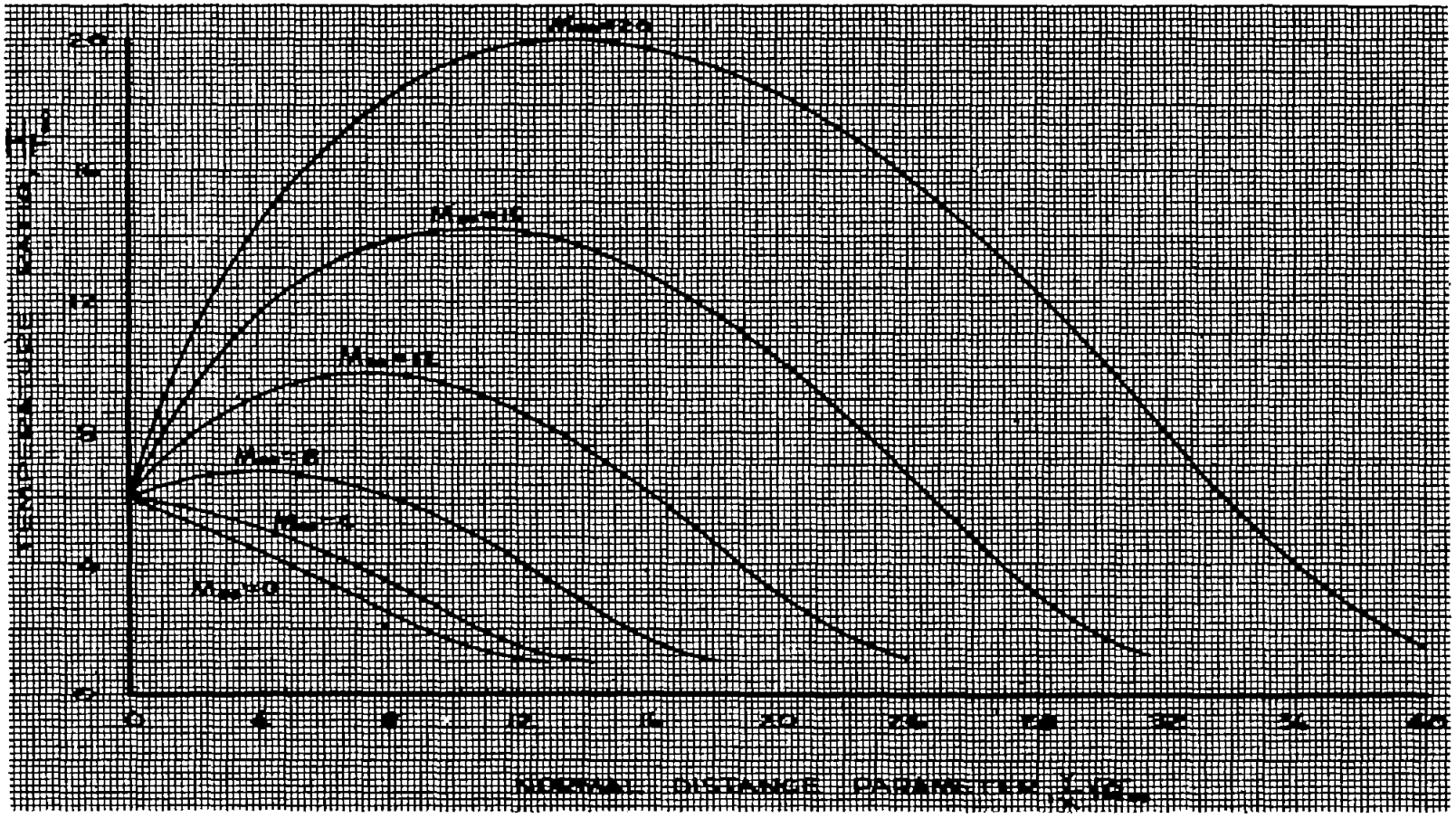

Figure 29.- Temperature distribution across laminar boundary layer for wall-to-free-stream temperature ratio of 6 and various Mach numbers. Prandtl number, 0.75; $\theta = 0.505$.

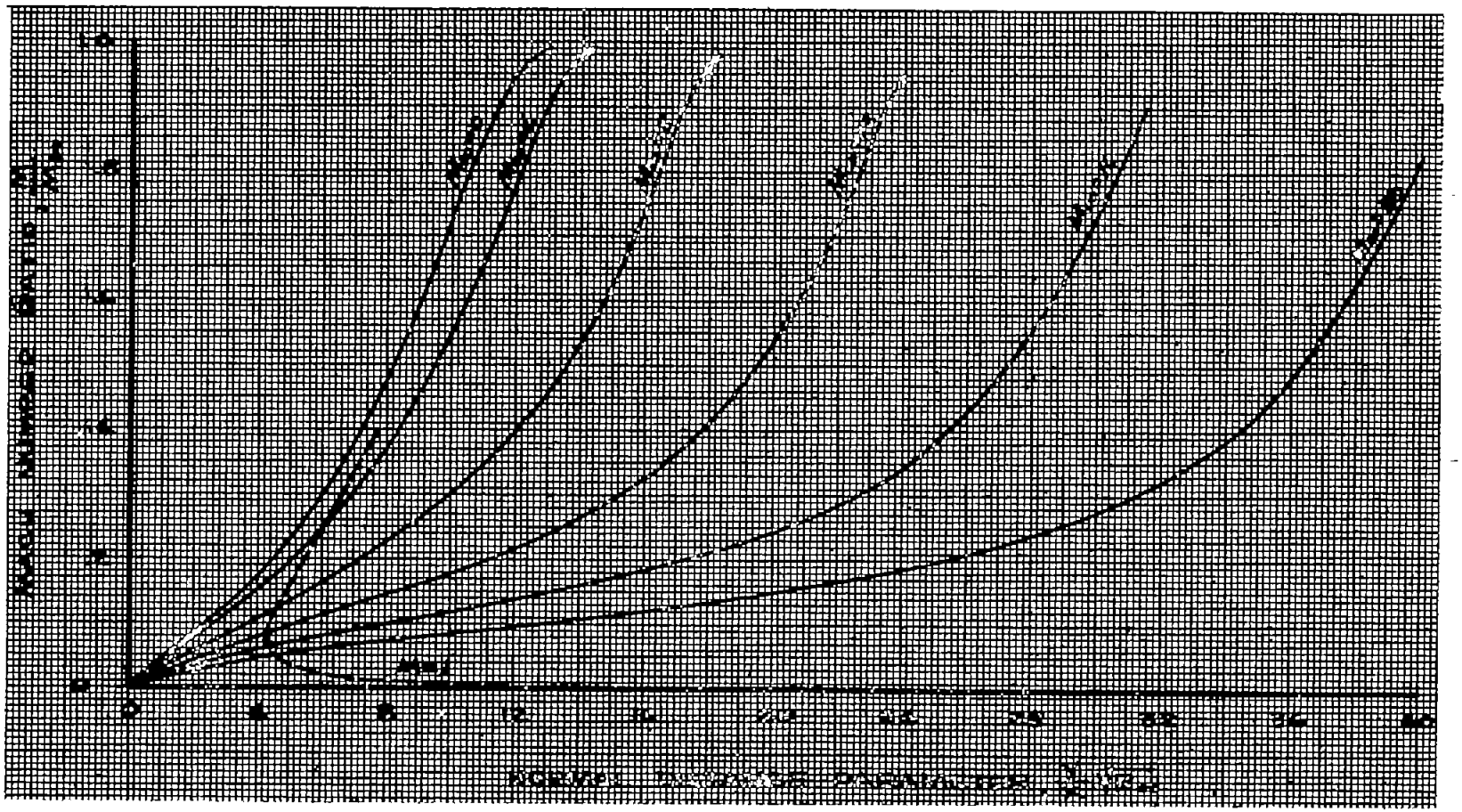

Figure 30.- Mach number distribution across laminar boundary layer for wall-to-free-stream temperature ratio of 6 and various Mach numbers. Prandtl number, 0.75; $\theta = 0.505$.

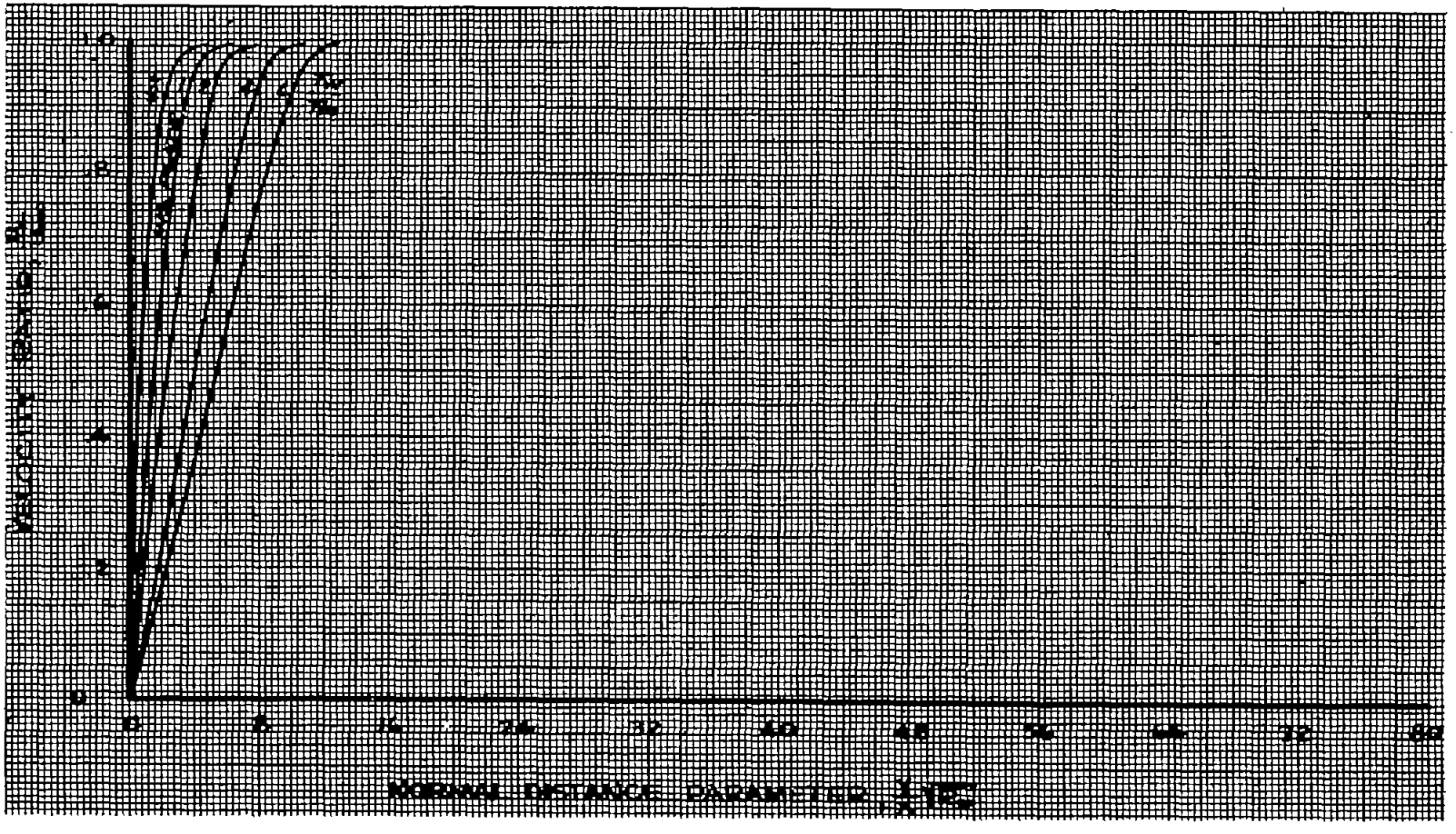

Figure 31.- Velocity distribution across laminar boundary layer for $M_\infty = 0$ and various wall-to-free-stream temperature ratios. Prandtl number, 0.75; $\theta = 0.505$.

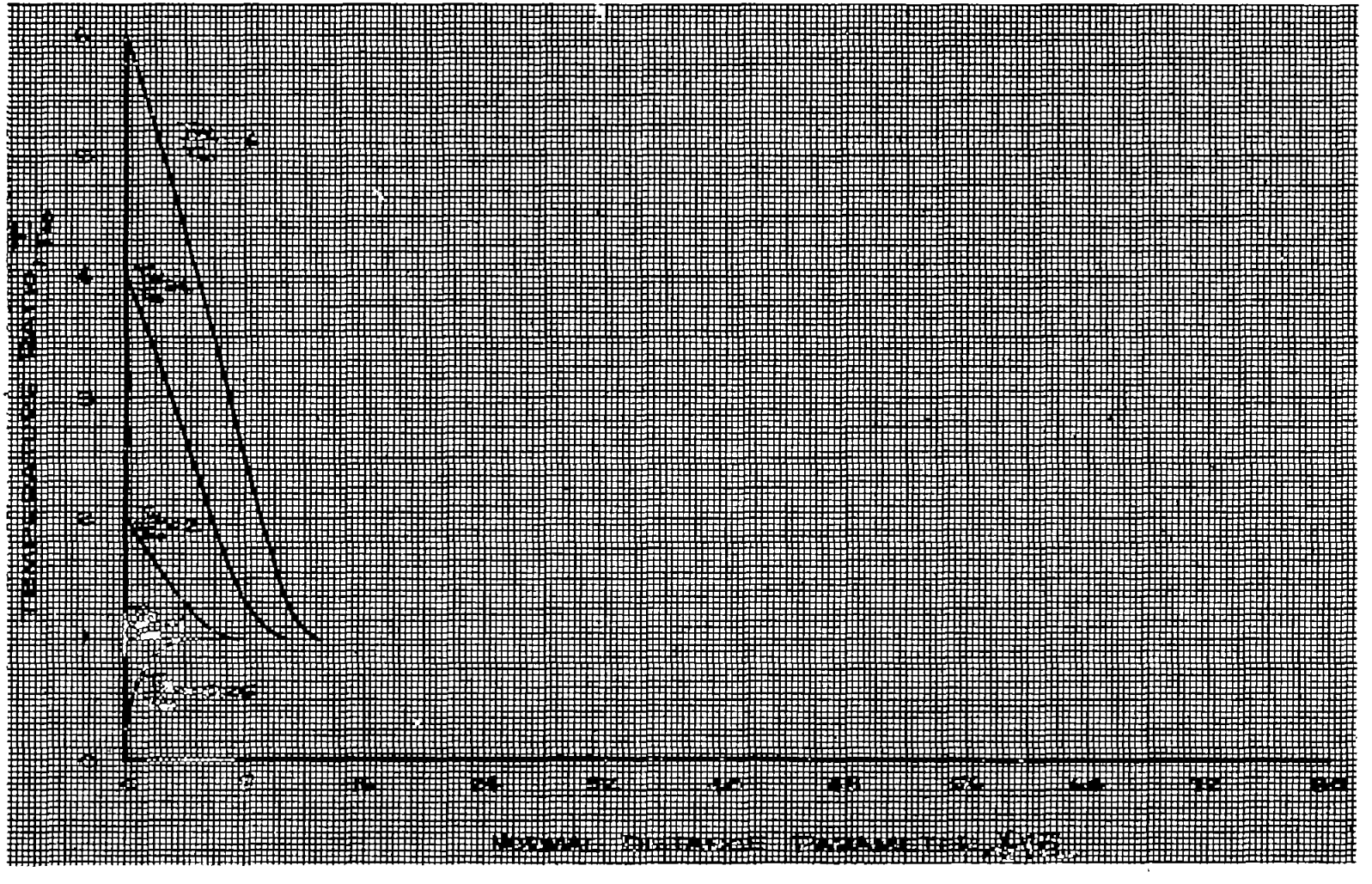

Figure 32.- Temperature distribution across laminar boundary layer for $M_\infty = 0$ and various wall-to-free-stream temperature ratios. Prandtl number, 0.75; $\theta = 0.505$.

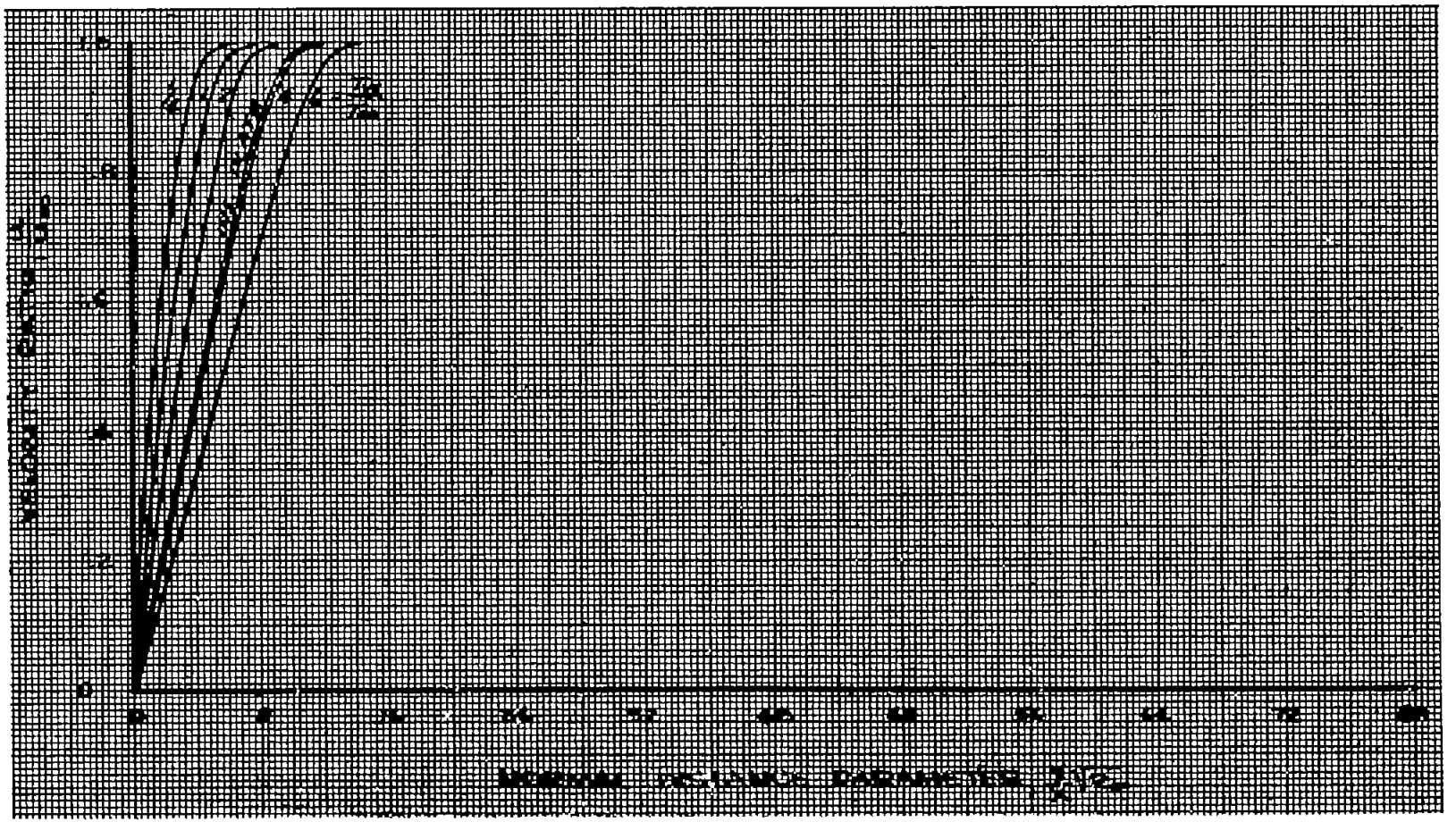

Figure 33.- Velocity distribution across laminar boundary layer for $M_\infty = 4$ and various wall-to-free-stream temperature ratios. Prandtl number, 0.75; $\theta = 0.505$.

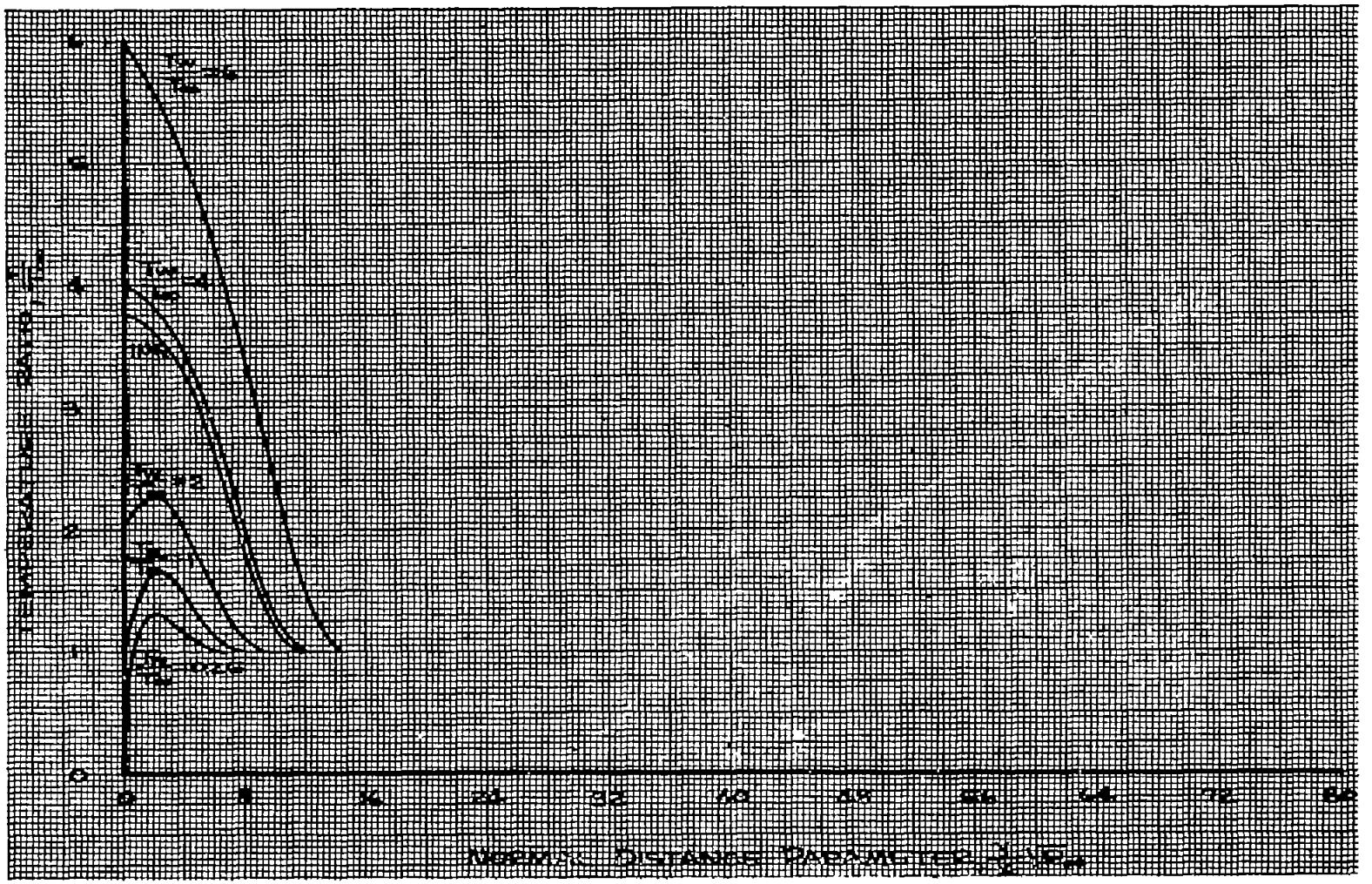

Figure 34.- Temperature distribution across laminar boundary layer for $M_\infty = 4$ and various wall-to-free-stream temperature ratios. Prandtl number, 0.75; $\theta = 0.505$.

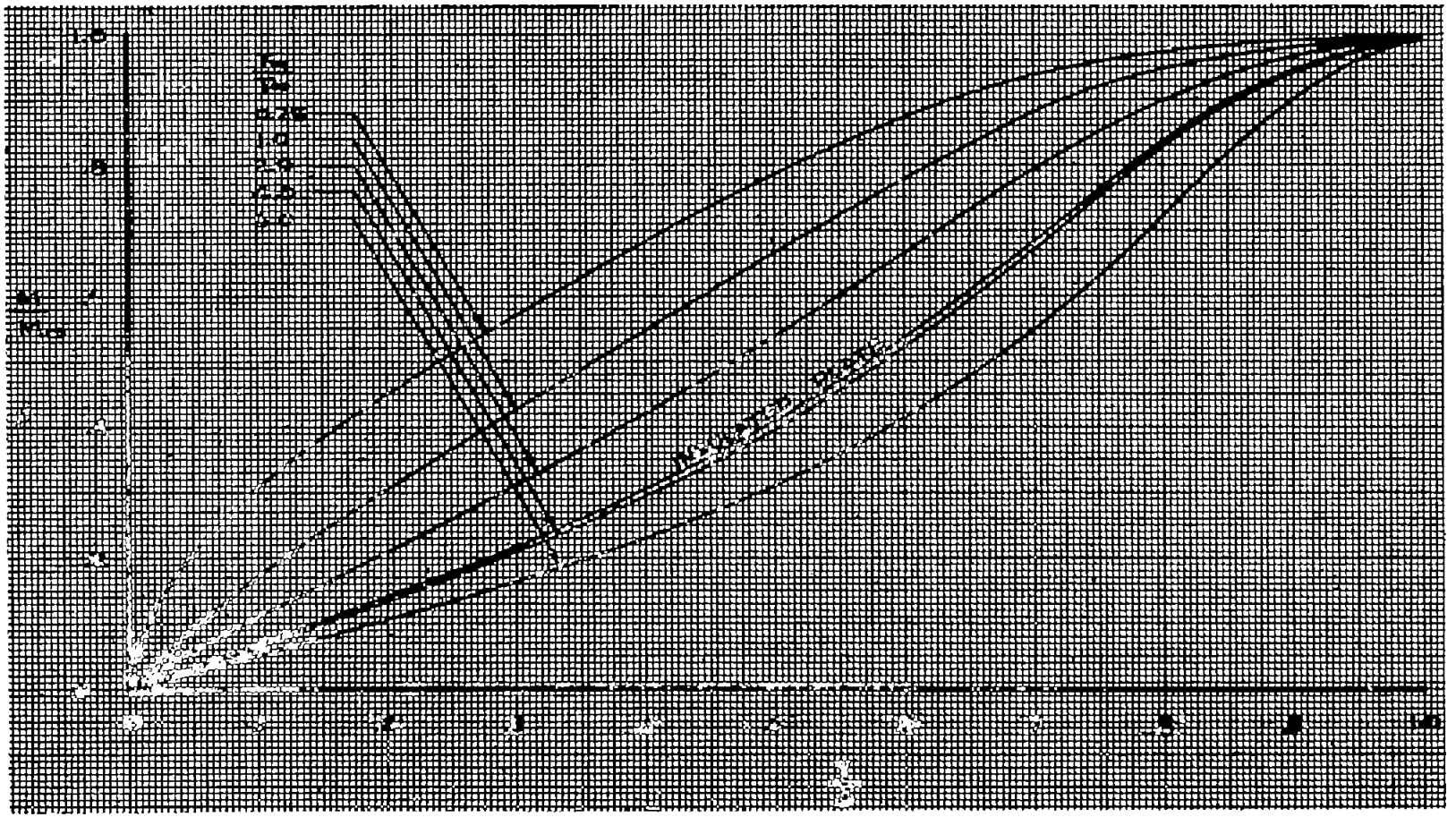

Figure 35.- Mach number distribution across laminar boundary layer for $M_\infty = 4$ and various wall-to-free-stream temperature ratios. Prandtl number, 0.75; $\theta = 0.505$.

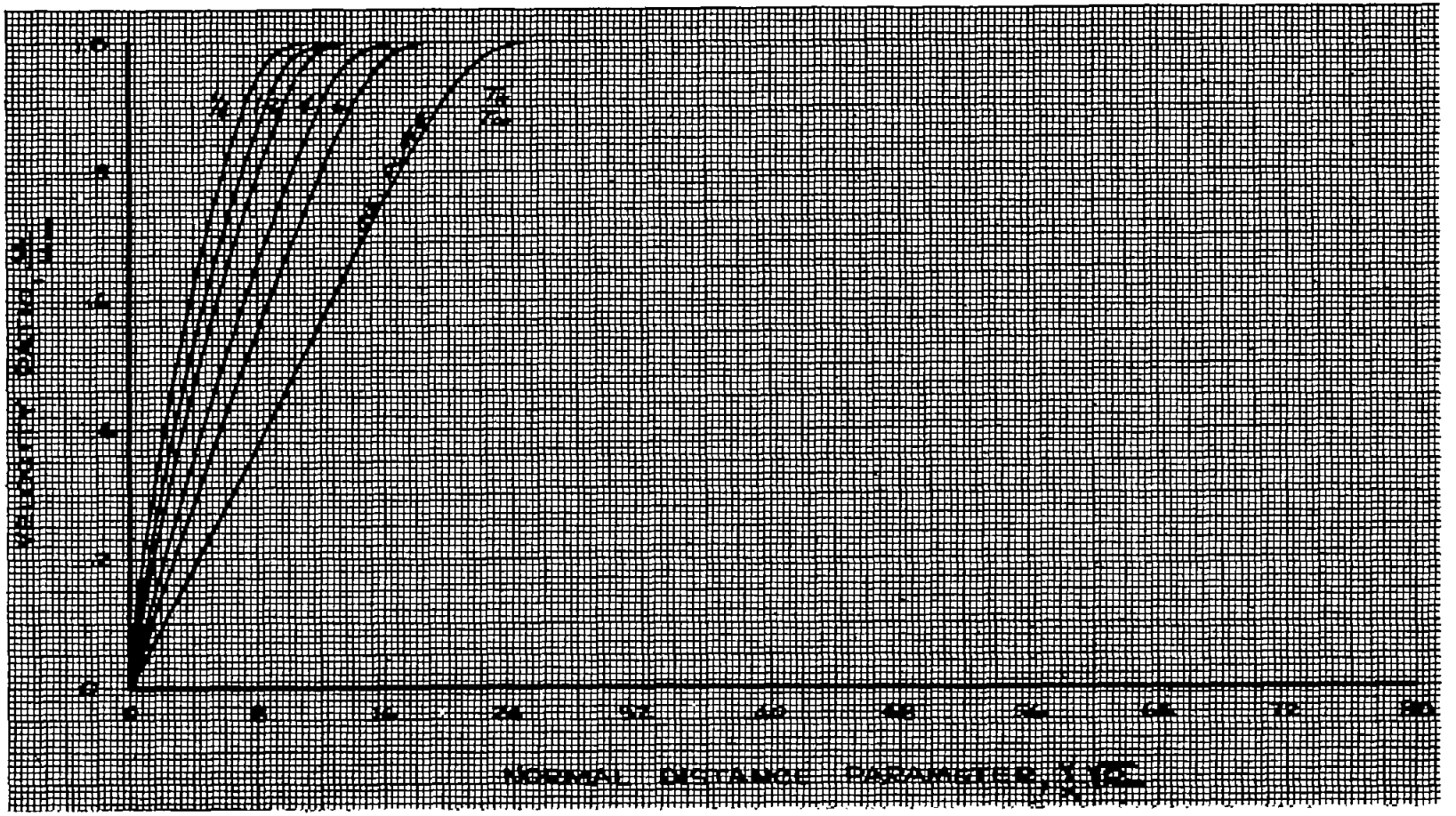

Figure 36.- Velocity distribution across laminar boundary layer for $M_\infty = 8$ and various wall-to-free-stream temperature ratios. Prandtl number, 0.75; $\theta = 0.505$.

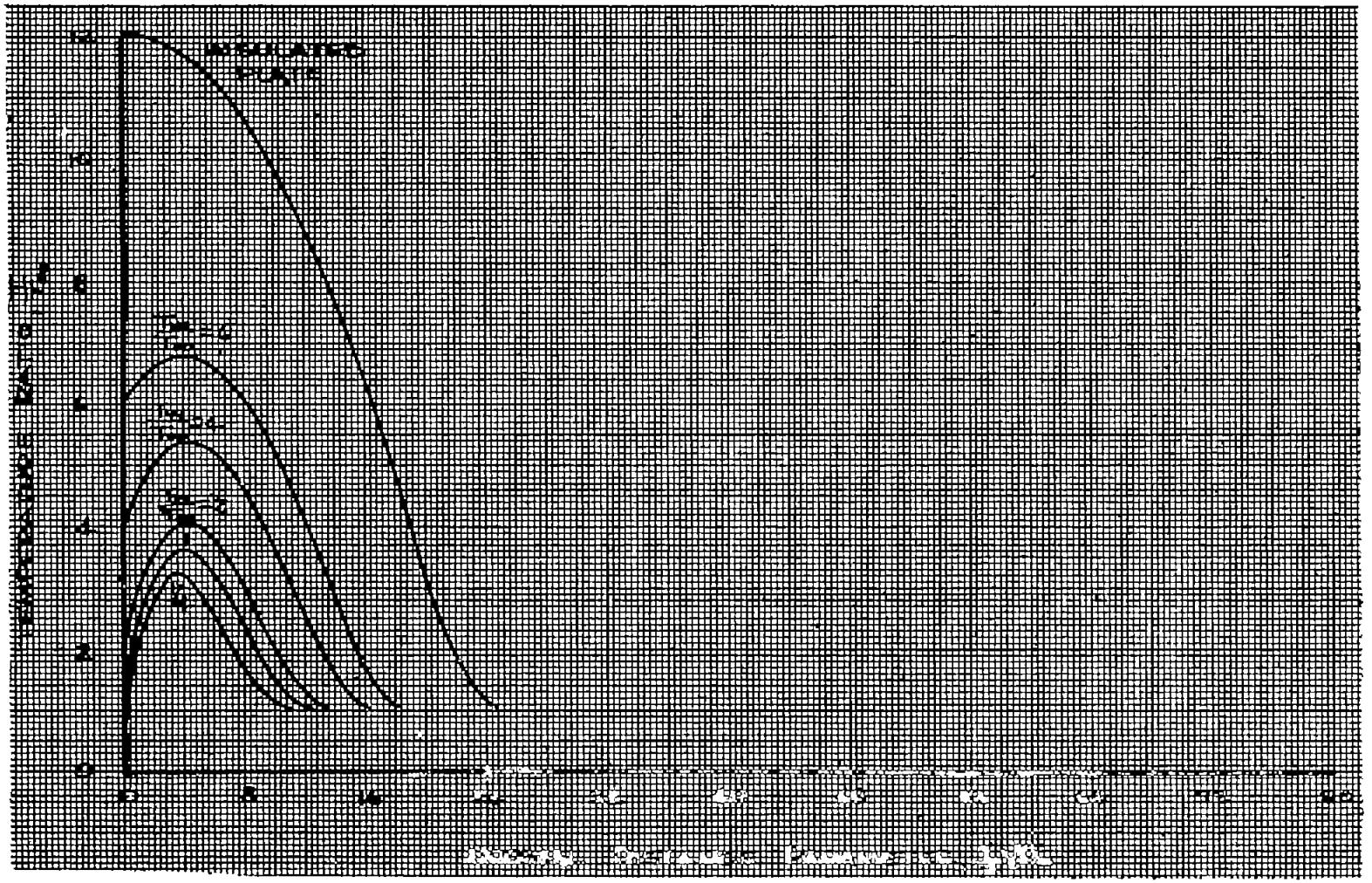

Figure 37.- Temperature distribution across laminar boundary layer for $M_\infty = 8$ and various wall-to-free-stream temperature ratios. Prandtl number, 0.75; $\theta = 0.505$.

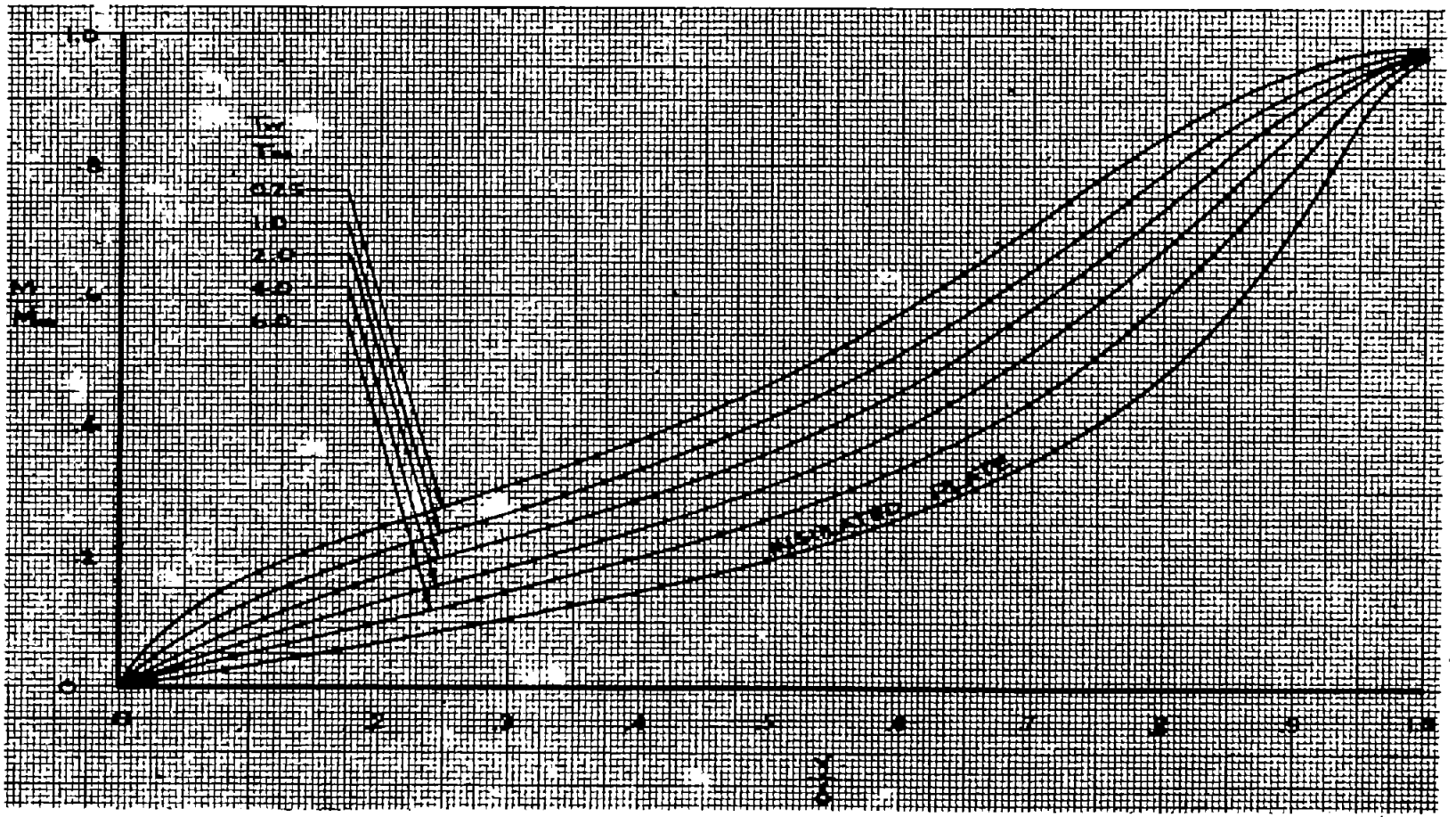

Figure 38.- Mach number distribution across laminar boundary layer for $M_\infty = 8$ and various wall-to-free-stream temperature ratios. Prandtl number, 0.75; $\theta = 0.505$.

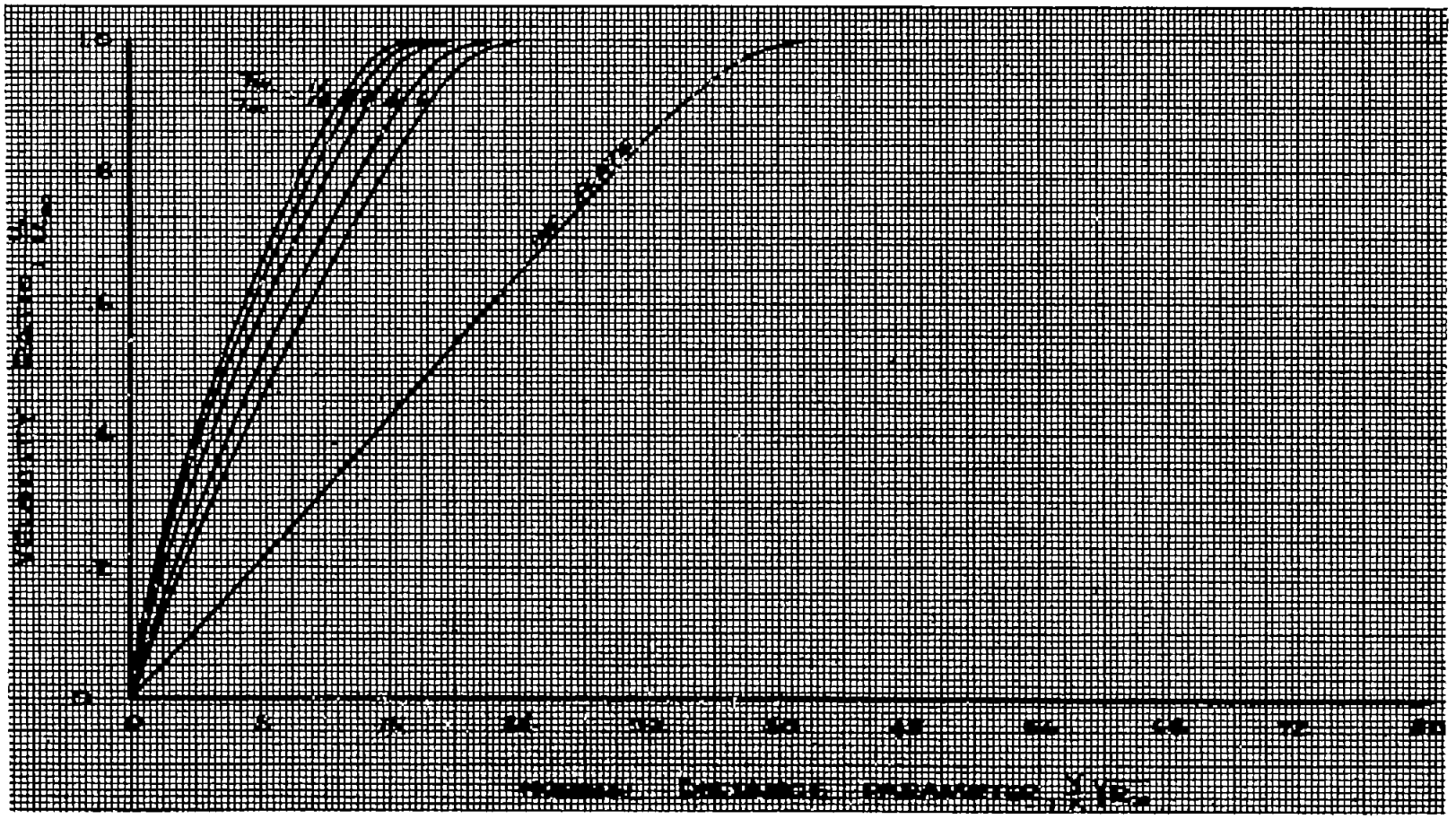

Figure 39.- Velocity distribution across laminar boundary layer for $M_\infty = 12$ and various wall-to-free-stream temperature ratios. Prandtl number, 0.75; $\theta = 0.505$.

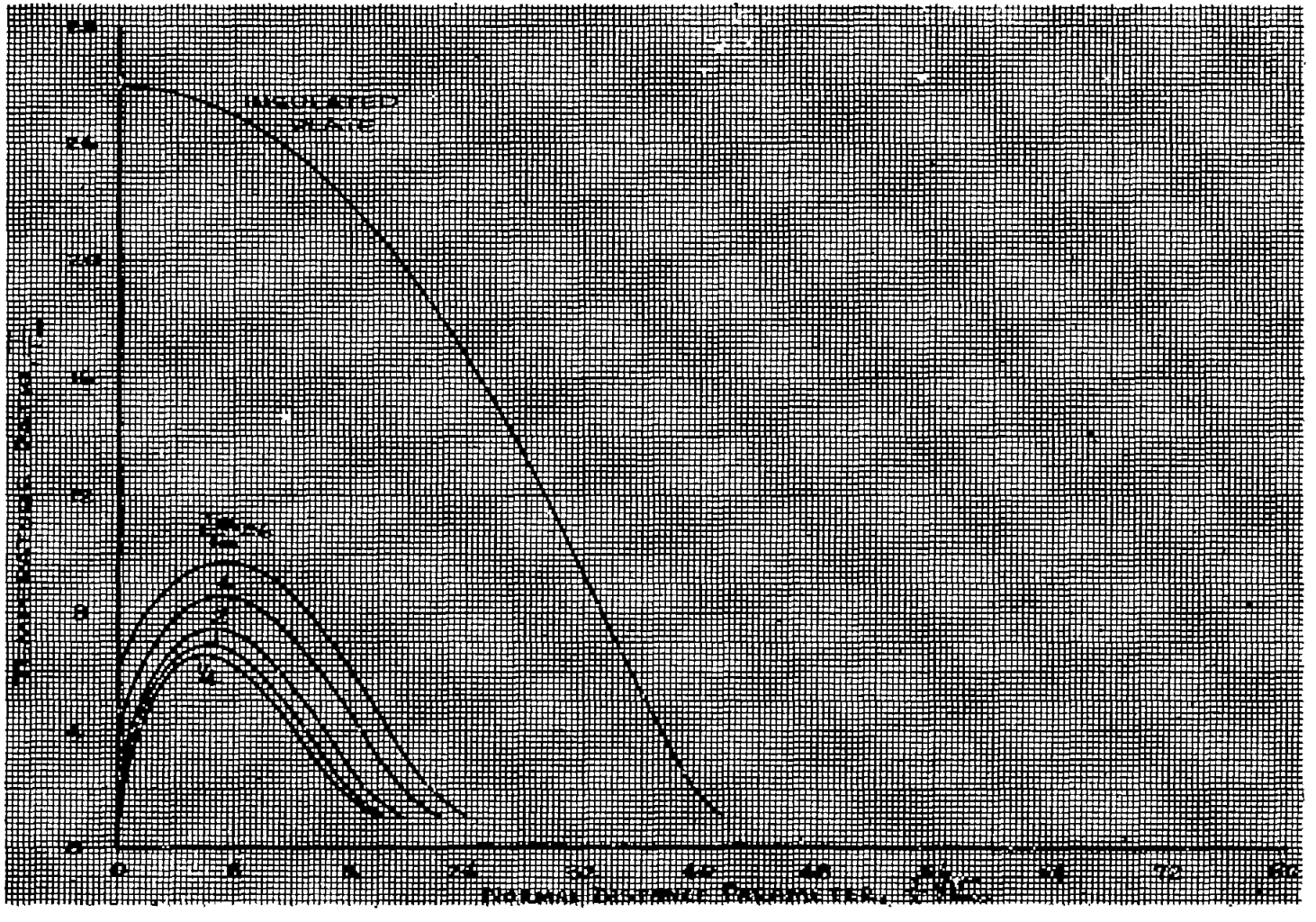

Figure 40.- Temperature distribution across laminar boundary layer for $M_\infty = 12$ and various wall-to-free-stream temperature ratios. Prandtl number, 0.75; $\theta = 0.505$.

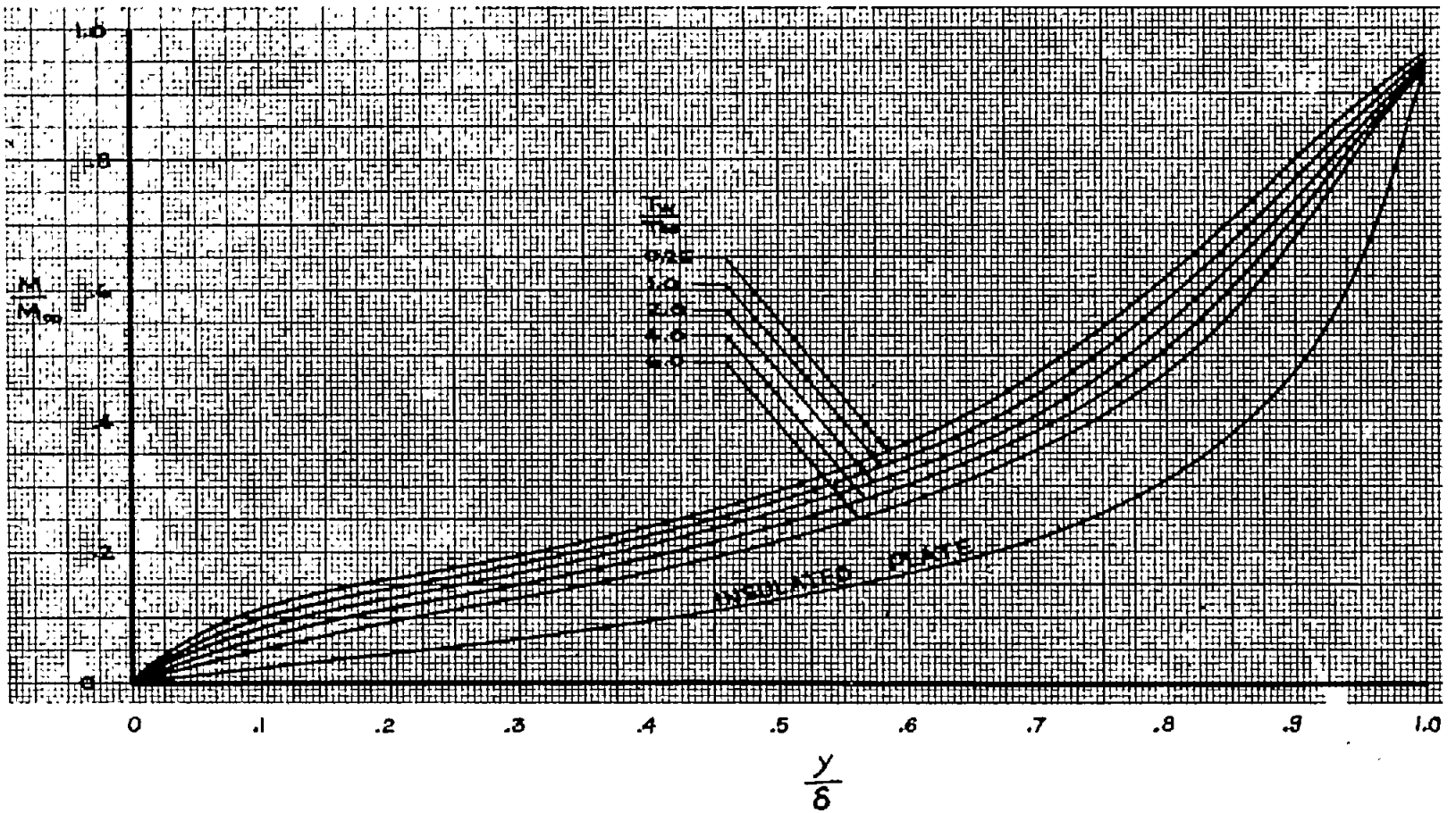

Figure 41.- Mach number distribution across laminar boundary layer for $M_\infty = 12$ and various wall-to-free-stream temperature ratios. Prandtl number, 0.75; $\theta = 0.505$.

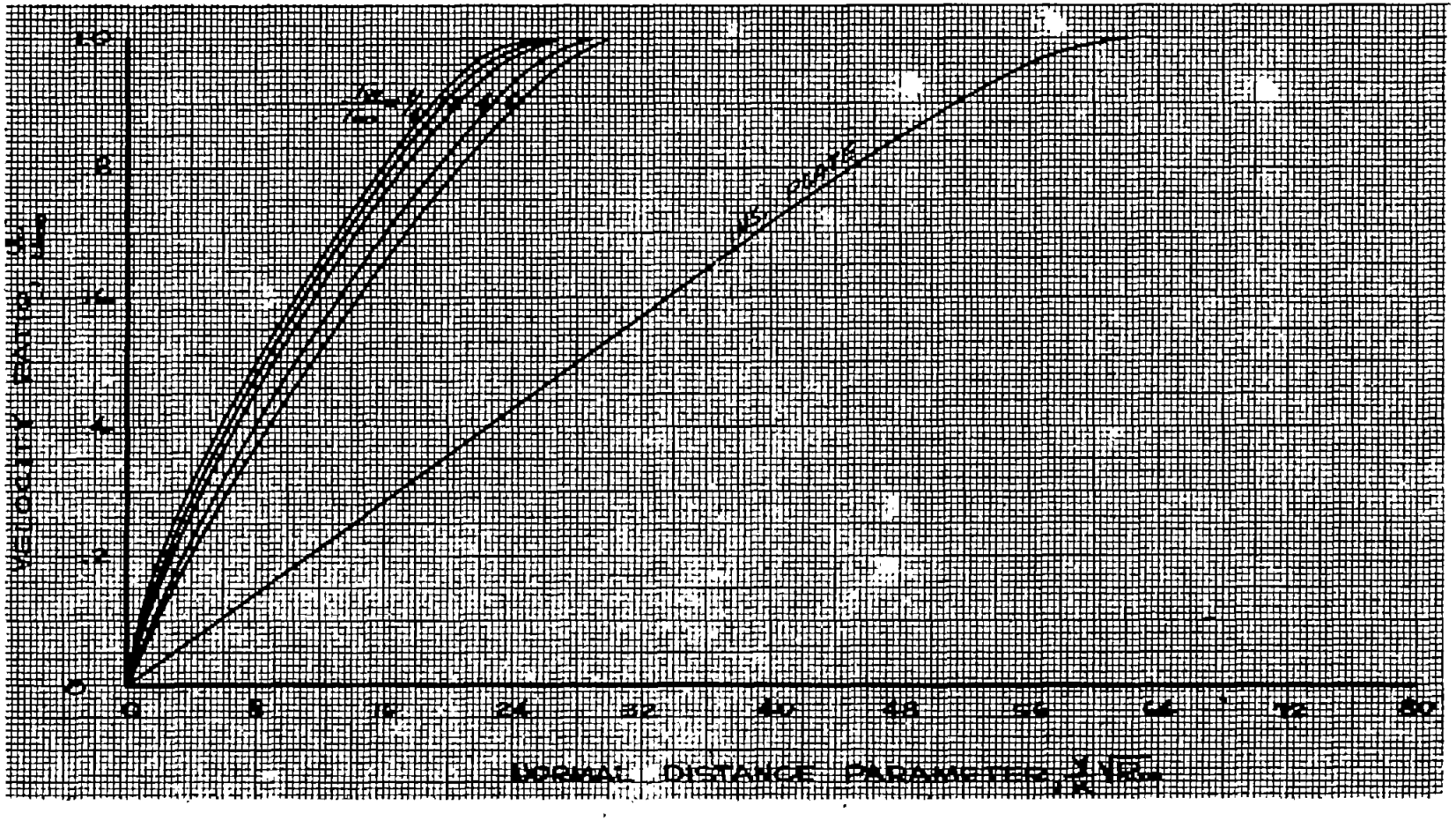

Figure 42.- Velocity distribution across laminar boundary layer for $M_\infty = 16$ and various wall-to-free-stream temperature ratios. Prandtl number, 0.75; $\theta = 0.505$.

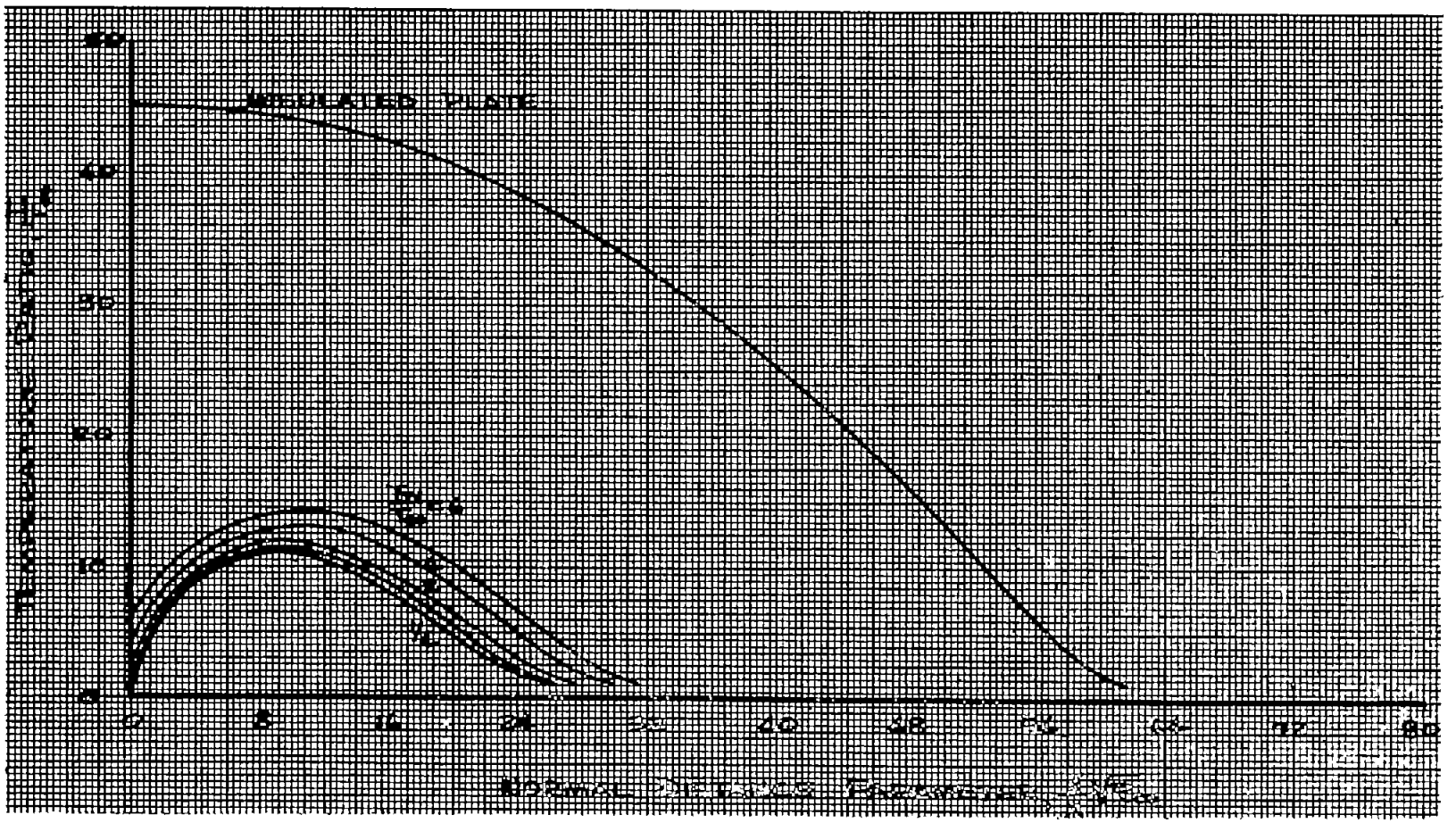

Figure 43.- Temperature distribution across laminar boundary layer for $M_\infty = 16$ and various wall-to-free-stream temperature ratios. Prandtl number, 0.75; $\theta = 0.505$.

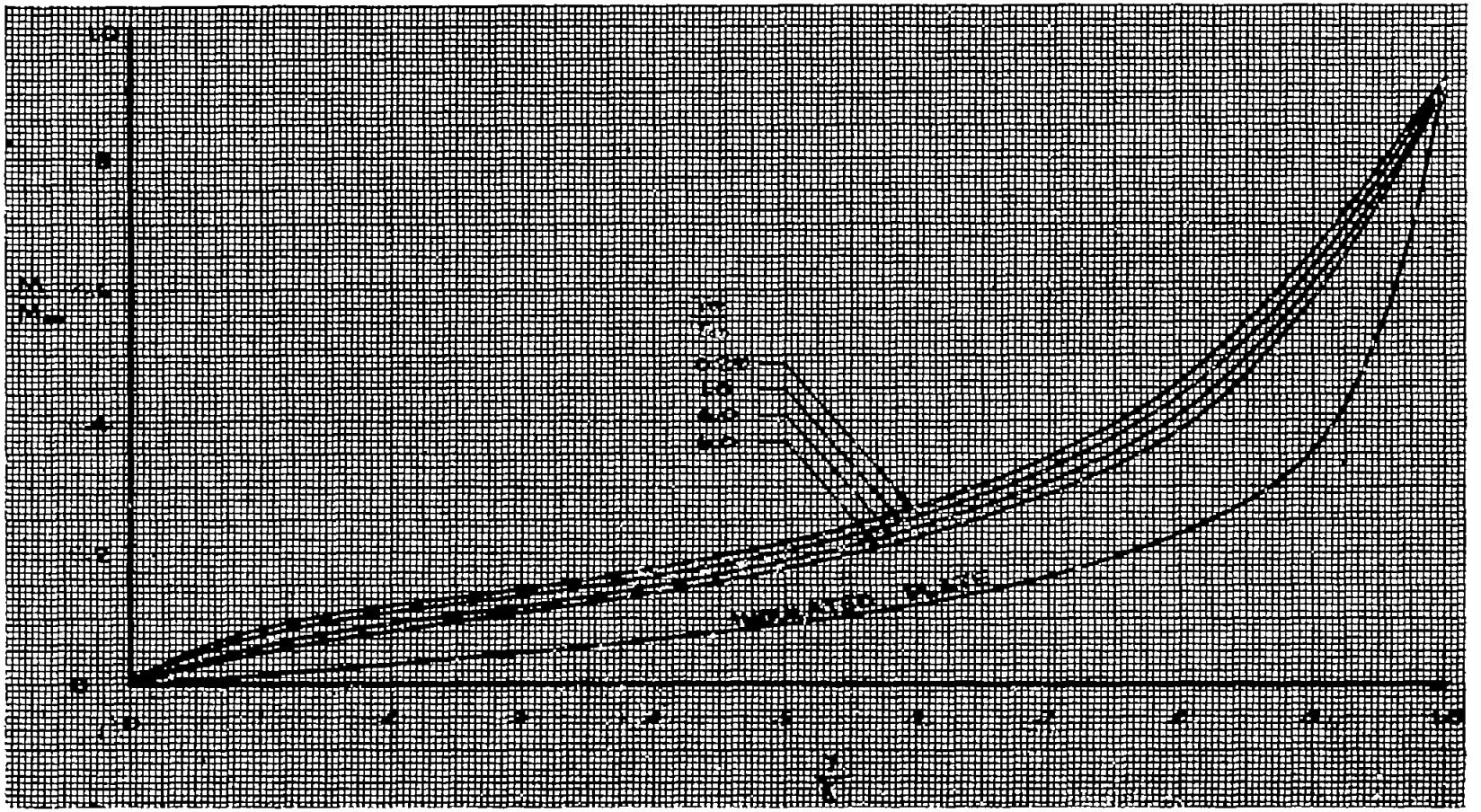

Figure 44.- Mach number distribution across laminar boundary layer for $M_\infty = 16$ and various wall-to-free-stream temperature ratios. Prandtl number, 0.75; $\theta = 0.505$.

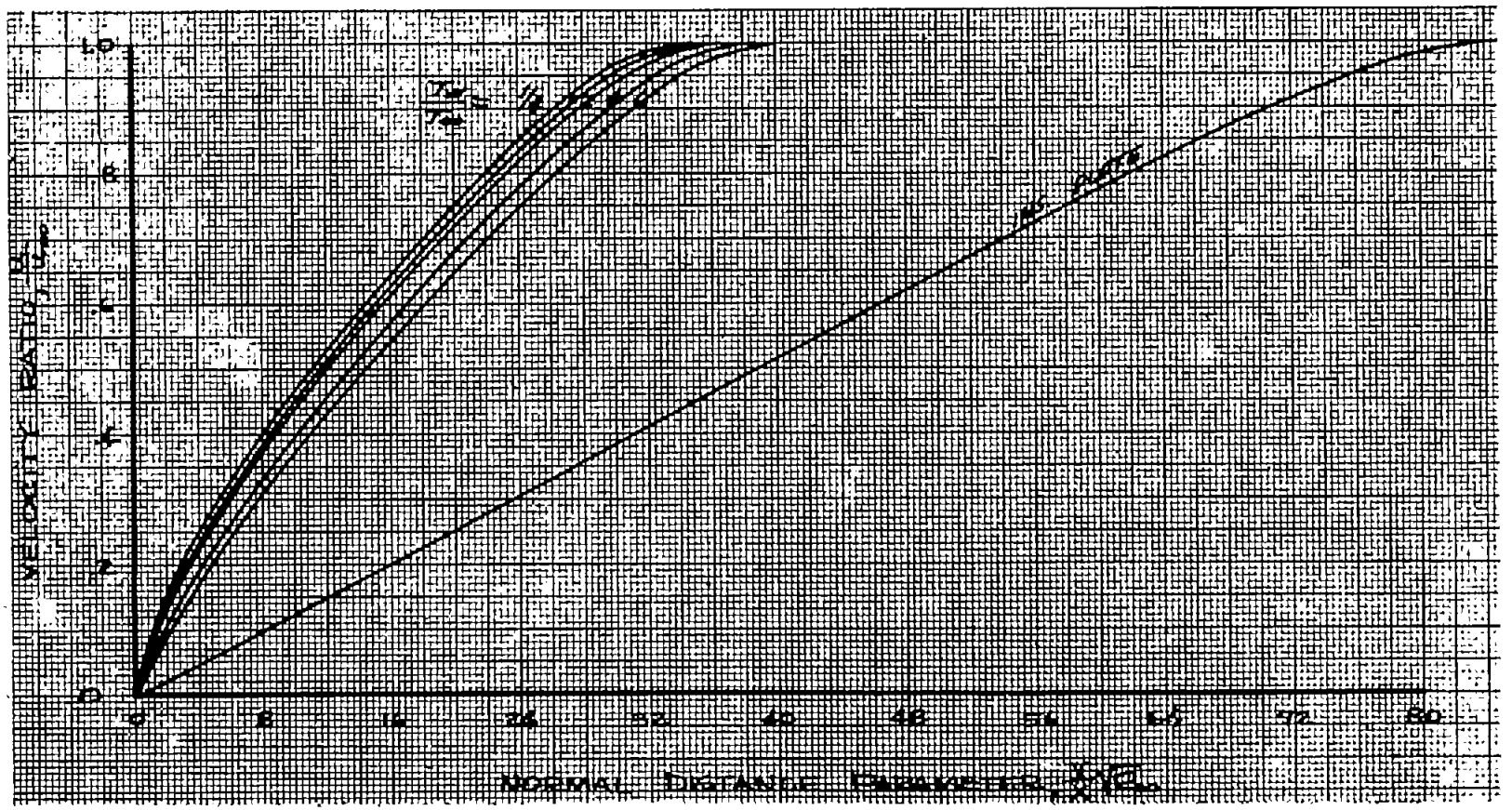

Figure 45.- Velocity distribution across laminar boundary layer for $M_\infty = 20$ and various wall-to-free-stream temperature ratios. Prandtl number, 0.75; $\theta = 0.505$.

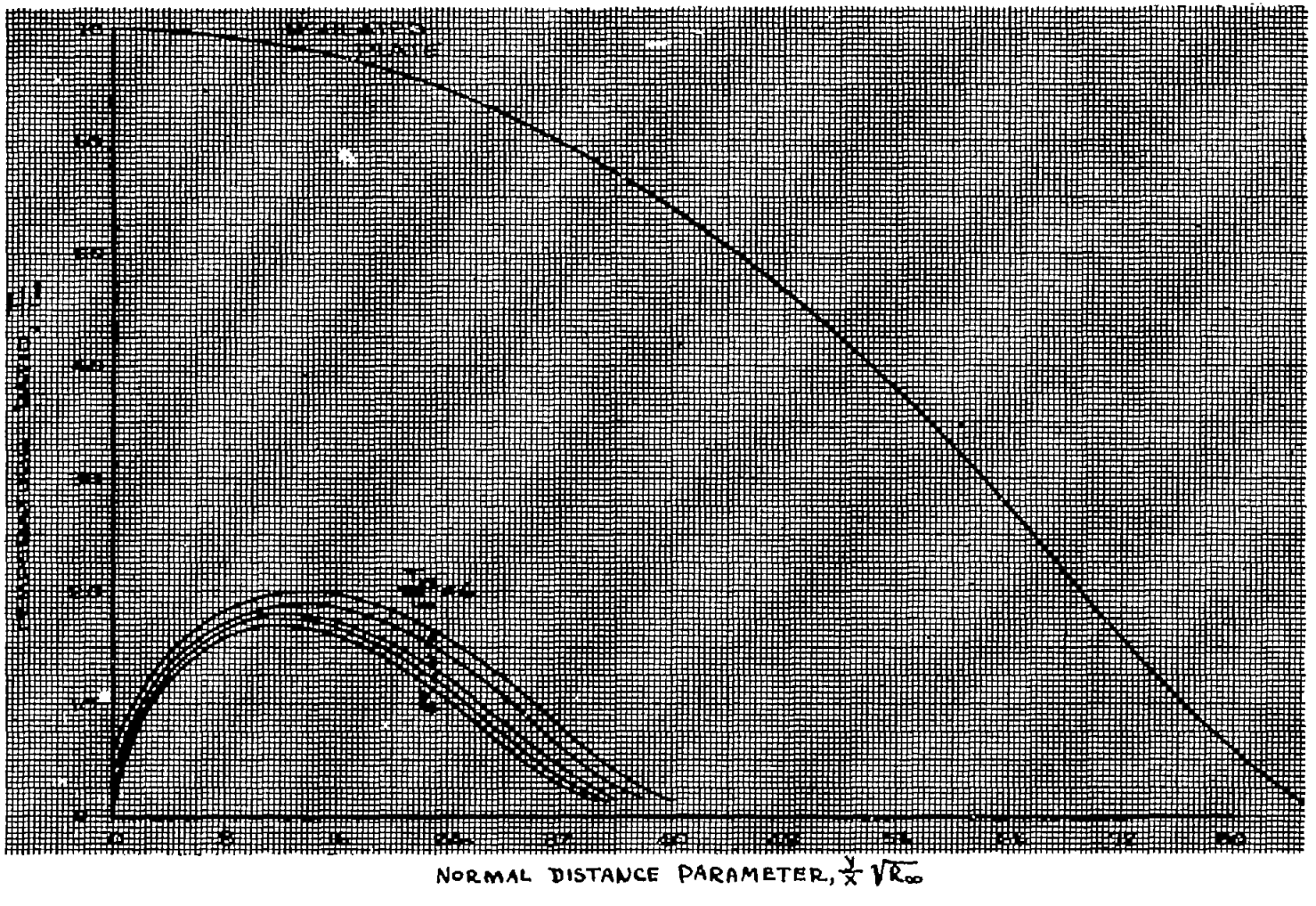

Figure 46.- Temperature distribution across laminar boundary layer for $M_\infty = 20$ and various wall-to-free-stream temperature ratios. Prandtl number, 0.75; $\theta = 0.505$.

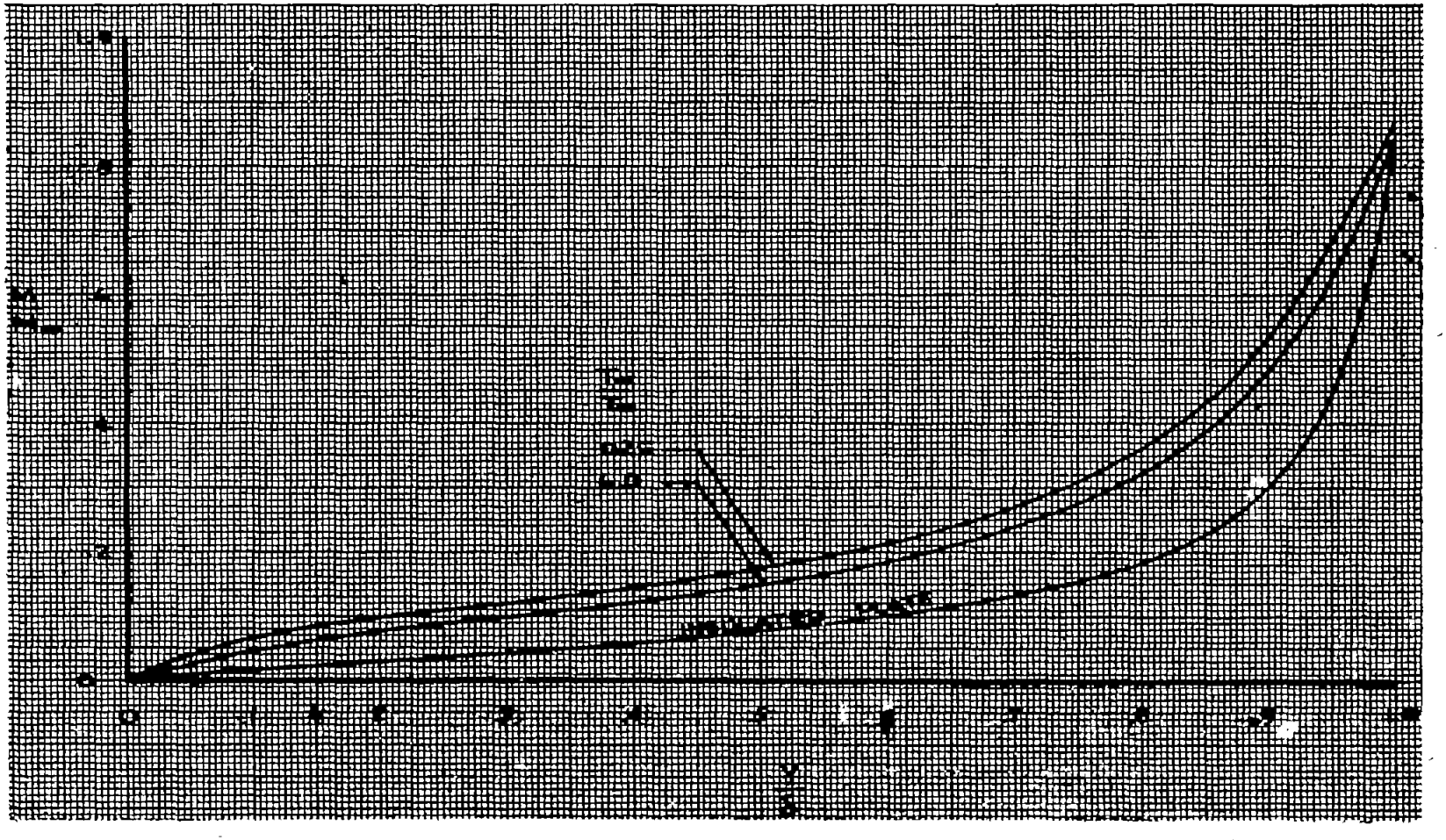

Figure 47.- Mach number distribution across laminar boundary layer for $M_\infty = 20$ and various wall-to-free stream temperature ratios. Prandtl number, 0.75; $\theta = 0.505$.

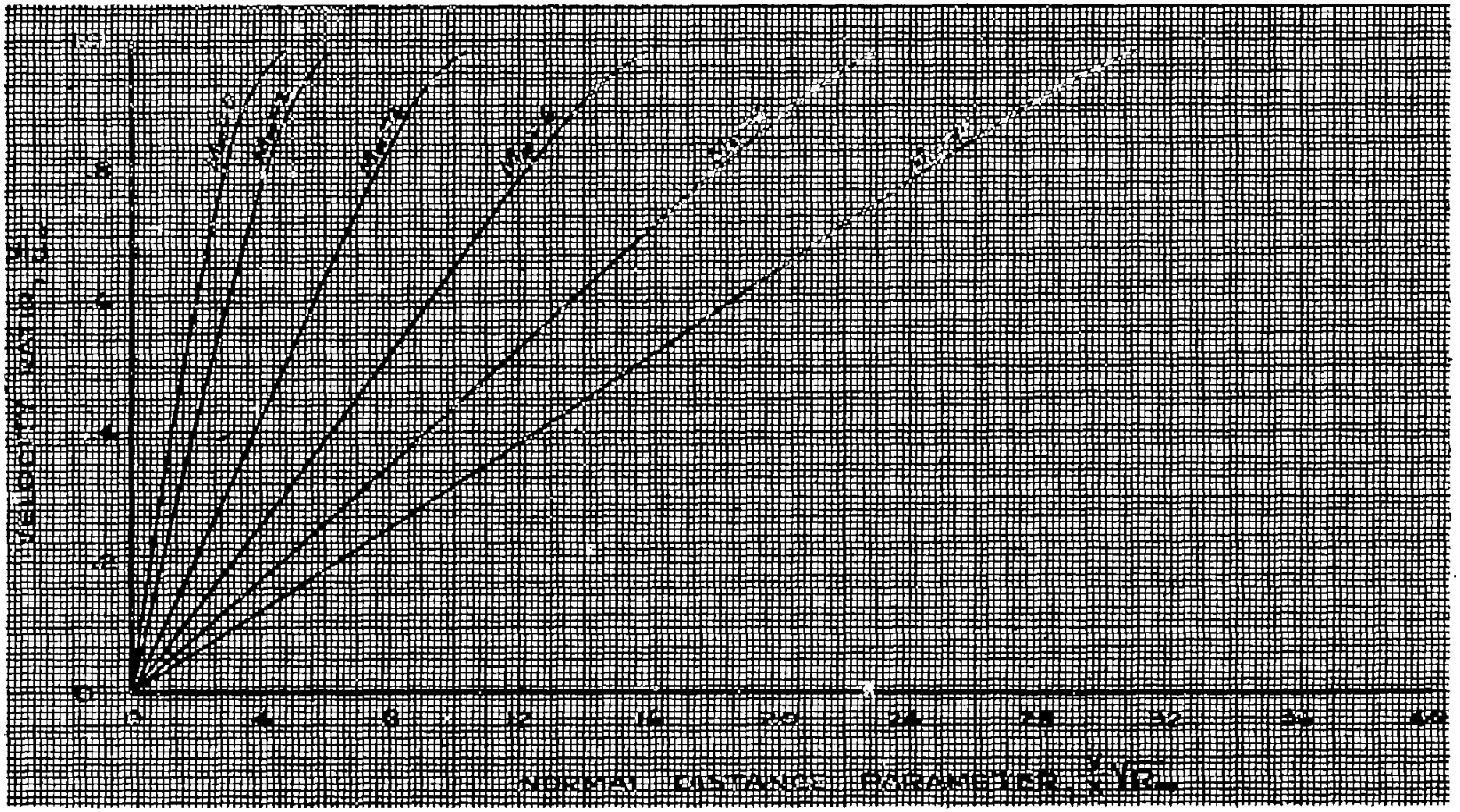

Figure 48.- Velocity distribution across laminar boundary layer on an insulated flat plate for various Mach numbers. Prandtl number, 1.0; $\theta = 0.505$.

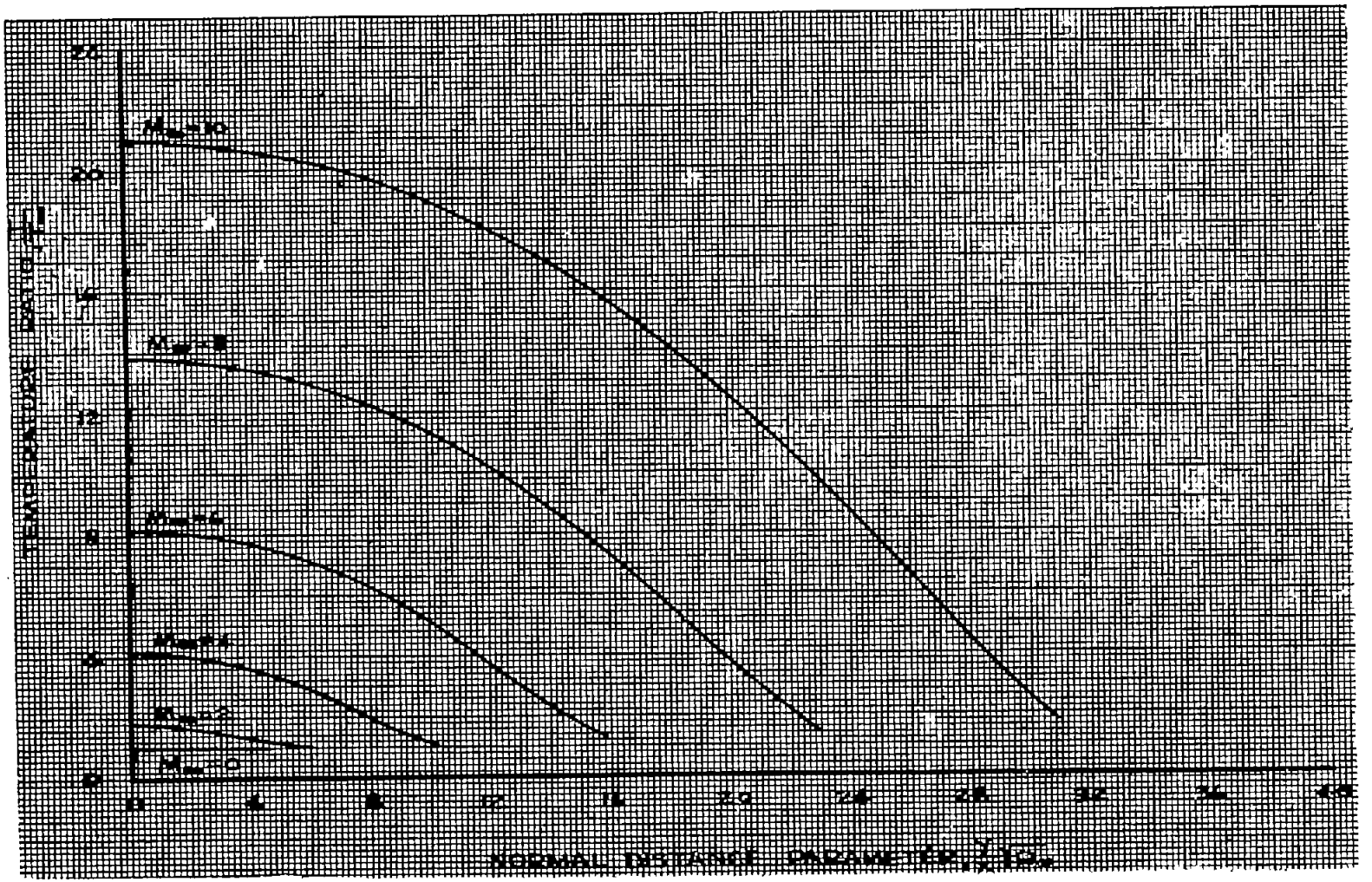

Figure 49.- Temperature distribution across laminar boundary layer on an insulated flat plate for various Mach numbers. Prandtl number 1.0; $\theta = 0.505$.

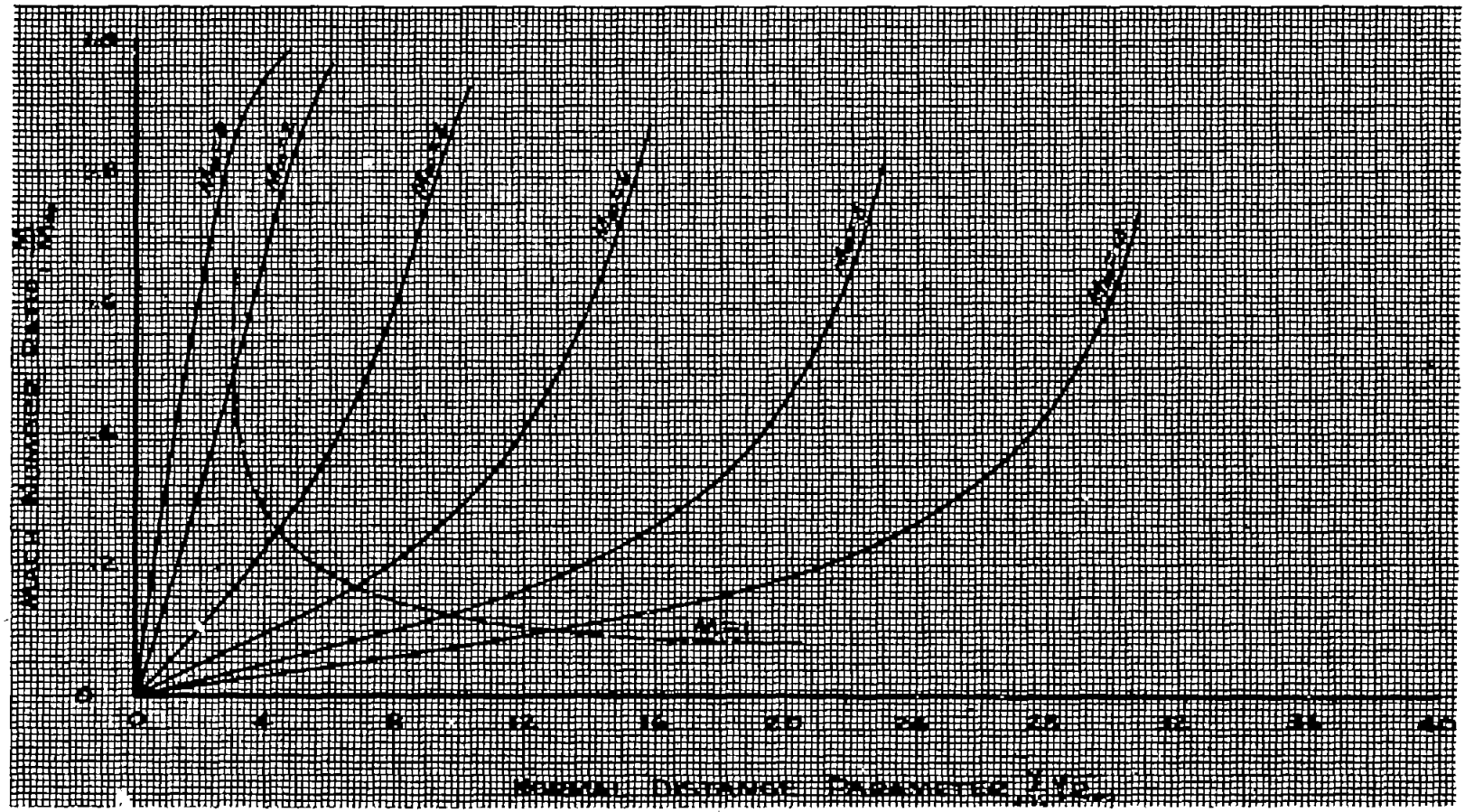

Figure 50.- Mach number distribution across laminar boundary layer on an insulated flat plate for various Mach numbers. Prandtl number, 1.0; $\theta = 0.505$.

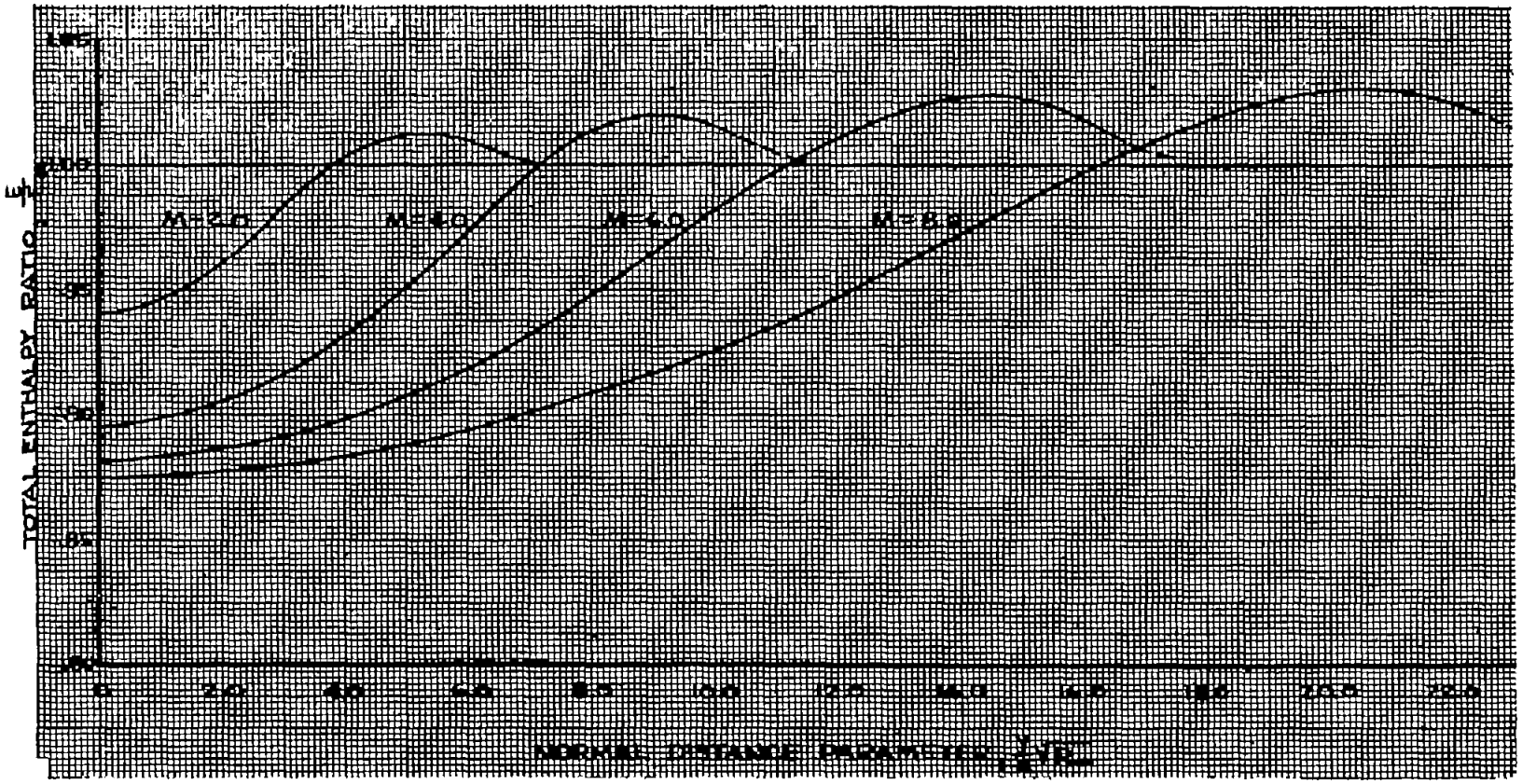

Figure 51.- Total enthalpy variation across laminar boundary layer of a compressible fluid flowing along an insulated flat plate at various free-stream Mach numbers. Prandtl number, 0.75; $\theta = 0.505$.